

**IZMIR KATIP CELEBI UNIVERSITY ★ GRADUATE SCHOOL OF SCIENCE**  
**ENGINEERING**

**THE EFFECT OF PULSED ELECTROMAGNETIC FIELDS FOR *IN VITRO***  
**WOUND HEALING EXPOSURE SYSTEMS**

**M.Sc. THESIS**

**Mehmet GÜMÜŞAY**

**Department of Biomedical Technologies**

**OCAK 2016**

**IZMIR KATIP CELEBI UNIVERSITY ★ GRADUATE SCHOOL OF SCIENCE**  
**ENGINEERING**

**THE EFFECT OF PULSED ELECTROMAGNETIC FIELDS FOR *IN VITRO***  
**WOUND HEALING EXPOSURE SYSTEMS**

**M.Sc. THESIS**

**Mehmet GÜMÜŞAY**  
**Y130101021**

**Department of Biomedical Technologies**

**Thesis Advisor: Prof. Dr. Adnan KAYA**

**OCAK 2016**

**İZMİR KATİP ÇELEBİ ÜNİVERSİTESİ ★ FEN BİLİMLERİ ENSTİTÜSÜ**

**DARBELİ ELEKTROMAGNETİK ALAN IŞIMA SİSTEMLERİNİN IN VITRO  
YARA İYİLEŞMESİNE ETKİSİ**

**YÜKSEK LİSANS TEZİ**

**Mehmet GÜMÜŞAY  
Y130101021**

**Biyomedikal Teknolojileri Anabilim Dalı**

**Tez Danışmanı: Prof. Dr. Adnan KAYA**

**OCAK 2016**

**Mehmet Gümüřay**, a **M.Sc.** student of **IKCU Graduate School of Science and Engineering** student ID **Y130101021**, successfully defended the **thesis/dissertation** entitled “**THE EFFECT OF PULSED ELECTROMAGNETIC FIELDS FOR *IN VITRO* WOUND HEALING EXPOSURE SYSTEMS**”, which he prepared after fulfilling the requirements specified in the associated legislations, before the jury whose signatures are below.

**Thesis Advisor :**      **Prof. Dr. Adnan KAYA**      .....

Izmir Katip Celebi University

**Jury Members :**      **Prof. Dr. Adnan KAYA**      .....

Izmir Katip Celebi University

**Prof. Dr. M. İbrahim TUĐLU**      .....

Celal Bayar University

**Asst. Prof. Utku Kürřat ERCAN**      .....

Izmir Katip Celebi University

**Date of Submission : 12 January 2016**

**Date of Defense : 11 January 2016**

*This thesis is dedicated to my family. For their endless love, support and encouragement,*

## **FOREWORD**

I would like to express my deep appreciation and thanks to my family, my colleagues who have supported during the preparation of the thesis. I would like to express my sincere gratitude to my thesis advisor, Prof. Dr. Adnan KAYA who has inspired me in this study and provided me precious suggestions and advice. Also, thank to our academic administrators who have been academically motivating and providing necessary equipments. This work was supported by IKÇÜ Graduate School Of Natural And Applied Sciences.

January 2016

Mehmet GÜMÜŞAY

## TABLE OF CONTENTS

	<u>Page</u>
<b>ABBREVIATIONS</b> .....	<b>viii</b>
<b>LIST OF TABLES</b> .....	<b>ix</b>
<b>LIST OF FIGURES</b> .....	<b>x</b>
<b>SUMMARY</b> .....	<b>xiii</b>
<b>ÖZET</b> .....	<b>xiv</b>
<b>1. INTRODUCTION</b> .....	<b>1</b>
1.1 Background.....	1
1.2 Research Aims.....	2
1.3 General Objective.....	3
1.4 Specific Objective .....	3
1.5 Thesis Organization and Description of Contributions .....	4
<b>2. LITERATURE REVIEW AND BACKGROUND UNDERSTANDING</b> .....	<b>5</b>
2.1 Overview .....	5
2.2 EMF Biological Effects.....	5
2.3 Possible PEMF/PRFE Mechanisms .....	6
<b>3. ELECTROMAGNETIC FIELDS AND WAVE EQUATIONS</b> .....	<b>9</b>
3.1 Objectives.....	9
3.2 Electric Fields.....	9
3.3 Magnetic Fields .....	11
3.4 Electromagnetic Field (EMF) Radiation .....	14
3.5 Maxwell's Equations .....	14
3.6 Wave Equations.....	16
3.7 Radio and Microwave Dielectric Properties of Biological Materials .....	16
3.8 Low-Loss Dielectric Materials.....	19
3.9 Lossy Dielectrics at Low Frequencies.....	20
3.10 Biological Materials .....	21
3.11 Propagation and Absorption in Tissue Media .....	22
3.11.1 Multiple Layers of Tissue .....	23
3.11.2 Spherical Tissue Models .....	25
3.11.3 Prolate Spheroidal Tissue Models.....	28
3.12 Theory-Biot-Savart Law.....	29
<b>4. PEMF COIL MODELS and PRFE ANTENNA PROTOTYPES</b> .....	<b>35</b>
4.1 Objectives.....	35
4.2 Modelling and Simulations.....	35
4.3 Numerical EM Modelling.....	35
4.4 Coil Model and Geometrical Parameters for PEMF Application .....	37
4.5 Antenna Model and Geometrical Parameters for PRFE Application.....	38
4.6 Fabrication of the Antenna Prototypes .....	39
4.6.1 Impedance Matching .....	39
4.6.2 PRFE Antenna with Artificial Magnetic Conductor (AMC) .....	42
4.6.3 A Multi layers Flexible Flat Spiral Antenna on PDMS/Kapton Substrate	44

4.6.4 Antimicrobial Effects of Non-Thermal Plasma on PDMS Layer of the Antenna .....	47
4.6.5 Comparison of the PRFE Applicator with Simulation Results.....	48
<b>5. PEMF PRFE EXPOSURE SYSTEMS, MEASUREMENTS and BIOLOGICAL RESULTS .....</b>	<b>50</b>
5.1 Overview .....	50
5.2 Experimental Equipment.....	50
5.3 The PEMF/PRFE exposure systems .....	52
5.4 <i>In Vitro</i> Wound Healing Assays.....	55
5.5 Simulation and Biological Results of PEMF/PRFE Exposure to MDA-MB-231, BMSC, and NA2B.....	58
5.6 The effect of PEMF and PRFE on mouse neuroblastoma (Na2b) and adipose tissue.....	60
5.7 The Effect of PEMF on 3T3 cells during <i>In Vitro</i> Wound Healing.....	62
5.8 Thermal Effect of Pulsed Electromagnetic Fields.....	66
<b>6. CONCLUSIONS .....</b>	<b>67</b>
<b>REFERENCES.....</b>	<b>69</b>
<b>APPENDICES .....</b>	<b>73</b>
<b>CURRICULUM VITAE.....</b>	<b>78</b>



## ABBREVIATIONS

<b>AC</b>	: Alternating Current
<b>AMC</b>	: Artificial Magnetic Conductor
<b>ASC</b>	: Adipose Tissue-Derived stem cell
<b>BMSC</b>	: Bone Marrow Mesenchymal Stem Cells
<b>CaM</b>	: Calmodulin
<b>CMS</b>	: Center for Medicare Services
<b>DC</b>	: Direct Current
<b>DFU</b>	: Diabetic Neuropathic Foot Ulcer
<b>DMEM</b>	: Dulbecco's Modified Eagle's Medium
<b>DMSO</b>	: Dimethyl Sulfoxide
<b>ECM</b>	: Extracellular Matrix
<b>ELF</b>	: Extremely Low Frequencies
<b>EMF</b>	: Electromagnetic Field
<b>eNOS</b>	: Endothelial Oxide Synthase Isoforms
<b>FDA</b>	: Food and Drug Administration
<b>FDTD</b>	: Finite Difference Time Domain
<b>FDM</b>	: Finite difference method
<b>FIT</b>	: Finite integration technique
<b>FEM</b>	: Finite Element Method
<b>FSS</b>	: Frequency Selective Surface
<b>GMT</b>	: Generalized Multipole Technique
<b>IF</b>	: Intermediate Frequencies
<b>iNOS</b>	: Inducible Nitric Oxide Synthase
<b>MLCK</b>	: Myosin Light Chain Kinase
<b>MoM</b>	: Method of Moments
<b>MRI</b>	: Medical Imaging
<b>Nb2a</b>	: Mouse Neuroblastoma Cell
<b>NO</b>	: Nitric Oxide
<b>NOS</b>	: Nitric Oxide Synthase
<b>nNOS</b>	: Neuronal Nitric Oxide Synthase Isoforms
<b>PBS</b>	: Phosphate Buffer Saline
<b>PDMS</b>	: Polydimethylsiloxane
<b>PEC</b>	: Perfect Electric Conductor
<b>PEMF</b>	: Pulsed Electromagnetic Field Therapy
<b>PRFE</b>	: Pulsed Radio Frequency Energy
<b>PrU</b>	: Pressure Ulcer
<b>RF</b>	: Radio Frequencies
<b>ROS</b>	: Reactive Oxygen
<b>RNS</b>	: Nitrogen Species
<b>SWD</b>	: Shortwave Diathermy
<b>TLM</b>	: Transmission Line Matrix Method
<b>VLU</b>	: Venous Leg Ulcer

## LIST OF TABLES

	<u>Page</u>
<b>Table 3.1:</b> Characteristics of electric and magnetic fields. ....	13
<b>Table 3.2:</b> Maxwell's equations and the continuity equation in differential and integral forms for time-varying fields. ....	15
<b>Table 3.3:</b> Dielectric constants and Conductivities of Select Tissues and Materials at 50 MHz (Michlovitz, Bellew, & Nolan, 2011). ....	22
<b>Table 4.1:</b> Performance Parameter results of Flat Spiral Antenna. ....	44
<b>Table A.1:</b> Dielectric properties of fat and muscle layers at different frequencies...	74

## LIST OF FIGURES

	<u>Page</u>
<b>Figure 3.1:</b> Pulsed electromagnetic field (PEMF) mechanism .....	7
<b>Figure 3.1:</b> (a) Electric field lines due to a single point charge. (b) Electric field produced by two uniform sheets of charge. ....	10
<b>Figure 3.2:</b> Magnetic field lines around a current-carrying conductor: (a) Less current flow. (b) Increased current flow.....	11
<b>Figure 3.3:</b> Magnetic flux density $\vec{B}$ emerging from an area A.....	13
<b>Figure 3.4:</b> Spectrum of the dielectric properties of cell suspensions and tissues. ...	17
<b>Figure 3.5:</b> Behavior of bound, charged particle in an applied electric field.....	17
<b>Figure 3.6:</b> Frequency permittivity associated with low-loss dielectric materials....	20
Figure 3.7: (a) Relative permittivity and (b) Conductivity of skin tissue samples from three rats (Karacolak et al., 2009). ....	22
<b>Figure 3.8:</b> Plane wave impinging on a composite fat-muscle layer. ....	23
<b>Figure 3.9:</b> (a) Magnitude of E-Field (V/m) for air-muscle-fat layers. (b) Reflection coefficient of air-fat-muscle model with frequency dispersive material parameters. ....	24
<b>Figure 3.10:</b> Predicted SAR distribution in a sphere whose size is extremely small compared to the wavelength. x, y, and z are the orthogonal coordinates of a rectangular system (James C Lin, Guy, & Johnson, 1973). ....	26
<b>Figure 3.11:</b> Diagrammatic representation of the behavior of electric and magnetic fields under quasi-static conditions of irradiation. ....	26
<b>Figure 3.12:</b> Frequency dependence of absorption in a spherical model of the human body.....	27
<b>Figure 3.13:</b> The incremental magnetic field strength, $\Delta\vec{B}$ , at point P is given by the.....	29
<b>Figure 3.14:</b> A pair of Helmholtz coils, each of radius R and separated by a R.....	32
Figure 3.15: Countour Plot of Z Component of Magnetic Field.....	33
Figure 3.16: The z component (x=-15 cm to x=15 cm) of magnetic field intensity ..	33
Figure 3.17: The z component (from x=-10 cm to x=40 cm) of magnetic field intensity for (a) Two ring coil, (b) Four ring coil.....	34
<b>Figure 4.1:</b> Magnetic coils used in PEMF application (a) Helmholtz coil, (b) coil prototypes, (c) 3-series Helmholtz coil) Antenna Structures operating at 27 MHz.....	38
<b>Figure 4.2:</b> Antenna Structures operating at 27 MHz. ....	39
<b>Figure 4.3:</b> There are four basic L-network configurations. The network to be used depends on the relationship of the generator and load impedance values. Those in (a) and (b) are low-pass circuits, and those in (c) and (d) are high-pass versions.....	40
<b>Figure 4.4:</b> Simulation results of the proposed antenna (a) Front view (b) Back view (c) Simulation and measurement result of S11 (d) Simulation result of S11 with matching (e) E-field simulation result (f) E-field result through 10 cm line from	

the antenna (g) H-field simulation result (f) H-field result through 10 cm line from the antenna.....	41
<b>Figure 4.5:</b> Designed AMC structures. ....	42
<b>Figure 4.6:</b> Simulation results of the proposed antenna with AMC (a) Front view (b) Back view (c) Simulation result of S11 (d) Simulation result of S11 with matching (e) E-field simulation result (f) E-field result through 10 cm line from the antenna (g) H-field simulation result (f) H-field result through 10 cm line from the antenna.....	43
<b>Figure 4.7:</b> Fabrication process for PDMS-Kapton substrate based antenna, (a) Mixing PDMS silicone gel and cure agent (10:1 v/v) (b) Degas for 30 minutes, (c) Pour the mixture into a container attached antenna with Kapton substrate at the bottom and degas for 1 hour (d) Fabricated Antenna Prototype.....	45
<b>Figure 4.8:</b> (a) Schematic diagram of the multilayer microstrip patch antenna identifying each layer and its thickness, (b) Simulation result of S11 (c) Simulation result of S11 with matching (d) E-field simulation result (e) E-field result through 10 cm line from the antenna (f) H-field simulation result (g) H-field result through 10 cm line from the antenna. ....	46
<b>Figure 4.9:</b> PDMS exposed for 5 mins to non-thermal plasma completely inhibited 10 <sup>4</sup> CFU/mL of E. Coli. ....	48
<b>Figure 4.10:</b> Flat spiral antennas simulation results (a) 1.6 mm FR4 $\epsilon_r=4.3$ , middle feeding (b) 1.6 mm FR4 $\epsilon_r=4.3$ , side feeding (c) 1.6 mm PDMS $\epsilon_r=2.4$ , side feeding (d), (e), (f) S11 results with and without matching circuit (g), (h), (i) E-field results (j), (k), (l) H-field results.....	48
<b>Figure 4.11:</b> (a) Measurement setup of S11 for middle feeding flat spiral antenna (b) S11 result of the antenna, (c) S21 result of the antenna (d) Measurement setup of S11 for side feeding flat spiral antenna flexible flat spiral antenna (e) S11 result of the antenna, (f) S21 result of the antenna .....	49
<b>Figure 5.1:</b> PEMF exposure System (a) Kikusui power generator (b) Pasco function generator and Pasco universal interface (c), (d) Pasco Helmholtz coils with cell cultures, (e) 75 Hz PEMF signal (f) B-Field (Tesla) measurement result with a hall effect sensor. ....	51
<b>Figure 5.2:</b> (a) PRFE system (b) AM signal of PRFE application (c) FSK application of PRFE.....	52
<b>Figure 5.3:</b> PEMF exposure setup and experimental timeline.....	53
<b>Figure 5.4:</b> Summary of steps for methodology of the study. (a) Inverted microscope, (b) Cell culture images, (c) Measured B-field in the Helmholtz coil, (d) Simulated B-field in the Helmholtz coil, (e) Measured power in dB, (f) Simulated H-field.....	54
<b>Figure 5.5:</b> <i>In Vitro</i> exposure systems and conditions. Cells: MDA-MB-231, (ASCs), (BMSC), (Nb2a), and 3T3; Exposure: PEMF (75 Hz, 1.3 ms pulse width, 1 mT, 5h) PRFE (27.12 MHz frequency, PSK or AM, 20 mW, 5h). ....	55
<b>Figure 5.6:</b> MTT metabolization to formazan salt in metabolically active cells. ....	56
<b>Figure 5.7:</b> PEMF and PRFE system simulations with petri dish, (a) PRFE application with petri dish, (b) PRFE simulation with petri dish, (c) PEMF application petri dish, (d) PEMF siulation with petri dish, (e) E-field simulation result of PRFE application, (f) H-field simulation result of PRFE application, (g) E-field simulation result of PEMF application, (h) H-field simulation result of PEMF application, (i) E-Field result of PRFE application trough 10 cm line from center of the applicator, (j) H-Field result of PRFE application through 10 cm line from center of the applicator, (k) E-Field result of PEMF application	

through 20 cm diameter of the applicator, (l) H-Field result of PEMF application through 20 cm diameter of the applicator.....	59
<b>Figure 5.8:</b> The death of cells were observed during the stage of proliferation and that is because oxidative stress (NOS), apoptosis (TUNEL), and inflammation (TGF-beta) increased.....	60
<b>Figure 5.9:</b> The effects of PEMF and PRFE Na2b in mouse neuron-like cell culture. ....	61
<b>Figure 5.10:</b> Oxidative stress (NOS), apoptosis (TUNEL) and increase of inflammation (TGF-beta) (a) Proliferation Stage (b) Differentiation Stage. ....	61
<b>Figure 5.11:</b> PEMF and PRFE system simulations with 24 well plate cell culture (a) PRFE application with 24 well plate (b) PRFE simulation with 24 well plate (c) PEMF application 24 well plate, (d) PEMF siulation with 24 well plate, (e) E-field simulation result of PRFE application, (f) H-field simulation result of PRFE application (g) E-field simulation result of PEMF application, (h) H-field simulation result of PEMF application (i) E-Field result of PRFE application trough 10 cm line from center of the applicator, (j) H-Field result of PRFE application through 10 cm line from center of the applicator, (k) E-Field result of PEMF application through 20 cm diameter of the applicator, (l) H-Field result of PEMF application through 20 cm diameter of the applicator. ....	63
<b>Figure 5.12:</b> Acquired microscope images of the Control and PEMF/PRFE exposure 3T3 fibroblast cell groups. ....	64
<b>Figure 5.13:</b> MTT result of Acquired microscope images of the Control and PEMF/PRFE exposure 3T3 fibroblast cell groups. ....	65
Figure 5.14: Percentage of wound closure of PEMF and PRFE treated groups .....	65
<b>Figure 5.15:</b> Thermal image of PEMF applied cultures. (a) Culture with PEMF coil, (b) Closer thermal images of culture dish. ....	66
<b>Figure A.1:</b> Induced electric and magnetic field by low frequency electromagnetic fields to human leg model. ....	75
<b>Figure A.2:</b> Simulation result of 27 Mhz electromagnetic field exposed of human tissue model by a loop antenna. ....	75
<b>Figure A.3:</b> E-field and H-field distributions generated by 27 MHz antenna in human tissue layers. ....	76

# THE EFFECT OF PULSED ELECTROMAGNETIC FIELDS FOR *IN VITRO* WOUND HEALING EXPOSURE SYSTEMS

## SUMMARY

Electromagnetic fields have achieved important role as stimulator and therapeutic facility in biology and medicine (Blank & Findl, 2013). The effects of low magnitude, low frequency pulsed electromagnetic fields have been a period of study since past few decades, which was mainly on the treating soft tissue injuries, skin ulcers, non-uniform bone fractures and degenerative nerve healing (Hug & Rösli, 2012b). Chronic wounds are a major healthcare problem for patient morbidity and contribute significantly to the cost of health care in the world. Chronic ulcers or wounds are breaks in the skin of greater than 6 weeks or with frequent recurrence. The most common etiologies of chronic ulcers include venous leg ulcers, pressure ulcers (PrUs), diabetic neuropathic foot ulcers (DFUs), and leg ulcers of arterial insufficiency (Markova & Mostow, 2012).

From this point of view, the main purpose of the present study is to investigate the effects of pulsed radio frequency energy (PRFE) at 27.12 MHz carrier frequency on the proliferation and migration of cells involved in wound healing *in vitro* with the ultimate aim of developing an applicator antenna. One of the aims of this study was to investigate effect of Pulsed electromagnetic field (PEMF) at 75 Hz frequency by applying on the same cell lines and investigated its effects on wound healing.

The applications of the developed PRFE and PEMF exposure systems have been investigated in terms of the experimental evaluation of *in vitro* Scratch Assay, MTT Assay, and Immunohistochemistry analyses. The PRFE antennas and PEMF coils were designed and simulated using CST Microwave studio software and measurements were carried out to verify the results.  $\vec{E}$ -field and  $\vec{H}$ -field simulations were also carried out with biological materials (tissue or cell culture in petri dishes).

Through this study, we experimentally proved that it is possible to optimize PRFE and PEMF parameters (frequency,  $f$ , and magnetic flux density,  $\vec{B}$ ) of the applied irradiation for accelerated wound healing. Obtained results showed that the application of PEMF and PRFE increase proliferation of non-cancerous cells while cease the proliferation of cancer cells stopped.

## DARBELİ ELEKTROMAGNETİK ALANLAR İLE KRONİK YARA İYİLEŞTİRME CİHAZI TASARIMI

### ÖZET

Elektromanyetik alanlar biyoloji ve tıpta stimülatör ve tedavi edici olarak önemli bir role sahiptir (Blank & Findl, 2013). Son yıllarda düşük frekans ve enerjiye sahip darbeli elektromanyetik alanların, yumuşak soku yaralanmaları, deri ülserleri uniform olmayan kemik kırıkları ve dejeneratik sinir iyileşmesi üzerinde çalışmalar yapılmaktadır (Hug & Röösli, 2012b). Kronik yaralar tüm dünyada büyük bir maliyete sahip önemli bir morbidite sağlık sorunudur. Kronik ülserler 6 haftadan uzun kalan ve sıkça nüks eden yaralardır. Kronik ülserlerin en yaygın etiyojileri arasında venöz bacak ülseri (VLUs), basınç ülseri (Prus), diyabetik nöropatik ayak ülseri (DFUs) ve arteriyel yetersizliğin bacak ülseri bulunmaktadır (Markova & Mostow, 2012).

Buradan yola çıkarak bu çalışmanın amacı, 27.12 MHz taşıyıcılı frekanslı darbeli radyofrekans enerji (PRFE) aplikatörü üretmek ve bu aplikatörün *in vitro* yara iyileşmesinde proloferasyon ve migrasyona etkisini incelemektir. Bu çalışmanın diğer bir amacı 75 Hz frekanslı darbeli elektromanyetik alan (PEMF) tedavisinin aynı hücre hatlarında yara iyileşmesi üzerindeki etkisini incelemektir.

PRFE ve PEMF ışınma sistemlerinin, hücre kültürlerinde *in vitro* Scratch deneyi, MTT deneyi ve immünohistokimyasal analizleri yapıldı. PRFE antenler ve PEMF bobinleri tasarlanmış ve CST Mikrodalga stüdyo yazılımı kullanılarak simüle edilmiş ve ölçümler sonuçları doğrulamak için yapılmıştır.  $\vec{E}$  – alan ve  $\vec{H}$  – alan simülasyonları biyolojik materyallerle (doku ve petri kaplarındaki hücre kültürleri) de yapılmıştır.

Bu çalışmalar sonucunda elde edilen bulgularda PRFE ve PEMF parametreleri (frekans, f ve manyetik alan yoğunluğu,  $\vec{B}$ ) yara iyileştirmesini hızlandırmak amacıyla optimize edilebilir. Elde edilen sonuçlar PEMF ve PRFE'nin kanseli olmayan hücrelerde prolofirasyonu arttırırken, kanserli hücrelerde ise prolofirasyonu durdurduğu gösterilmiştir.

# 1. INTRODUCTION

## 1.1 Background

Wound healing is the process of repair after skin injury. If the protective skin barrier is disrupted, an orchestrated cascade of events is activated. Local wound factors and systemic mediators mediate the healing process. It is estimated that about 1–2 % of the population in the so-called developed countries suffer from chronic wounds. Current studies have revealed important molecular mechanisms in wound healing. The healing process can be divided into three overlapping phases: (i) inflammatory phase; (ii) proliferative phase or new tissue formation (neoangiogenesis, proliferation, re-epithelialization); and (iii) tissue remodeling (remodeling of extracellular matrix, ECM (Behm, Babilas, Landthaler, & Schreml, 2012).

In the last century, there have only been a handful of technical advances that have contributed to changes in the discipline of wound management. Despite these advancements, wound management is still extremely challenging due to its subjectivity, the complexity of the wound healing process itself, and patient variability (Dargaville et al., 2013).

Electromagnetic fields are physical phenomena (a field) that permeates through all of space. It arises from electrically charged objects and is one of the four fundamental forces of nature, which is found almost everywhere. All electromagnetic fields are force fields, carrying energy and capable of producing an action at a distance. These fields have characteristics of both waves and particles. This energy is utilized in various ways, though we still lack a full understanding of its fundamental properties. Many inventions of the late twentieth century, ranging from everyday home and office appliances to satellite systems and mobile phones, are so important and so advantageous, we wonder how we ever lived without them (R. Habash, 2007). Table 1.1 shows a few examples of electromagnetic field sources.



**Table 1.1 :** Typical sources of magnetotherapy (Markov, 2007).

Frequency range	Frequencies	Some examples of exposure sources
Static	0 Hz	MRI (medical imaging) and other diagnostic or scientific instrumentation
ELF [Extremely Low Frequencies]	0-300 Hz	PEMF are usually low-frequency fields with very specific shapes and amplitudes.
Radiofrequency range:	13.56, 27.12, and 40.68MHz	PRFE utilize the selected frequencies in the radiofrequency range:

Biological effects of magnetic fields are classified into three categories; the effects of (1) time-varying magnetic fields, (2) DC or static magnetic fields, and (3) multiplication of both static fields and other energy such as light and radiation. For each category, a different strategic approach is required to explain the biomagnetic effects. Time-varying magnetic fields produce eddy currents that stimulate excitable tissues at low frequencies. Biological effects of static magnetic fields have been poorly understood (Ueno, 1996).

Recently, several reports have evaluated effects of extremely low frequency electromagnetic fields (EMFs) on tissue repair (Pesce, Patruno, Speranza, & Reale, 2013). Present thesis focuses on determining the effect of PEMF and PRFE on skin wound healing, along with emerging details of the anti-inflammatory effects of EMFs.

## 1.2 Research Aims

Hug et al, 2012 have demonstrated the effectiveness of PEMF in healing soft-tissue wounds non-union bone fractures and there are many PEMF products as an adjuvant therapy. However, this therapy still has some clinical implementation problems.

To overcome these situations, interaction of EMF with biological tissues should be elaborated and simulate this process. So choosing the best parameters will be easier. The main aim of this study is to design a practical or clinical device that can be used to accelerate wound healing by low frequency electromagnetic fields.

Research aims for this thesis can be presented in the following manner:

- Design of applicators for PRFE applications that have higher performance, versatility and directivity features.
- Fabrication of PEMF coil with 75 Hz frequency and square waveform has been produced to obtain the best interaction with biological tissue,
- In Vitro test of designed system,
- Design of a functional and high beneficial device designed which may be a great potential method of treatment in the world.

### **1.3 General Objective**

The general objective of this research is to investigate the effects of pulsed electromagnetic field (PEMF) on wound healing. This investigation consists of: a) Simulation of applicators b) Simulation of biological models with applicators c) Experimental system design and d) Experimental evaluation.

### **1.4 Specific Objective**

A wide range of studies has shown that the application of PEMF can promote cell proliferation, increase the rate of healing, reduces pain and swelling. However, future advances in wound healing needs to emphasize methods that has influence on the repair processes of damaged tissue.

Up to date, researchers have used PEMF stimulators to promote healing, with the results varying significantly and there are discrepancies between the usages of PEMF parameters. Most of the exposure systems for studying PEMF effects on biological samples utilize electric coils to generate electromagnetic exposures. A uniform field can be obtained using antenna/applicator. In this respect, the objectives of the study;

- Design of high performance, easily integrated, biocompatible applicators,
- Development of portable device that could be used for chronic wound healing and pain management.
- To set adjustable frequency and waveform depending on different applications.
- Evaluate two different signal types that are PEMF (up to 300 Hz) and PRFE (27.12 MHz) therapy obtions.

## **1.5 Thesis Organization and Description of Contributions**

To document the details of this research, this thesis is divided into six sections:

Chapter 1 presents an introduction to the research. This preamble includes research aims, and objectives. It also presents the motivating factors behind undertaking this study and briefly outlines the approach taken towards the aim of outcome of this particular research.

Chapter 2 lays focus on the literature reviews and essential understanding of PEMF devices; its application, characterization and major limitations pertaining to experiments concerning PEMF and PRFE exposure on biological samples. Conducted literature survey also discuss the process of wound healing, conventional methods of treating wound, and their conventional treatment methods and limitations.

Chapter 3 presents a summary of electromagnetic fields and wave equation. A brief theoretical analysis of the systems configuration has been documented.

Chapter 4 provides the design and development of the PEMF system based on a core Helmholtz coil configuration capable of producing a uniform time varying magnetic field (magnetic flux density, 0.5–5 mT over the frequency range,  $f$ , 1-300Hz) and PRFE system built on the antenna/applicator. CST simulation program was used to evaluate the induced electric and magnetic field distribution and their region of uniformity is provided. Theoretical and experimental results.

Chapter 5 reports the PEMF and PRFE system measurements and the performance parameters of proposed applicators. Some applications of the lab built PEMF and PRFE systems by studying the effect of varying parametric changes on wound healing are given. Concerned materials and methodology are presented. A comparative analysis of change in the wound healing process of the exposed and unexposed biological tissue for selected frequencies and magnetic flux densities is provided. Results reveal that wound healing can be accelerated at particular frequencies for PEMF for magnetic flux density of 1 mT.

Chapter 6 presents a summary of the research contribution and provides suggestions to future works. This section is rounded up by a list of peer-reviewed publication yielding form this research project.

## **2. LITERATURE REVIEW AND BACKGROUND UNDERSTANDING**

### **2.1 Overview**

Electromagnetic fields at all frequencies are one of the most common environmental issues and there is a growing concern and speculation. All populations are now exposed to varying degrees of EMFs, and the levels will continue to increase as technological inventions advance which have become an integral part of our modern life (R. Habash, 2007).

The aim of this thesis is to introduce EMF interactions and applications, and focus on biological effects, aiming for breakthrough, new discoveries and innovative biomedical technologies. This covers a frequency range from 0 Hz to about 300 Hz and 27.12 MHz carrier frequency. Biological effects of EMFs are discussed in this chapter to present the current hypothesis on impact and mechanism of PEMF for wound healing purpose. PEMF therapeutic systems are discussed in greater details in particular the advantages of using such systems for promotion of wound healing. The design and constructed prototype of the PEMF system are presented along with their characterization. Special attention was given to the output module of the PEMF system (treatment coils system/applicator) for reasons made apparent through this literature review. Key concepts revolving around wound healing (types, process, and treatment methods) for both normal and infected wounds are explained in considerable details.

### **2.2 EMF Biological Effects**

The basic question in biomagnetism is to know the range of waveform parameters which recognized by cells for a given signal type (Behari, 2009). The mechanisms of these interactions and the possibility of the signals to modulate cell and tissue functioning remain to be unclear (Singh & Kapoor, 2015). The scientific and medical communities still lack of understanding why the same magnetic fields applied to different tissues can cause different effects (Hug & Rössli, 2012a).

The medical part of the equation requires proper diagnostics and identification of the exact target as well as the “dose” of EMF that the target needs to receive. Then, physicists and engineers should offer the appropriate protocol and exposure system that will secure that the target tissue received the required magnetic flux density. Therefore, theoretical models and biophysical dosimetry could be instrumental in selection of the appropriate signals for engineering and clinical application of new PEMF therapeutic devices. Historically, the largest benefit from magnetic field therapy has been reported for victims of musculoskeletal disorders, wounds, and pain (Trock, 2000). Today, the largest interest in public is in the potential of EMF to help in the alleviation of pain. The National Institute of Health estimates that more than 48 million Americans suffer chronic pain that results in a \$65 billion loss of productivity and over \$100 billion spent on pain care (Harden et al., 2007). The better part of this money is spent for pain-relief medications with little benefit. It should be noted that the musculoskeletal disorders, related to bone fractures and chronic wounds, remain another large target for magnetic/electromagnetic field therapy. Recent advances in the magneto therapy suggest that carefully selected magnetic fields may be helpful for treatment of diseases such as Parkinson’s, Alzheimer’s, as well as Reflex Sympathetic Disorders for which contemporary medicine has little help to offer (Fleming & Bauer, 2014). Thus, the clinical effects of PEMF often constitute the method of choice when all conventional care has failed to produce adequate clinical results.

It should be pointed out that for the majority of pharmaceutical treatments administered medication spreads over entire body, thereby causing adverse effects in different organs, which sometimes should be significant (Pirmohamed et al., 2004). One should not forget that in order to deliver the medication dose needed to treat the target tissue/organ; patients routinely receive medication doses that may be hundreds of times larger than the dose needed by the target. Compared to regular pharmaceuticals, PEMF offers an alternative with fewer, if any, side effects.

### **2.3 Possible PEMF/PRFE Mechanisms**

A large body of literature deals with biological effects of extremely low-frequency magnetic fields (ELF MFs) have been studied *in vitro*. Despite the multitude of studies, no coherent picture has evolved regarding the plausibility of effects at low-flux densities or regarding the interaction mechanisms. .

The proposed EMF signal transduction pathway relevant to tissue maintenance, repair and regeneration, begins with voltage-dependent  $\text{Ca}^{2+}$  binding to calmodulin (CaM), which is driven by increase in cytosolic  $\text{Ca}^{2+}$  concentrations in response to chemical and/or physical insults (including EMF itself) at the cellular level. Calcium binding to CaM activates CaM (CaM\*) which subsequently binds to and activates cNOS (cNOS\*) thus catalyzing the synthesis of the signaling molecule NO from L-arginine. This pathway is shown in its simplest schematic form in Figure 2.1. The proposed mechanism does not imply a direct EMF effect on the level of free cytosolic  $\text{Ca}^{2+}$  or on the activity of voltage-gated  $\text{Ca}^{2+}$  channels, but rather, an EMF effect on voltage-dependent  $\text{Ca}^{2+}$  binding to CaM, following the original proposal of the ECM model.

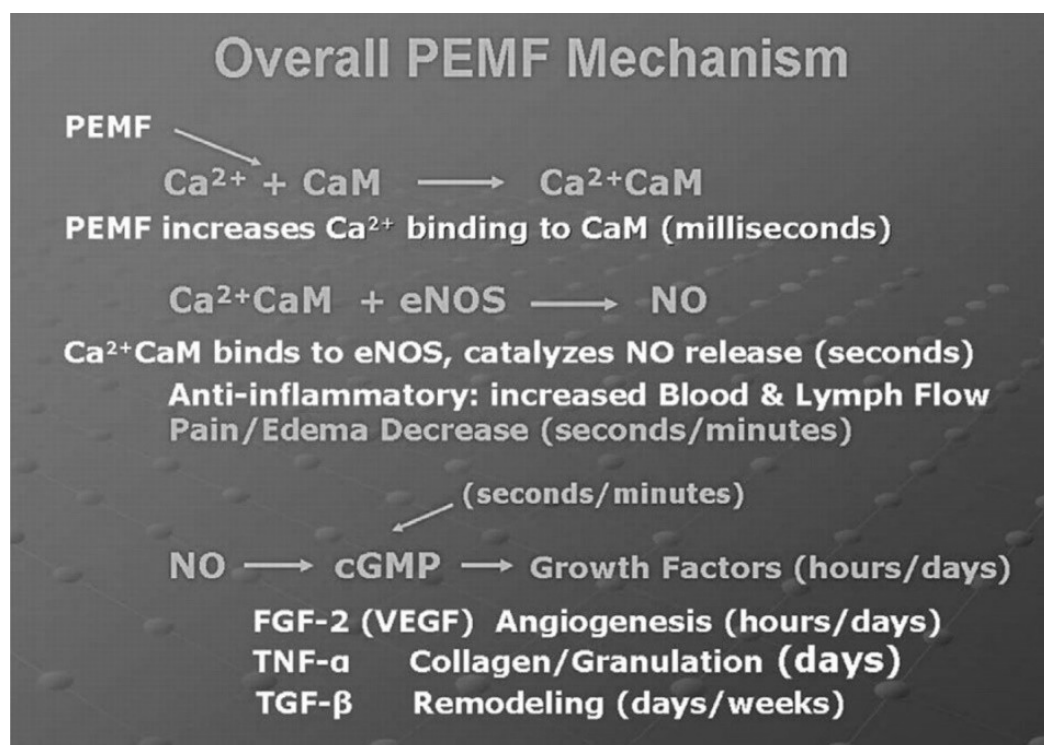


**Figure 3.1:** Pulsed electromagnetic field (PEMF) mechanism

Pulsed electromagnetic field (PEMF) transduction mechanism based on evidence to date that many athermal PEMF effects depend upon nitric oxide cascades. PEMFs can be configured to modulate calcium-binding kinetics to calmodulin. Calcium/calmodulin then activates nitric oxide synthase and the relevant cascade ensues dependent upon stage of tissue repair process. This mechanism has been proposed as a working.

One of the biological end points that have been frequently investigated is the oxidative status of the biological system. That it is reasonable to assume that early responses to

external stressors involve changes in oxidative homeostasis, discussed in several recent reviews. Possible lasting effects on the oxidative balance could affect a number of cellular processes in such a way that disease conditions can develop. In this context, extremely low-frequency magnetic field exposure consistently triggers oxidative responses in cultured mammalian cells. Taking the complexity of both the exposure situation (with various frequencies, waveforms, modulations, flux densities, presence of other MF, duration, exposure periodization, etc.) and the multitude of biological processes that are more or less relevant endpoints into consideration, it is clear that it is not necessarily easy to test this hypothesis. The hypothesis cannot be rejected due to that the majority of investigated studies showed positive effects, over a broad range of cell types, exposure durations, and flux densities (Wade, 2013).

Another important effect of PEMF is the ability of magnetic fields to restore “equilibrium in ROS (free radical)/antioxidant chemistry. One can consider that since both reactive oxygen species (ROS) free radicals such as superoxide anion ( $O_2^-$ ) and hydroxyl anion ( $OH^-$ ) are paramagnetic, they will be affected by a magnetic field. This forced vibration (similar to the effect on ions such as  $K^+$ ,  $Na^+$ ,  $Cl^-$ ,  $Ca^{2+}$ ) is thought to enhance the homeostasis between ROS and antioxidants. It is unequivocal that all chronic diseases result from a lack of homeostasis between free radicals and antioxidants. While both free radicals and antioxidants are normal and vital for processes such as cellular respiration and immunity, an imbalance could lead to cell and tissue death, DNA damage, and protein and fat degradation (Gordon, 2007).

### 3. ELECTROMAGNETIC FIELDS AND WAVE EQUATIONS

#### 3.1 Objectives

This thesis is deal with the effects of electromagnetic fields on biological systems. However, in the literature there exists a lack of the theoretical calculation and simulation on interaction of electromagnetic field with biological media. The source of the external electromagnetic stimulus are electric fields and magnetic fields. It has been observed that a series of parameters such as pulse waveform and frequency should be carefully chosen in order to achieve effective treatments. The objective of this chapter is to make progress in the area of bioelectromagnetics by analytic solution of wave equation with biological media.

#### 3.2 Electric Fields

Electromagnetic fields can be viewed as the combination of an electric field and a magnetic field. Electric field  $\vec{E}$  exists whenever electric charges are present, which means, whenever electricity is in operation or when positive and negative charges are separated. The basic unit for  $\vec{E}$  field is newton per coulomb (N/C), which is dimensionally equivalent to volts per meter (V/m). Electric fields could be represented graphically by two ways as shown in Figure 3.1. The first way shows the  $\vec{E}$  field due to a single point charge where the arrows indicate the direction of the field, and its magnitude is higher near the charge but decreases while going away from the charge (Figure 3.1a). The second way shows the  $\vec{E}$  field produced by two uniform sheets of charge representing a parallel-plate capacitor (Figure 3.1b). Several  $\vec{E}$  field lines originate from positive charges and terminate on negative charges. The  $\vec{E}$  field is uniform near the center of the conducting sheets and it bends (fringes) around the edges.



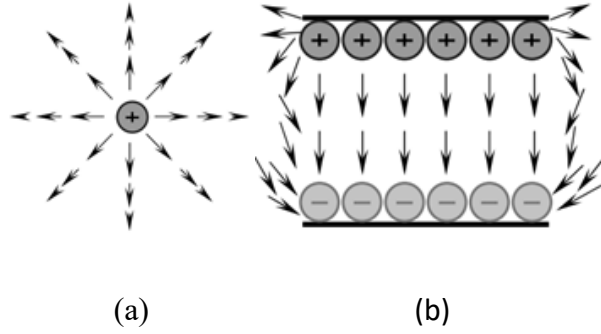


**Figure 3.1:** (a) Electric field lines due to a single point charge. (b) Electric field produced by two uniform sheets of charge.

Electric flux density or electric displacement, denoted as  $\vec{D}$ , is a measure of the  $\vec{E}$  field in terms of equivalent charge per unit area. The unit for  $\vec{D}$  is coulombs per square meter ( $C/m^2$ ).  $\vec{D}$  in a dielectric medium (e.g., biological tissues) is directly proportional to  $\vec{E}$ , as represented by the following equation:

$$\vec{D} = \epsilon \vec{E} \quad (3.1)$$

where  $\epsilon$  is the permittivity of the dielectric medium in farads per meter (F/m). The term permittivity refers to a fundamental property of the dielectric medium. It may be defined as the electric flux density per unit of electric field intensity within the medium. Basically, dielectric material is an insulating material. Generally, three different quantities describe the permittivity of the medium:  $\epsilon$ ,  $\epsilon_0$ , and a dimensionless quantity known as the relative permittivity  $\epsilon_r$  or the dielectric constant, which is defined as the permittivity relative to that of free space. The three quantities are related by the following equation:

$$\epsilon = \epsilon_0 \epsilon_r \quad (3.2)$$

The relative permittivity of free space is  $\epsilon_r = 1$ . This value is assumed for air in most applications. Values of dielectric constant for most biological materials range from 1 to about 80 or so.  $\vec{D}$  and  $\vec{E}$  are vectors with the same direction. This is real for all isotropic media, i.e., media whose properties do not depend on direction. The quantities  $\vec{E}$  and  $\vec{D}$  establish one of two key pairs of electromagnetic fields. The other pair consists of magnetic fields (R. Habash, 2007).

### 3.3 Magnetic Fields

The  $\vec{E}$  field was explained by means of force between charges that act on a line between the charges. With the movement of charges, another kind of force is exerted on one another along the line between the charges. This force stands for the magnetic field intensity, denoted as  $\vec{H}$ , which is a vector quantity created due to moving charges in free space or within conductors. Magnetic fields run perpendicular to the electric current. This means, while electric current runs in a straight line, magnetic fields surround the line in a circular fashion as shown in Figure 3.2. They control the motion of moving charges. The unit of magnetic field is amperes per meter (A/m). If we have direct current (DC), the magnetic field will be steady, like that of a permanent magnet. If we have alternating current (AC), the magnetic field will fluctuate at the same frequency as the E field does and it becomes an electromagnetic field, because it contains both  $\vec{E}$  and  $\vec{H}$  fields. Table 3.1 shows characteristics of these fields.

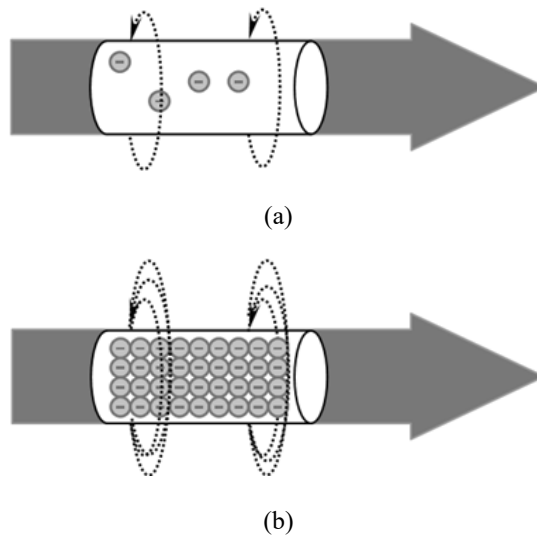


**Figure 3.2:** Magnetic field lines around a current-carrying conductor: (a) Less current flow. (b) Increased current flow.

Significant magnetic fields emanate from sources such as transmission and distribution lines, substations, transformers, network protectors, feeders, switch gears, distribution busways, electric panels, wiring systems, motors, and various electric appliances. Magnetic fields may easily penetrate materials, including people, buildings, and most metals. They are not shielded by most common materials and pass easily through them (R. W. Y. Habash, 2001).

When magnetic field penetrates a cross-sectional area of a medium, it is converted to magnetic flux density  $\vec{B}$ . It is related to  $\vec{H}$  via the vector relation

$$\vec{B} = \mu \vec{H} \quad (3.3)$$

where  $\mu$  is the permeability of the medium. The term permeability refers to the magnetic property of any material. It is a measure of the flux density produced by a magnetizing current. The basic unit of permeability is henries per meter (H/m). Three different quantities describe the permeability of the medium:  $\mu$ ,  $\mu_0$ , and a dimensionless quantity known as the relative permeability  $\mu_r$ , which is defined as the permeability relative to that of free space. The three quantities are related by

$$\mu = \mu_0 \mu_r \quad (3.4)$$

The relative permeability of free space is  $\mu_r = 1$ . The traditional unit of magnetic flux density  $B$  is webers per square meter (Wb/m<sup>2</sup>) (a weber is the same as a volt-second). It is usually measured in tesla (T), named after Nikola Tesla, or in gauss (G), named after Karl Friedrich Gauss, the nineteenth-century German pioneer in magnetism. In the United States, magnetic field is generally measured in CGS units; Oersted (Oe) and Gauss (G). In most of the rest of the world, it is measured in tesla (T). Since most extremely low frequency (ELF) environmental exposures involve magnetic field intensities that are only a fraction of teslas or gauss, the commonly used units for measurements are either microteslas ( $\mu$ T) or milligauss (mG). The following conversions may assist when dealing with units:

$$1 \text{ G} = 10^{-4} \text{ T}$$

$$1 \text{ T} = 1 \text{ Wb/m}^2$$

$$0.1 \mu\text{T} = 1 \text{ mG}$$

The magnetic flux  $\Phi$  (in webers) linking the surface  $A$  is defined as the total magnetic flux density passing through  $A$ . Figure 3.3 shows that  $\vec{B}$  is perpendicular to the area.

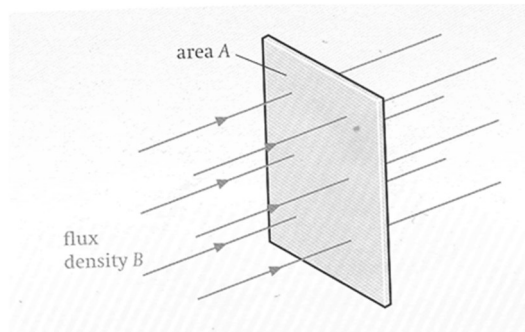


**Figure 3.3:** Magnetic flux density  $\vec{B}$  emerging from an area  $A$ .

The magnetic flux,  $\Phi$ , is then defined as the integral of the flux density over some surface area. For the simplified (but often useful) case of magnetic flux lines perpendicular to a cross-sectional area  $A$ , we can see that the flux is given by the following integral (Goswami, 2004):

$$\Phi = \int_A \vec{B} \cdot d\vec{A} \quad (3.5)$$

**Table 3.1:** Characteristics of electric and magnetic fields.

<b>Electric fields</b>	<b>Magnetic fields</b>
1. Electric fields arise from voltage	1. Magnetic fields arise from current flows.
2. Their strength is measured in volts Per meter (V/m).	2. Their strength is measured in amperes per meter (A/m). Commonly emf investigators use a related measure flux density in microtesla ( $\mu\text{T}$ ) or millitesla (mT) instead.
3. An electric field can be present even when a device is switch off.	3. Magnetic fields exist as soon as a device is switch on and current flows.
4. Field strength decreases with distance from the source.	4. Field strength decreases with distance from the source.
5. Most building materials shield electric fields to some extent.	5. Magnetic fields are not attenuated by most materials.

### **3.4 Electromagnetic Field (EMF) Radiation**

Electromagnetics is the study of the electric and magnetic phenomena caused by electric charges at rest or in motion. A time-varying electric field is accompanied by a magnetic field, and vice versa. In other word, time-varying electric and magnetic fields are coupled, resulting in an electromagnetic field. Under certain conditions, time-dependent electromagnetic fields produce waves that radiate from the source (Cheng, 1993). The study of electromagnetics includes both theoretical and applied concepts.

The theoretical concepts are described by a set of basic laws formulated primarily through experiments conducted during the nineteenth century by many scientists; Faraday, Ampere, Gauss, Lenz, and others. They were then combined into a consistent set of vector equations by Maxwell. These are the widely acclaimed Maxwell's equations. The applied concepts of electromagnetics are formulated by applying the theoretical concepts to the design and operation of practical systems.

### **3.5 Maxwell's Equations**

In general, electric and magnetic fields are vector quantities that have both magnitude and direction. The relations and variations of the electric and magnetic fields, charges, and currents associated with electromagnetic waves are governed by physical laws, which are known as Maxwell's equations. These equations, as we have indicated, were arrived at mostly through various experiments carried out by different investigators, but they were put in their final form by James Clerk Maxwell, a Scottish physicist and mathematician. These equations can be written either in differential or in integral form, see in table 3.2 (Balanis, 2012).

**Table 3.2:** Maxwell's equations and the continuity equation in differential and integral forms for time-varying fields.

Differential form	Integral form
$\vec{\nabla}_x \vec{E} = -\vec{M}_i - \frac{\partial \vec{B}}{\partial t}$ (3.6)	$\oint_c \vec{E} \cdot d\vec{l} = -\iint_s \vec{M}_i \cdot d\vec{s} - \frac{\partial}{\partial t} \iint_s \vec{B} \cdot d\vec{s}$ (3.7)
$\vec{\nabla}_x \vec{H} = \vec{j}_i + \vec{j}_c + \frac{\partial \vec{D}}{\partial t}$ (3.8)	$\oint_c \vec{H} \cdot d\vec{l} = \iint_s \vec{j}_i \cdot d\vec{s} + \iint_s \vec{j}_c \cdot d\vec{s} + \frac{\partial}{\partial t} \iint_s \vec{D} \cdot d\vec{s}$ (3.9)
$\vec{\nabla} \cdot \vec{D} = q_{ev}$ (3.10)	$\oiint_s \vec{D} \cdot d\vec{s} = Q_e$ (3.11)
$\vec{\nabla} \cdot \vec{B} = 0$ (3.12)	$\oiint_s \vec{B} \cdot d\vec{s} = 0$ (3.13)
$\vec{\nabla} \cdot \vec{j}_{ic} = -\frac{\partial q_{ev}}{\partial t}$ (3.14)	$\oiint_s \vec{j}_{ic} \cdot d\vec{s} = -\frac{\partial}{\partial t} \iiint_v q_{ev} \cdot dv = -\frac{\partial Q_e}{\partial t}$ (3.15)

All these field quantities “ $\vec{E}$ ,  $\vec{H}$ ,  $\vec{D}$ ,  $\vec{B}$ ,  $\vec{j}$ ,  $\vec{M}_i$ ,  $\vec{j}_{ic}$ , and  $q_v$ ” are assumed to be time-varying, and each is a function of the space coordinates and time, that is,  $\vec{E} = \vec{E}(x, y, z; t)$ . The definitions and units of the quantities are

$\vec{E}$  = electric field intensity (volts/meter)

$\vec{H}$  = magnetic field intensity (amperes/meter)

$\vec{D}$  = electric flux density (coulombs/square meter)

$\vec{B}$  = magnetic flux density (webers/square meter)

$\vec{j}_i$  = impressed (source) electric current density (amperes/square meter)

$\vec{j}_c$  = conduction electric current density (amperes/square meter)

$\vec{j}_{ic}$  = the variations of the current density

$\vec{M}_i$  = impressed (source) magnetic current density (volts/square meter)

$q_{ev}$  = electric charge density (coulombs/cubic meter)

### 3.6 Wave Equations

Equations (3.16) and (3.17) are a set of coupled equations both containing electric and magnetic field quantities. In a medium with finite electrical conductivity  $\sigma$ , a conduction current density  $\vec{j} = \sigma \vec{E}$  will exist and this will give rise to energy loss to Joule heating. The wave equations in media of this type have a loss term (Zhang & Li, 2013),

$$(\nabla^2 + \omega^2 \mu \epsilon - j \omega \mu \sigma) \vec{E} = 0 \quad (3.16)$$

$$\left( \nabla^2 + \omega^2 \mu \epsilon - j \omega \mu \sigma \right) \vec{H} = 0 \quad (3.17)$$

### 3.7 Radio and Microwave Dielectric Properties of Biological Materials

Dielectric properties of tissue materials have been extensively studied (Duck, 2013). A basic understanding has been achieved on the mechanisms and structures that determine the electromagnetic properties of tissue materials. It has been demonstrated that tissue materials are nearly nonmagnetic, and thus have permeabilities close to that of free space and are independent of frequency. On the other hand, the electrical properties of tissue materials have been shown to display a characteristic dependence on frequency. They possess very high dielectric constants compared with many other types of homogeneous liquids and solids. Biological tissues are a mixture of water, ions, and organic molecules organized in cells, sub-cellular structures, and membranes, and its dielectric properties are highly frequency-dependent in the range from Hz to GHz. The spectrum is characterized by three main dispersion regions referred to as  $\alpha$ ,  $\beta$ , and  $\gamma$  regions at low, intermediate, and high frequencies. Biological materials can show large dispersions, especially at low frequencies (Figure 3.4). Low frequencies are mainly caused by interfacial polarizations at the surfaces between the different materials of which a cell is composed. Reviews of the dielectric properties of cells and the different dispersions are given in the literature (Hilger et al., 2013).

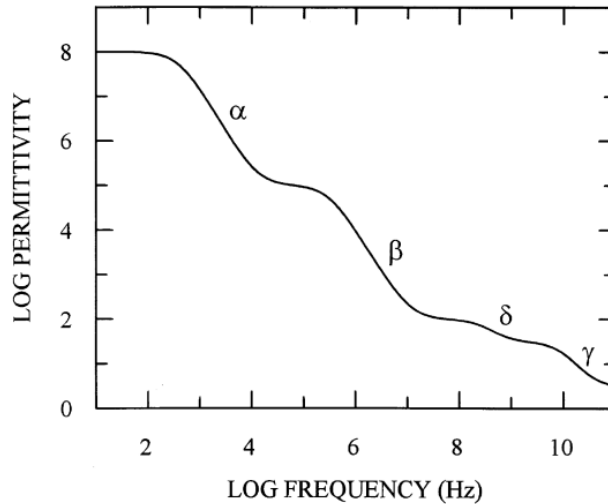


**Figure 3.4:** Spectrum of the dielectric properties of cell suspensions and tissues.

When the dipole distribution is uniform, the positive charges of one dipole cancel the effect of the negative charge from an adjacent dipole. But when the dipole distribution changes from point to point, this complete cancellation cannot occur. At an interface especially, the ends of the dipoles leave an uncancelled charge on the surface, which becomes an equivalent "bound" charge in the material. The relaxation behaviour may therefore be examined by considering the response of bound charges in an applied electric field. For the model shown in Figure 3.5, the dynamic force equation is

$$m \frac{d^2x}{dt^2} = q\vec{E} - m\omega_s^2x - m\xi \frac{dx}{dt} \quad (3.18)$$

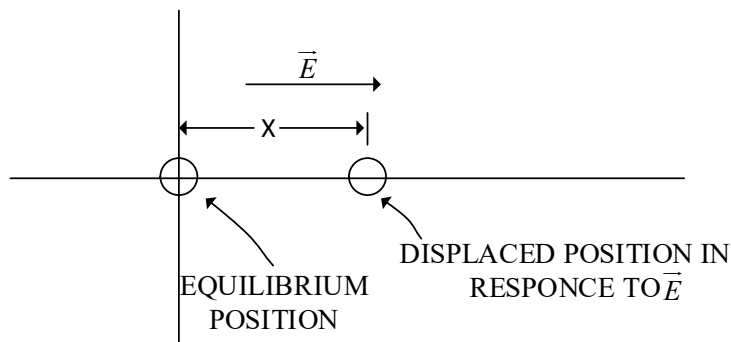


**Figure 3.5:** Behavior of bound, charged particle in an applied electric field.



where  $x$  is the particle displacement,  $\bar{E}$  is the electric field, and  $q$  and  $m$  are the particle charge and mass, respectively. The force given by mass times particle acceleration, on the left-hand side of the equation, consists of the electric driving force  $q\bar{E}$ , an elastic restoring force proportional to displacement  $x$  with spring constant conveniently denoted as  $m\omega_s^2$ , and a retarding damping force proportional to velocity  $dx/dt$  with damping constant  $m\xi$ . The spring and damping constants are chosen in this notation because  $\omega_s$  is the characteristic frequency of the spring-mass system and  $\xi$  is the particle collision frequency.

If the field varies harmonically in time ( $e^{j\omega t}$ ), (3.18) may be rearranged to give

$$x(\omega) = \frac{(q/m)/E}{\omega_s^2 - \omega^2 + j\omega\xi} \quad (3.19)$$

A dipole moment  $\bar{p}$  of charge  $q$  times the displacement  $x$  is formed. For a medium with volume-bound charge density  $\rho$ , the total dipole moment per unit volume or polarization  $\bar{P}$  is

$$\bar{P} = \rho\bar{p} = \frac{\rho(q^2/m)E}{\omega_s^2 - \omega^2 + j\omega\xi} \quad (3.20)$$

The electric flux density  $\bar{D}$  may be expressed in terms of the electric field  $\bar{E}$  and polarization  $\bar{P}$  as  $\bar{D} = \epsilon_0\bar{E} + \bar{P}$ . For isotropic media the permittivity  $\epsilon$  may be related to  $\bar{D}$  by the expression  $\bar{D} = \epsilon\bar{E}$ . These relations, together with (3.20), give an expression for the permittivity,

$$\epsilon = \epsilon_0 \left( 1 + \frac{\omega_p^2}{\omega_s^2 - \omega^2 + j\omega\xi} \right) \quad (3.21)$$

Where  $\omega_p^2 = \rho q^2 / m\epsilon_0$  and  $\epsilon_0$  is the free-space permittivity. Clearly  $\epsilon$  is a complex number and can be denoted by

$$\epsilon = \epsilon' - j\epsilon'' \quad (3.22)$$

where  $\epsilon'$  and  $\epsilon''$  are the real and imaginary parts of the permittivity and can be obtained by equating the real and imaginary parts of (3.21) and (3.22).

The velocity of bound charge motion  $v = dx / dt$  is obtained from (3.19):

$$\vec{v}(\omega) = \frac{(q/m)\vec{E}}{\xi - j[(\omega_s^2 - \omega^2)/\omega]} \quad (3.23)$$

The finite velocity of charge motion in the material indicates that the particles cannot respond instantaneously to a suddenly applied electric field. This time-delay phenomenon gives rise to a frequency-dependent behaviour of charge displacement leading to changes in permittivity with frequency or relaxation. Relaxation is exhibited by all biological tissues and many physical materials. In what follows, the general development will focus on two classes of dielectric materials of interest to the biophysical aspects of electromagnetic interaction with biological systems.

### 3.8 Low-Loss Dielectric Materials

For low-loss dielectric materials characterized by low collision frequency,  $\xi$ ,  $\epsilon'$  and  $\epsilon''$  can be easily derived from (3.21) where  $\omega \neq \omega_s$ .

$$\epsilon' / \epsilon_0 = 1 + \left[ \omega^2 / (\omega_s^2 - \omega^2) \right] \quad (3.24)$$

$$\epsilon'' / \epsilon_0 = \omega \xi \omega_p^2 / (\omega_s^2 - \omega^2)^2 \quad (3.25)$$

A graphical representation of this result is shown in Figure 3.6. The real part of the permittivity is usually high at low frequencies, increasing to extremely high values at the characteristic frequency  $\omega_s$  and then returning to  $\epsilon_0$  at higher frequencies. The imaginary part of the permittivity is small at all frequencies except near  $\omega_s$ . It is high there because of the large particle displacement at the characteristic frequency (Michaelson & Lin, 1987), giving rise to large collisional and thus absorption effects.

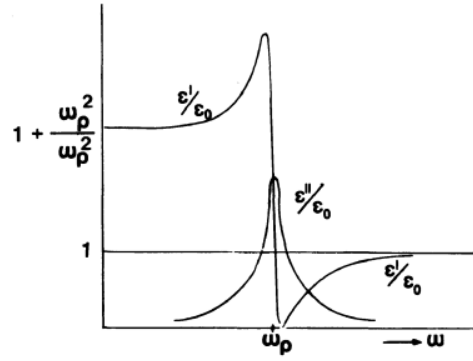


**Figure 3.6:** Frequency permittivity associated with low-loss dielectric materials.

For most solid dielectric materials of practical interest to microwave biophysics (e.g., Plexiglas), the frequency  $\omega_s$  is in the optical spectrum or above. They are thus characterized by low loss and slowly increasing dielectric constant with frequency.

### 3.9 Lossy Dielectrics at Low Frequencies

At frequencies low compared to the characteristic frequency ( $\omega \ll \omega_s$ ), (3.21) reduces to

$$\frac{\epsilon}{\epsilon_0} = 1 + \frac{\omega_p^2 / \omega_s^2}{1 + j\omega\xi / \omega_s^2} \quad (3.26)$$

This equation may be expressed in terms of the permittivity at zero frequency,

$$\epsilon(0) = \epsilon_0 \left(1 + \omega_p^2 / \omega_s^2\right) \quad (3.27)$$

and the permittivity at infinite frequency  $\epsilon(\infty) = \epsilon_0$ . Note that both these limiting values of complex permittivity are real numbers. Thus, (3.26) written in the Debye form becomes

$$\epsilon = \epsilon(\infty) + \frac{\epsilon(0) - \epsilon(\infty)}{1 + j\omega\tau} \quad (3.28)$$

where  $\tau = \xi / \omega_s^2$  is the relaxation time and is inversely related to the relaxation frequency  $\omega_r$ . In living matter it is impossible to separate the two contributions from measurements made at a given frequency. Therefore, the presence of a finite  $\epsilon'$  has the effect of producing a total electrical conductivity  $\sigma$ , and a finite conductivity is equivalent to a total imaginary part of the permittivity as  $\epsilon''$ . The relationship between  $\sigma$  and  $\epsilon''$  may be derived from two of Maxwell's equations, (3.6) and (3.8), or

$$\sigma = \omega \epsilon'' \quad (3.29)$$

where  $\sigma$ , an equivalent conductivity representing all losses, is given by

$$\sigma = \frac{\omega^2 \tau [\epsilon(0) - \epsilon(\infty)]}{1 + (\omega \tau)^2} \quad (3.30)$$

It is also convenient to define a relative dielectric constant by dividing  $\epsilon'$  by the free-space permittivity  $\epsilon_0$ :

$$\epsilon_r = \epsilon' / \epsilon_0 \quad (3.31)$$

### 3.10 Biological Materials

The dielectric properties of tissue materials are complex and require a distribution of relaxation processes for representation throughout the radio and microwave frequency region. In this case, the dielectric behaviour may be modelled as a sum of relaxation processes, with each process being a non-instantaneous exponential relaxation from one state to another. The corresponding responses in the frequency domain are of the form

$$\epsilon = \epsilon_\infty + \sum_{n=1}^N \frac{\Delta \epsilon_n}{1 + j \omega \tau_n} \quad (3.32)$$

where  $\Delta \epsilon_n$  is the difference between the permittivity far below and far above the relaxation frequency, and  $\tau_n$  is the relaxation time associated with each relaxation process.

In general, the dielectric constant and conductivity of tissues with low water content are an order of magnitude lower than the corresponding values for tissues with higher water content. Figure 3.7 shows the average relative permittivity and conductivity of rat skin sample from 200 MHz to 20 GHz (Karacolak, Cooper, & Topsakal, 2009).

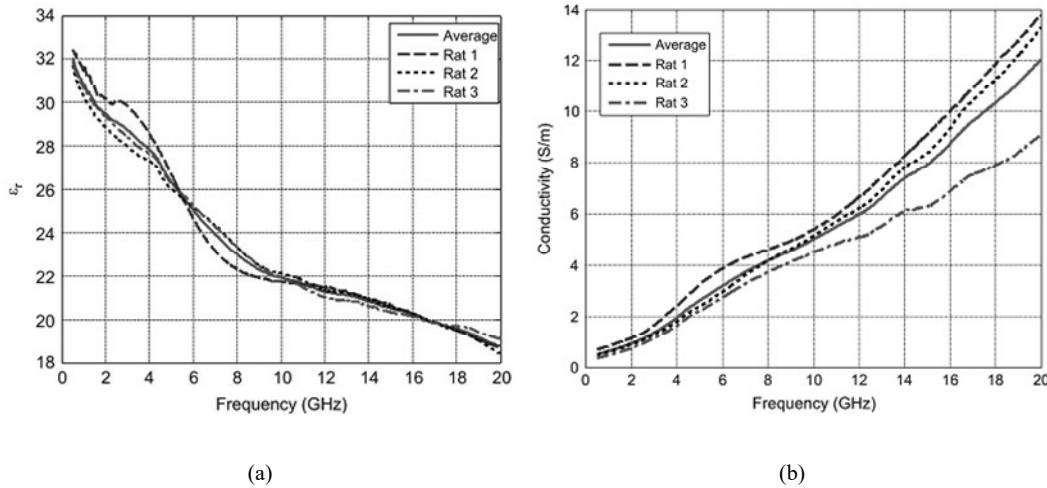


Figure 3.7: (a) Relative permittivity and (b) Conductivity of skin tissue samples from three rats (Karacolak et al., 2009).

The dielectric constants and conductivities for some other tissues with high water content are listed in Table 3.3.

**Table 3.3:** Dielectric constants and Conductivities of Select Tissues and Materials at 50 MHz (Michlovitz, Bellew, & Nolan, 2011).

Tissues/Materials	Dielectric Constants ( $\epsilon$ )	Conductivity ( $\sigma$ ) [S/m]
Blood	80	11.7
Muscle/Skin	85-100	0.7-0.9
Bone Marrow	7-8	0.02-0.04
Fat Tissue	11-13	0.04-0.06
Distilled Water	80	$2 \times 10^4$
Oil	2	$10^{11}$
Metals	-	$10^4$ - $10^7$

### 3.11 Propagation and Absorption in Tissue Media

The propagation of electromagnetic waves in biological materials is governed by the dielectric constant, conductivity, source configuration, and the geometrical factors that describe the tissue structure. These parameters also determine the quantity of energy a given biological body extracts from the propagating wave. When the radius of curvature of the body surface is large compared to the wavelength and beam width of

the impinging radiation, planar tissue models may be used to estimate the absorbed energy and its distribution inside the body. Otherwise, the absorbed energy will be dictated by the size of the body, the curvature of its surface, the ratio of body size to wavelength, and the source characteristics.

### 3.11.1 Multiple Layers of Tissue

When there are several layers of different tissues, the reflection and transmission characteristics become more complicated. Multiple reflections can occur between the skin and subcutaneous tissue boundaries, with a resulting modification of the reflection and transmission coefficients (Faktorová & Isteniková, 2011).

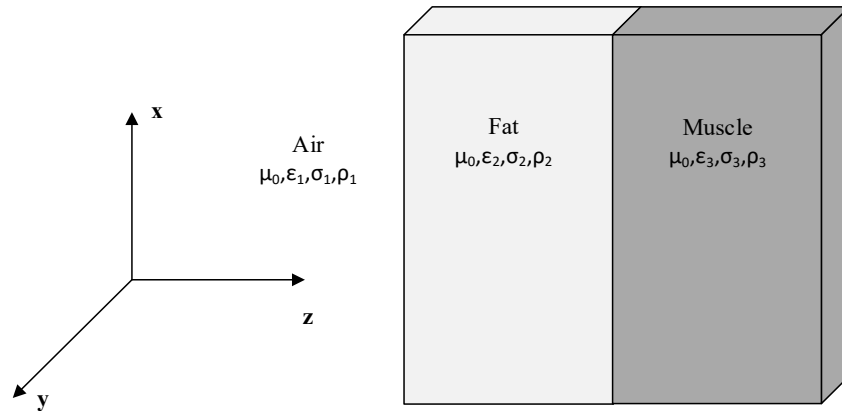


**Figure 3.8:** Plane wave impinging on a composite fat-muscle layer.

In general, the transmitted wave will combine with the reflected wave to form standing waves in each layer. This phenomenon becomes especially pronounced if the thickness of each layer is less than the penetration depth for that tissue medium. Plane waves impinging on the human body considered as consisting of parallel layers of subcutaneous fat and more deeply lying muscle have been studied. For the situation depicted in Figure 3.8, the electric field strength in the fat layer is given by

$$\vec{E}_f = F_1 \vec{E}_0 \left[ e^{-(\alpha_2 + j\beta_2)z} + R_{32} e^{(\alpha_2 + j\beta_2)z} \right] \quad (3.33)$$

and the electric field in the underlying muscle tissue is given by

$$\vec{E}_m = F_t \vec{E}_0 e^{-(\alpha_3 + j\beta_3)z} \quad (3.34)$$

where  $\alpha_2$ ,  $\beta_2$  and  $\alpha_3$ ,  $\beta_3$  are the attenuation and propagation coefficients in fat and muscle, respectively. The layer function  $F_1$  and the transmission function  $F_t$  are given by

$$F_1 = F_{12} / \left[ e^{-(\alpha_2 + j\beta_2)l} + R_{12}R_{32}e^{-(\alpha_2 + j\beta_2)l} \right] \quad (3.35)$$

$$F_t = T_{12}T_{23} / \left[ e^{(\alpha_2 + j\beta_2)l} + R_{21}R_{32}e^{-(\alpha_2 + j\beta_2)l} \right] \quad (3.36)$$

where  $T_{12}$  and  $T_{23}$  are the transmission coefficients at the air-fat and fat-muscle boundaries, respectively.  $R_{21}$  and  $R_{32}$  denote, respectively, the reflection coefficients at these boundaries;  $l$  is the thickness of the fat layer. The EM field computations are analytically done for air-fat-muscle three layer system with the frequency dispersive material parameters (Appendix A). The reflection coefficient and magnitude of electric field are shown in Figure 9 (a) for the fat thickness of 10mm and 28mm muscle thickness at six different frequencies. As shown in Figure 3.9 (b), the electric field penetrates into the fat and muscle layers at larger distances for the frequency of low reflection coefficient.

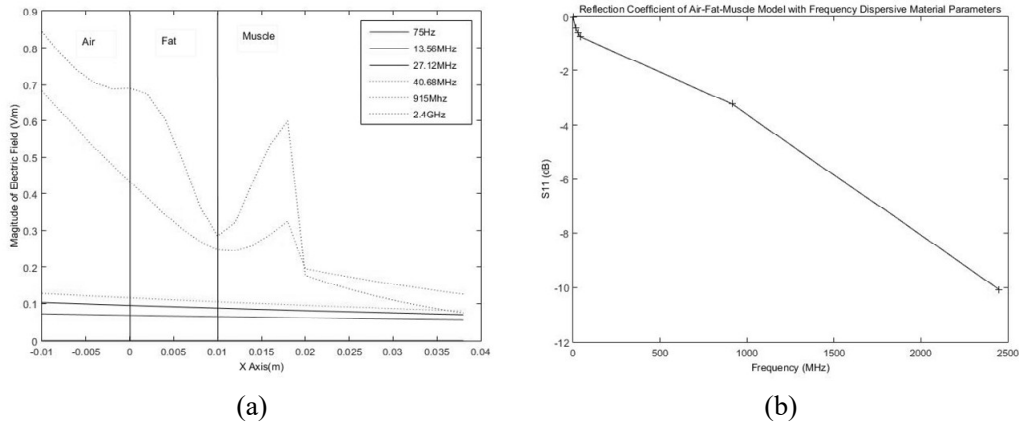


**Figure 3.9:** (a) Magnitude of E-Field (V/m) for air-muscle-fat layers. (b) Reflection coefficient of air-fat-muscle model with frequency dispersive material parameters.

### 3.11.2 Spherical Tissue Models

If the sphere is extremely small compared with a wavelength, the absorbed energy distribution becomes nearly uniform in the  $x$  and  $y$  directions but decreases continuously with distance from the exposed surface (see Figure 3.10). This behaviour can be explained by a quasi-static field theory. Accordingly, for a plane wave polarized in the  $x$  direction that propagates in the  $z$  direction, the induced electric field inside a dielectric sphere is given by (James C Lin & Michaelson, 2013).

$$\vec{E}_t = \vec{E}_0 e^{j\omega t} \left[ \frac{3}{\varepsilon} \hat{x} - j \frac{kr}{2} (\cos \phi \hat{\theta} - \cos \theta \sin \phi \hat{\phi}) \right] \quad (3.37)$$

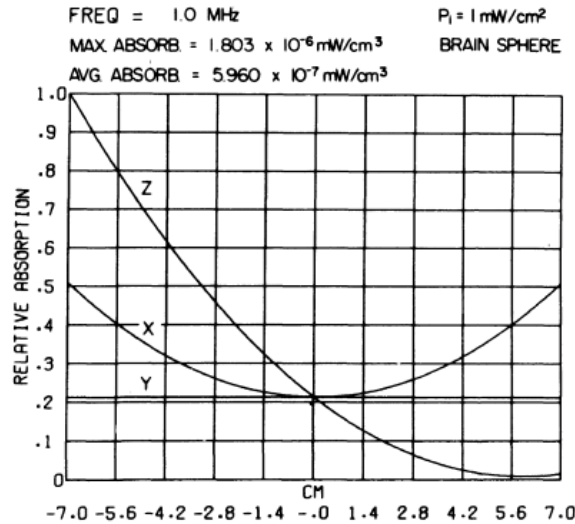
where  $\vec{E}_0$  is the strength of the incident electric field and  $r$  is the radial variable. The whole-body absorption rate is given by

$$P_a = \frac{1}{2} \sigma \vec{E}_0^2 V \left[ \frac{9}{|\varepsilon|^2} + \frac{1}{10} (ka)^2 \right] \quad (3.38)$$

where  $V$  and  $a$  are respectively the volume and radius of the spherical model.

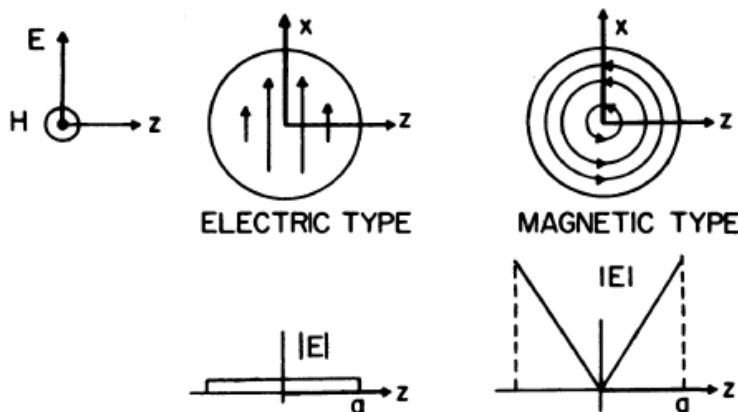
The electric field component of the incident plane wave couples to the object in the same fashion as an electrostatic field. This gives rise to a constant induced electric field inside the sphere that has the same direction but is reduced by  $3/\varepsilon$  from the applied electric field for biological materials and is independent of sphere size. Similarly, the magnetically induced electric field inside the body is identical to the quasi-static solution whose magnitude is given by  $\vec{E} = \pi f \mu r \vec{H}$ , where  $f$  is the frequency,  $\mu$  is the permeability,  $r$  is the radius, and  $\vec{H}$  is the magnetic field component. Thus, the magnetic field component of the incident plane wave produces an internal electric field that varies directly with distance away from the axis and in proportion to the frequency.





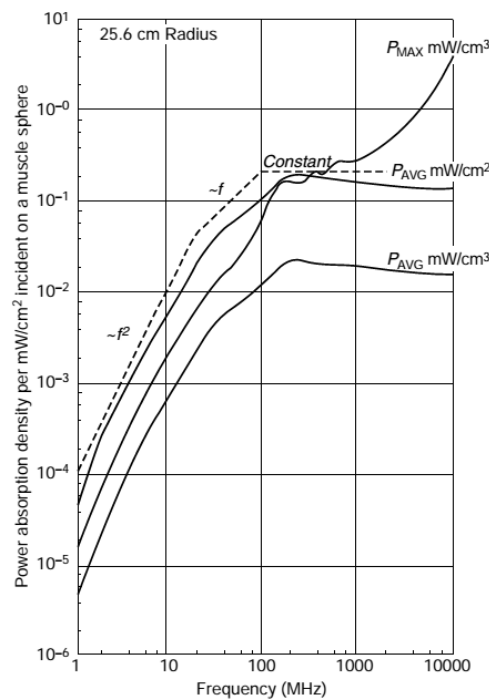
**Figure 3.10:** Predicted SAR distribution in a sphere whose size is extremely small compared to the wavelength. x, y, and z are the orthogonal coordinates of a rectangular system (James C Lin, Guy, & Johnson, 1973).

Figure 3.11 depicts how the induced electric fields combined inside the sphere. The magnetically induced electric field encircles the y axis (magnetic axis) and gives rise to an eddy current whose magnitude increases with distance away from the y axis. This indicates that while the H-induced energy absorption in a mouse or larger animal is much greater than the E-induced component, electrically and magnetically induced absorption may be equally significant in even smaller animals at lower frequencies (below 30 MHz). Moreover, for a small insect or pupa the electric field will be the predominant factor. The variation of average and maximum energy absorption with frequency for a human-size sphere is illustrated in Figure 3.12.



**Figure 3.11:** Diagrammatic representation of the behavior of electric and magnetic fields under quasi-static conditions of irradiation.

Inspection of the maximum absorption rate induced by a plane wave, a quasi-static electric field, and a quasi-static magnetic field shows that absorption in the frequency range 1-20 MHz is primarily due to the magnetic induction and is characterized by a square-of-frequency dependence. The approximate frequency dependence of average or total energy absorption throughout the frequency range 1 MHz-10 GHz is indicated by the dashed line. For frequencies between 1 and 20 MHz, the average absorption varies as the square of the frequency. In the frequency range 20-200 MHz, the average absorption increases directly in proportion to frequency and reaches a maximum of about  $2 \times 10^{-3}$  W/kg per W/m<sup>2</sup> of incident power at 200 MHz. The average absorption rate remains fairly constant with increasing frequency. (It actually is inversely proportional to frequency for higher frequencies.) There is thus little doubt that electromagnetic energy absorption varies both with frequency and with body size, and in a predictable manner (J.C. Lin & Michaelson, 2014).



**Figure 3.12:** Frequency dependence of absorption in a spherical model of the human body.

### 3.11.3 Prolate Spheroidal Tissue Models

Since the bodies of humans and experimental animals are seldom spherical, we need a more appropriate model to analytically and numerically describe the induced fields and absorbed energy inside experimental subjects. A prolate spheroid approaches more closely the shape of mammalian bodies, but most analyses have been restricted to homogeneous models for humans and experimental animals.

The induced electric fields inside a dielectric prolate spheroid ( $a$ , semi major axis;  $b$ , semi minor axis) in a plane wave electromagnetic field with long wavelength ( $\lambda > a$ ) may be represented by

$$\vec{E}_e = \frac{\vec{E}_0}{C_1} \hat{z} - j \frac{1}{2} E_0 \frac{\omega \mu_0}{377} (z \cos \phi \hat{\rho} - z \sin \phi \hat{\phi} - \rho \cos \phi \hat{z}) \quad (3.39)$$

for  $\vec{E}$  polarization and

$$\vec{E}_h = \frac{-\vec{E}_0 \hat{y}}{C_2} + \frac{1}{2} \vec{E}_0 \frac{\omega \mu_0 \rho \hat{\phi}}{377} \quad (3.40)$$

for  $\vec{H}$  polarization. The whole-body energy absorption rate is generally given by

$$P_a = \frac{1}{2} \sigma \int_{\text{volume}} \vec{E} \cdot \vec{E}^* dv \quad (3.41)$$

where  $\sigma = \omega \varepsilon_0 \varepsilon''$  is the electrical conductivity and  $\vec{E}^*$  denotes the complex conjugate of the induced field  $\vec{E}$  inside the body. The whole body rates of absorbed energy by substituting equations (3.39) and (3.40) into (3.41) are

$$P_{ae} = \frac{1}{2} \sigma \vec{E}_0^2 \left( \frac{4}{3} \pi a b^2 \right) \left[ \frac{1}{C_1^2} + \frac{1}{20} \left( \frac{\omega \mu_0}{377} \right)^2 (a^2 + b^2) \right] \quad (3.42)$$

For  $\vec{H}$  polarization the constant  $C_1$  is given by

$$C_1 = (1 - \varepsilon) \eta_0 \left[ (1 - \eta_0^2) \coth^{-1} \eta_0 + \eta_0 \right] + \varepsilon \quad (3.43)$$

### 3.12 Theory-Biot-Savart Law

The Biot–Savart law is used for computing the magnetic field ( $\vec{B}$ ) generated at some arbitrary point (P) by a steady current (i). It relates this incremental magnetic field, located a distance from an incremental length of wire, with the current flowing in the direction of the incremental length. It relates both the magnitude and direction of the magnetic field to the magnitude of the current, the magnitude and direction of the incremental length, and the distance from the increment of length to the point of interest. The magnetic field is calculated by summing up all the increments of B resulting from incremental lengths of current that produce the magnetic induction. The law is named for Jean-Baptiste Biot and Felix Savart, who first formulated this relationship in 1820. Using the principle of symmetry, the Biot-Savart law used in this study to determine the magnetic field strength as a function of distance along the axis of a single circular coil of wire carrying current I (Figure 3.13). The result used to determine the magnetic field of a pair of Helmholtz coils along their axis of symmetry

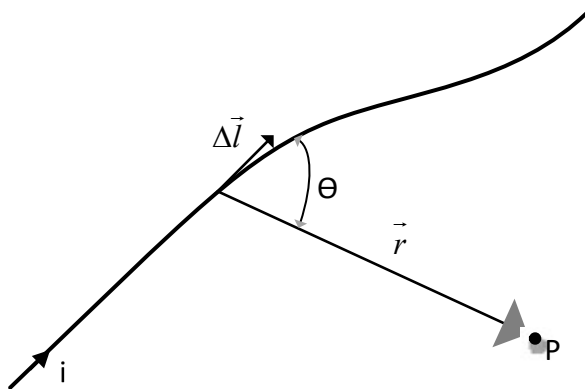


**Figure 3.13:** The incremental magnetic field strength,  $\Delta \vec{B}$ , at point P is given by the.

$$\text{Biot-Savart law, } \Delta \vec{B} = \frac{\mu_0 i}{4\pi} \frac{\Delta \vec{l} \sin \Theta}{r^2} \text{ or in vector form, } \Delta \vec{B} = \frac{\mu_0 i}{4\pi} \frac{\Delta \vec{l} \times \vec{r}}{r^3}$$

The Biot-Savart law can be better understood and applied by considering Figure 3.13, which depicts a randomly-shaped wire with a steady current i flowing in it. According to the Biot-Savart law, the magnetic field  $\Delta \vec{B}$  resulting from the current flowing in a small length of the wire  $\Delta l$  at some arbitrary distance r away is given by the equation

$$\Delta \vec{B} = \frac{\mu_0 i}{4\pi} \frac{\Delta l \sin \Theta}{r^2} \quad (3.44)$$

The vector  $\Delta \vec{B}$  can be resolved into parallel and perpendicular components with respect to the central axis along x using the unit vectors  $\hat{i}$  and  $\hat{j}$  so that

$$\Delta \vec{B} = \Delta B_{\parallel} \hat{i} + \Delta B_{\perp} \hat{j} \quad (3.45)$$

where  $\Delta \vec{B}_{\parallel}$  is a component along the x-axis and  $\Delta \vec{B}_{\perp}$  is a component perpendicular to the x-axis.  $\Delta \vec{B}_{\parallel}$  and  $\Delta \vec{B}_{\perp}$  are related to the magnitude of  $\Delta \vec{B}$ ,  $\Delta \bar{B}$ , by the following equations

$$\Delta \bar{B}_{\parallel} = \Delta \bar{B} \cos \alpha \quad (3.46)$$

and

$$\Delta \bar{B}_{\perp} = \Delta \bar{B} \sin \alpha \quad (3.47)$$

where  $\alpha$  is the angle between the plane of the loop and the vector from the line segment  $\Delta \vec{l}$  to point P.

The total magnetic field is then found by summing all the increments of  $\Delta \vec{B}$  for every increment of  $\Delta \vec{l}$  so that

$$\vec{B} = \sum \Delta \vec{B} = \sum \Delta B_{\parallel} \hat{i} + \sum \Delta B_{\perp} \hat{j} \quad (3.48)$$

Since the components  $\Delta \vec{B}_{\perp}$  are all equal and point in all directions, their sum will be zero so that

$$\vec{B}_{\perp} = \sum \Delta \vec{B}_{\perp} = 0 \quad (3.49)$$

This leaves

$$\vec{B} = \sum \Delta \bar{B}_{\parallel} \hat{i} \quad (3.50)$$

Substituting Equation (3.46) into Equation (3.50) and Equation (3.44) into the result yields

$$\vec{B} = \sum \Delta \bar{B}_{\parallel} = \sum \frac{\mu_0 i}{4\pi} \frac{\Delta \vec{l} \sin \theta}{r^2} \cos \alpha = \frac{\mu_0 i}{4\pi} \frac{\sin \theta}{r^2} \cos \alpha \sum \Delta \vec{l} \quad (3.51)$$

Since  $\theta = 90^\circ$  and  $r = \sqrt{R^2 + x^2}$ , then

$$\sin \theta = 1 \quad (3.52)$$

and

$$\cos \alpha = \frac{R}{\sqrt{R^2 + x^2}} \quad (3.53)$$

By making these substitutions, Equation (3.51) becomes

$$\vec{B} = \frac{\mu_0 i}{4\pi} \frac{1}{R^2 + x^2} \frac{R}{\sqrt{R^2 + x^2}} \sum \Delta \vec{l} = \frac{\mu_0 i}{4\pi} \frac{R}{(R^2 + x^2)} \sum \Delta \vec{l} \quad (3.54)$$

Since all the  $\Delta \vec{l}$ 's can be made arbitrarily as small as they need to be, their sum will equal the circumference of the circular coil and

$$\sum \Delta \vec{l} = 2\pi R \quad (3.55)$$

Inserting Equation (3.55) into Equation (3.54) produces the final result

$$\vec{B} = \frac{\mu_0 i}{4\pi} \frac{R}{(R^2 + x^2)^{3/2}} 2\pi R = \frac{\mu_0 i}{2} \frac{R^2}{(R^2 + x^2)^{3/2}} \quad (3.56)$$

and

$$\vec{B} = \frac{\mu_0 i}{2} \frac{R^2}{(R^2 + x^2)^{3/2}} \quad (3.57)$$

Equation (3.58) provides the magnitude of the magnetic field of a single circular turn of wire of radius R carrying a current i as a function of distance x from the center of the coil to a point P on the central axis of symmetry. The constant  $\mu_0$  is called the permeability of free space and is equal to  $1.26 \times 10^{-6}$  Tesla·meter/Ampere (T·m/A). For a coil of N turns of wire carrying a current i, Equation (3.57) becomes

$$\vec{B} = \frac{\mu_0 Ni}{2} \frac{R^2}{(R^2 + x^2)^{3/2}} \quad (3.58)$$

This equation can now be used to determine the magnetic field of a pair of Helmholtz coils as shown in Figure 3.14. The two coils are separated from each other by a distance equal to their radii, R. Each coil has N turns of wire with a current i flowing in each in the same direction

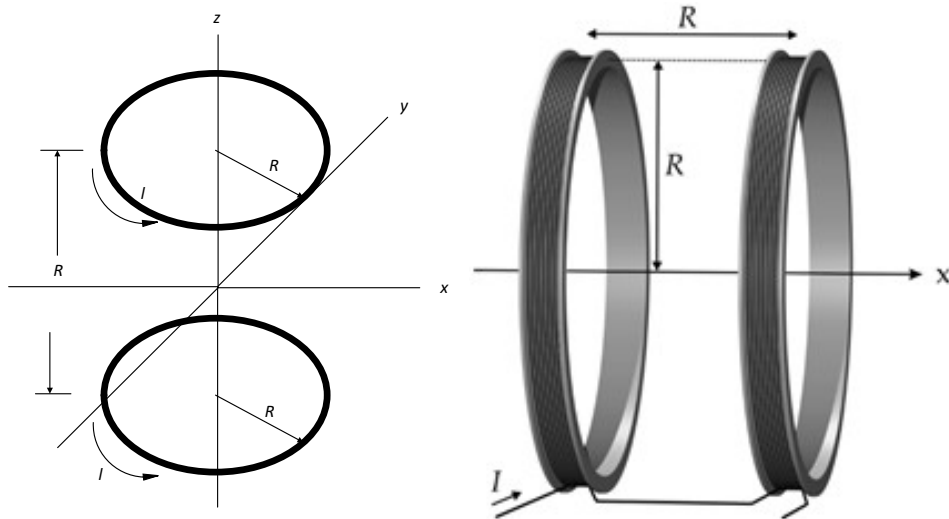


**Figure 3.14:** A pair of Helmholtz coils, each of radius  $R$  and separated by a  $R$

In this work, a pair of Helmholtz coils for enhancing the healing process was designed and used. 75 Hz magnetic field is produced by an identical pair of Helmholtz coils which was powered with a function generator. This device was made up of two parallel coaxial circular coils (500 turns in each loop, wound in series) which were separated from each other by a distance equal to the radius of one coil (10 cm). The windings of our Helmholtz coil were made of standard 0.95mm diameter copper wire to provide the maximum possible current.

In Figure 3.15, the  $z$  component of magnetic field density is analytically calculated for two and four axially oriented circular rings of radius 10 cm separated from each other with the separation distance of 10 cm starting from  $z=0$ . The contour, 2D and 3D surface plots of  $B_z$  are sketched at  $z=15$  cm in the middle point of circular rings from  $x=-30$  cm to  $x=30$  cm and  $y=-30$  cm to  $y=30$  cm (Appendix A). In Figure 3.16, the  $z$  component of magnetic field intensity is sketched from  $x=-15$  cm to  $x=15$  cm for two and four coils on the same axis. From both of these figures, how the dominant component of magnetic field intensity is made to be more homogenous and larger in magnitude on horizontal plane by the use of additional coils can be visualized. We have used two axially oriented circular rings in our PEMF system. The cell culteres were placed in the middle of two coils where the magnetic field intensity is maximum.

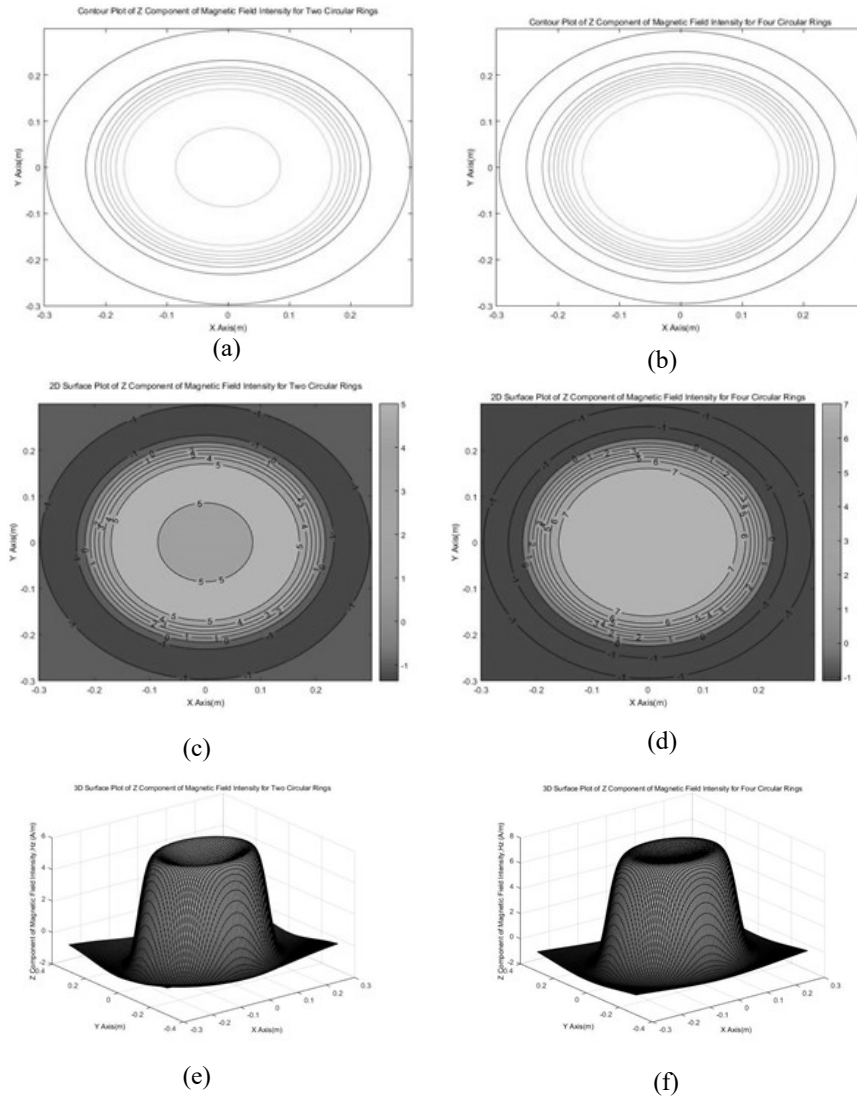


**Figure 3.15:** Countour Plot of Z Component of Magnetic Field

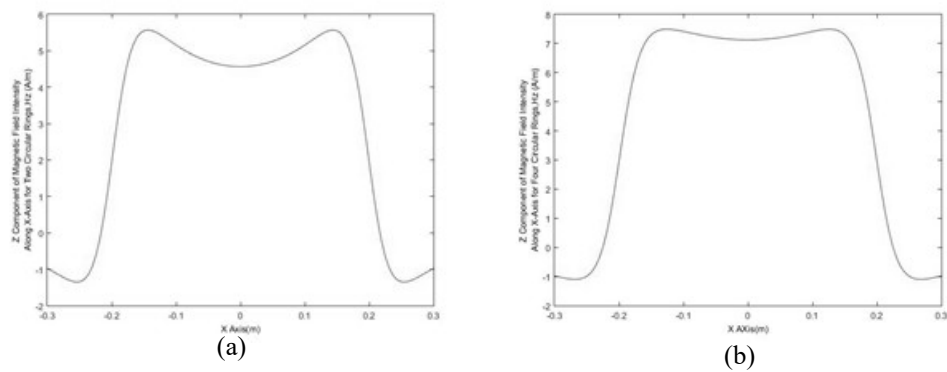


**Figure 3.16:** The z component ( $x=-15$  cm to  $x=15$  cm) of magnetic field intensity



In Figure 3.17, the z component of magnetic field intensity is additionally sketched from  $x=-10$  cm to  $x=40$  cm for two and four coils on the z- axis in order to observe how the z component of magnetic field intensity is formed to be more homogenous and higher in magnitude by the use of axially oriented coils along axial direction.

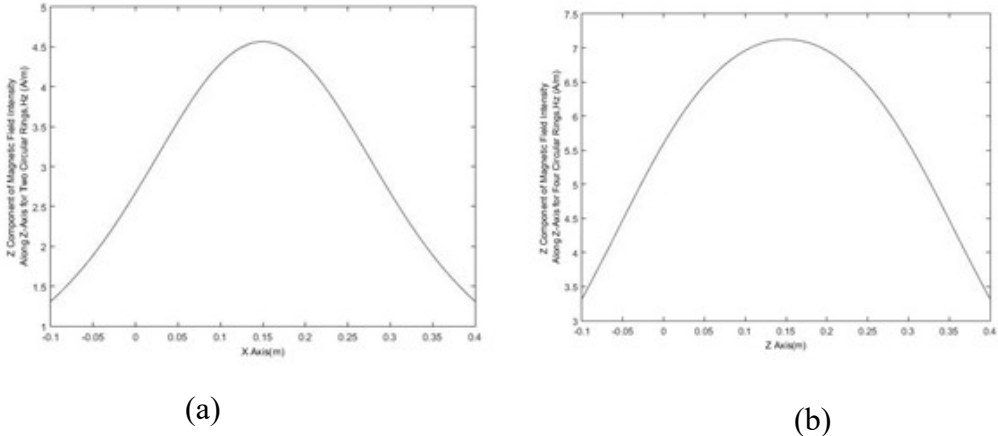


**Figure 3.17:** The z component (from  $x=-10$  cm to  $x=40$  cm) of magnetic field intensity for (a) Two ring coil, (b) Four ring coil

## **4. PEMF COIL MODELS and PRFE ANTENNA PROTOTYPES**

### **4.1 Objectives**

The use of antennas in medical applications, tissue parameters analysis and epidemiological studies has been the research topic of many investigators in the last few years.

This Chapter discusses the design and modelling/analytical aspect of PEMF and PRFE exposure systems for *in vitro* experiments. The PEMF exposure system is built based on a 2-Axis air core Helmholtz coil configuration that produce a uniform time varying magnetic field and the PRFE exposure system is designed as flat spiral antennas. All simulations performed by CST Microwave Studio. Instrumentation and experimental setup required for generating and measuring magnetic flux density within the PEMF system have also been presented in considerable details.

### **4.2 Modelling and Simulations**

The area of the new antenna will be large to support performances at lower frequencies. The antenna is crucial enabling component which allows communication between sensors, and with other off-body systems. But the antenna operates in a particularly challenging environment, in close proximity to the human body. The design of these antennas is thus challenging, and numerical simulation is an indispensable tool for antenna engineer.

### **4.3 Numerical EM Modelling**

Analytical methods are very good at analyzing certain problems with a high degree of symmetry and they can provide a great deal of insight into the behavior of many configurations. However, an accurate evaluation of most realistic electromagnetic configurations requires a numerical approach. Numerical methods are mainly used to solve Maxwell's equations and determine both electric and magnetic fields in a simulation domain.

A short overview of the most common numerical techniques for solving light scattering problems will be discussed under this title.

- i. **Finite difference method (FDM):** In mathematics, finite-difference methods (FDM) are numerical methods for solving differential equations by approximating them with difference equations, in which finite differences approximate the derivatives. FDMs are thus discretization methods. Today, FDMs are the dominant approach to numerical solutions of partial differential equations.
- ii. **Method of Moments (MoM):** Numerical techniques based on the method of weighted residuals are called moment methods. EM modelers have come to use the term "moment method" synonymously with "boundary element method". The boundary element method is a moment method applied to the solution of surface integral equations. In general, moment method techniques do an excellent job of analyzing unbounded radiation problems and they excel at analyzing PEC (perfect electric conductor) configurations and homogeneous dielectrics. They are not well-suited to the analysis of complex inhomogeneous geometries.
- iii. **Finite Element Method (FEM):** Finite element techniques require the entire volume of the configuration to be meshed as opposed to surface integral techniques, which only require the surfaces to be meshed. However each mesh element may have completely different material properties from those of neighboring elements. In general, finite element techniques excel at modeling complex inhomogeneous configurations. However, they do not model unbounded radiation problems as effectively as moment method techniques.
- iv. **Finite Difference Time Domain (FDTD):** Finite difference time domain (FDTD) techniques also require the entire volume to be meshed. Normally, this mesh must be uniform, so that the mesh density is determined by the smallest detail of the configuration. Unlike most finite element and moment method techniques, FDTD techniques work in the time domain. This makes them very well-suited to transient analysis problems. FDTD techniques are often the method of choice for modeling unbounded complex inhomogeneous geometries.

- v. **Finite integration technique (FIT):** The finite integration technique (FIT) was first introduced in 1977 and since then has been applied to solve different electromagnetic wave problems. The discretization method of FIT is similar to the FDTD method for homogeneous media. However, the FIT transforms Maxwell's equations, in their integral form, to a linear system of equations. This technique treats interfaces between different media in a more accurate manner. It is flexible in geometrical modeling and handles curved boundaries and complex shapes with more accuracy (Cooke, Shtokhamer, Mondelli, & Levush, 2006).
- vi. **Other Techniques:** There are numerous other electromagnetic modeling techniques. Methods such as the Transmission Line Matrix Method (TLM), Generalized Multipole Technique (GMT), and others each have their own set of advantages for particular applications (Garg, 2008; Hubing, 1991).

Many researchers have studied their basic characteristics and major efforts were also devoted to determining the resonant frequency, bandwidth, radiation etc. Although printed antennas appear simple and easy to manufacture, but to seek the electromagnetic properties that meet all the conditions is a complicated task (Didouh, Abri, & Bendimerad, 2012).

In this thesis CST Microwave Studio Software based on finite integration technique (FIT) is used to design 27.12 MHz applicators and simulation with biological materials. Also PEMF coils with biological material are simulated with biological materials in CST EM Studio tool.

#### **4.4 Coil Model and Geometrical Parameters for PEMF Application**

The major field parameters are frequency, waveform, and intensity of the field and duration of exposure. The delivery of induced electric field at the site of stimulation is very important. For this reason, it has been recognized that coil shape and size are important parameters for effective stimulation. Coils shaped differently induce electric fields with different characteristics. When broad areas are to be stimulated, it is necessary for the field to be uniform over the area. In such conditions, it is desirable to have a coil system (like the Helmholtz's and Ruben's) which provides a uniform

magnetic field over a considerable volume and which is easily accessible from outside the coil. The coil types used in this study are shown in Figure 4.1.

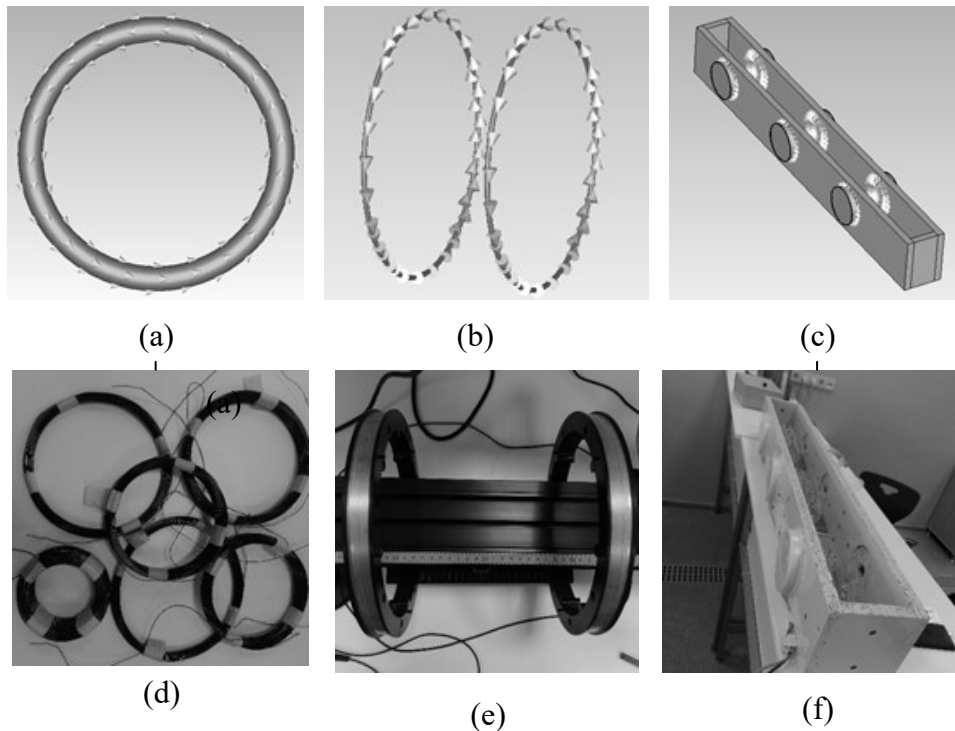


**Figure 4.1:** Magnetic coils used in PEMF application (a) Helmholtz coil, (b) coil prototypes, (c) 3-series Helmholtz coil) Antenna Structures operating at 27 MHz.

#### 4.5 Antenna Model and Geometrical Parameters for PRFE Application

The basic element chosen for the antenna design was a microstrip patch antenna. The patch conductor can be assumed at any shape, but generally, simple geometries are used which simplifies the analysis and performance prediction. Different miniaturization, input impedance and bandwidth enhancement techniques have been used in the design of the proposed applicator. The antenna was initially designed in free space conditions, and later optimized close to a simulated biological material. To meet the initial design requirements (operating frequency=27 MHz) various analytical approximate approaches may be used. The proposed antenna has dimensions 120 mm x120 mm x1.6 mm and it has 14 turn numbers with 2.2 mm thickness. A matching circuit adjusts the antenna frequency. Figure 4.2 shows the geometry of the simulated antennas resonant at 27 MHz. The antennas are modelled and implemented on FR4 dielectric substrate of thickness  $h = 1.6$  mm.

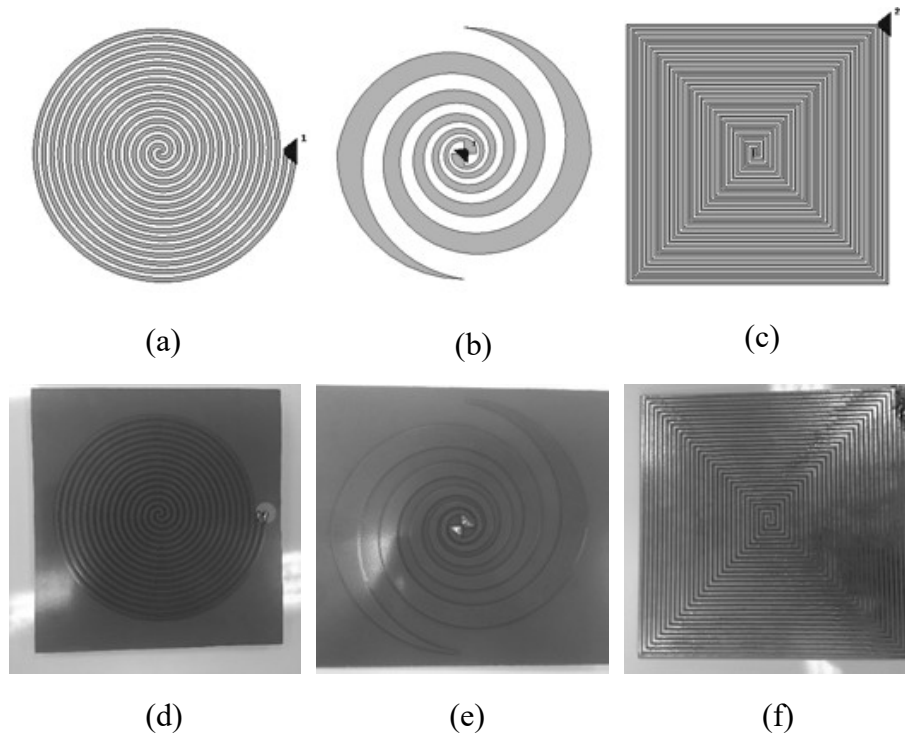


**Figure 4.2:** Antenna Structures operating at 27 MHz.

#### 4.6 Fabrication of the Antenna Prototypes

The antenna designs had to be validated by measurements and tested with biological materials. Therefore, all antenna elements described in this chapter were constructed. The impedance of the proposed antenna is measured using Anritsu 37269B vector network analyzer, MS2721B Anritsu and GW INSTEK GSP-830 spectrum analyzers. The measured values are compared with the simulated values. Figure 4.4 shows a patch with microstrip line feed from the side of the patch. This method of feeding is very widely used because it is very simple to design and analyze and very easy to manufacture.

##### 4.6.1 Impedance Matching

Input impedance of the antenna feedline has to match to the output of a transceiver or power amplifier so the amplifier has the proper resistive load and to reduce unwanted emissions (mainly harmonics) to a very low value. The input impedance circuit is usually required to transform a complex impedance with both resistance and reactance to a purely resistive value, usually  $50 \Omega$ .

To perform this task, the circuit cancels the reactive part of the impedance and then transforms the remaining resistive portion to the desired value (Silver & Wilson, 2008). L-networks are useful in matching one amplifier output to the input of a following stage. Another use is matching an antenna impedance to a transmitter output or a receiver input. Any RF circuit application covering a narrow frequency range is a candidate for an L-network. There are four basic versions of the L-network, with two low-pass versions and two high-pass versions (Figure 4.3)

In this study simple inductor-capacitor (LC) impedance matching networks are designed and simulated by CST Microwave Studio mini match tool. That will provide transform the antenna load impedance to the desired value (50 Ω).

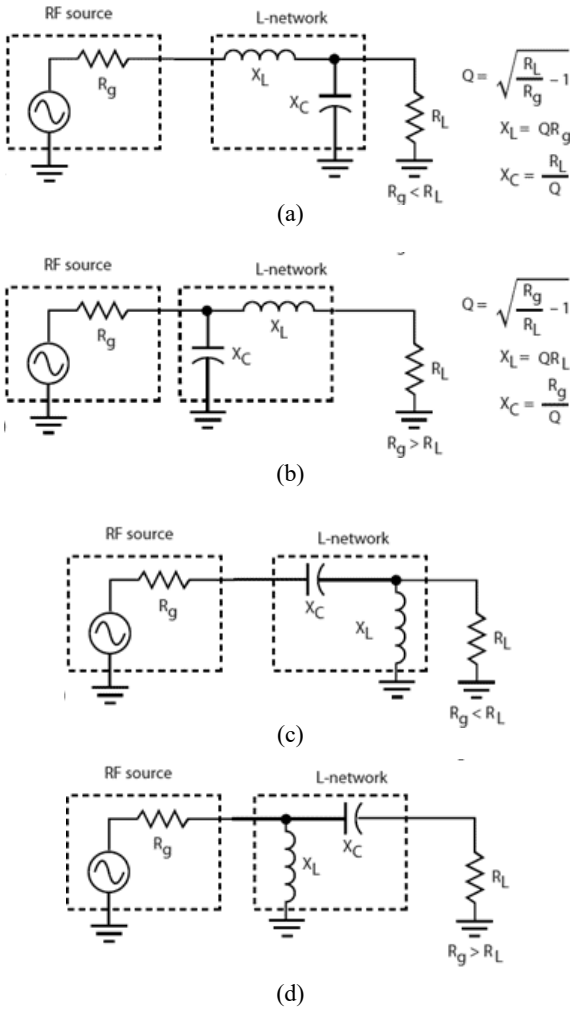


**Figure 4.3:** There are four basic L-network configurations. The network to be used depends on the relationship of the generator and load impedance values. Those in (a) and (b) are low-pass circuits, and those in (c) and (d) are high-pass versions.

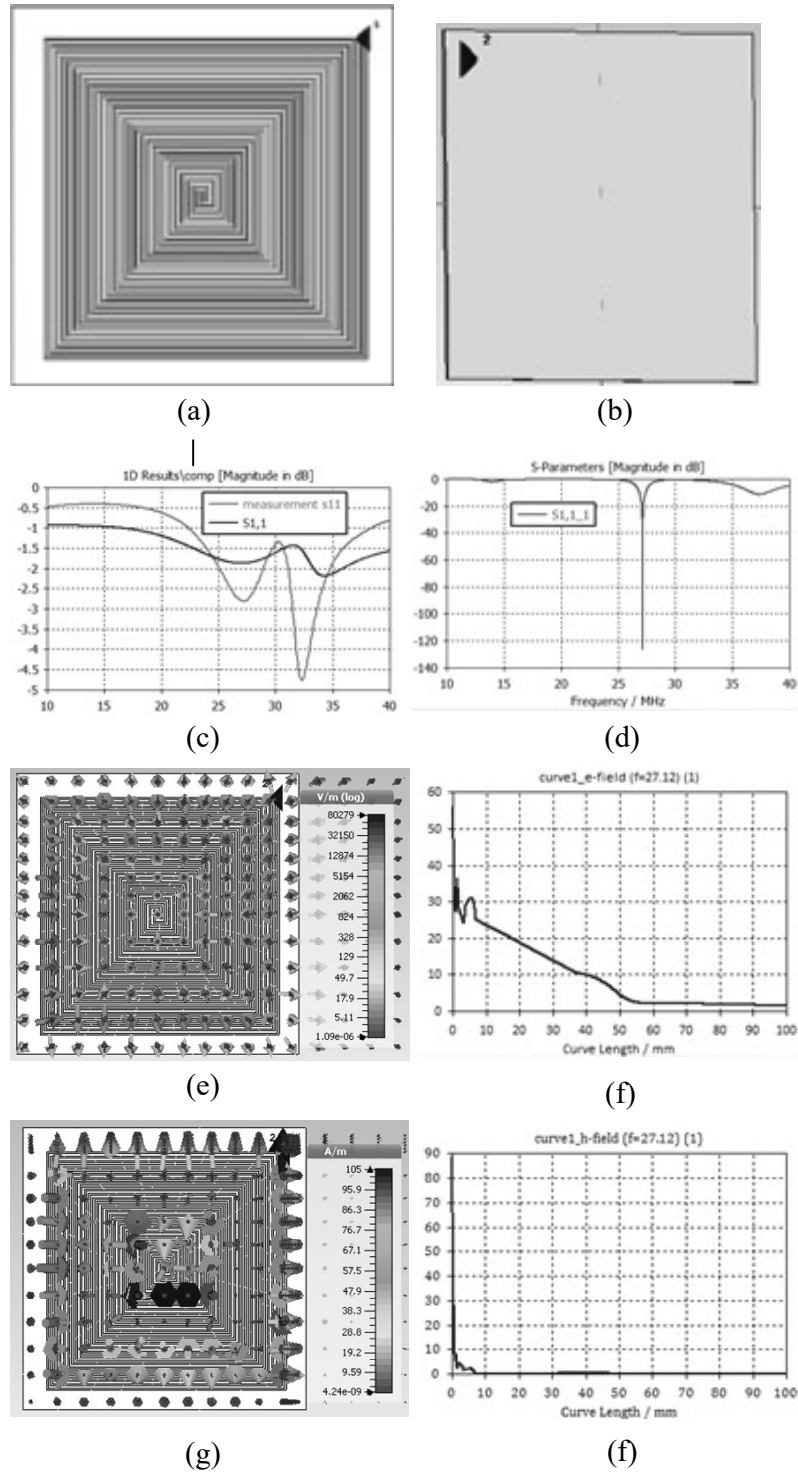


**Figure 4.4:** Simulation results of the proposed antenna (a) Front view (b) Back view (c) Simulation and measurement result of S11 (d) Simulation result of S11 with matching (e) E-field simulation result (f) E-field result through 10 cm line from the antenna (g) H-field simulation result (h) H-field result through 10 cm line from the antenna.



#### 4.6.2 PRFE Antenna with Artificial Magnetic Conductor (AMC)

An artificial magnetic conductor (AMC) is a type of metamaterial that emulates a magnetic conductor over a limited bandwidth. An AMC ground plane enables conformal antennas with currents flowing parallel to the surface because parallel image currents in the AMC ground plane enhance their sources. However, AMCs are limited by their bandwidth, which is proportional to the AMC inductance, which in turn is proportional to the substrate thickness and permeability. Some designed AMC structures can be seen in Figure 4.5.

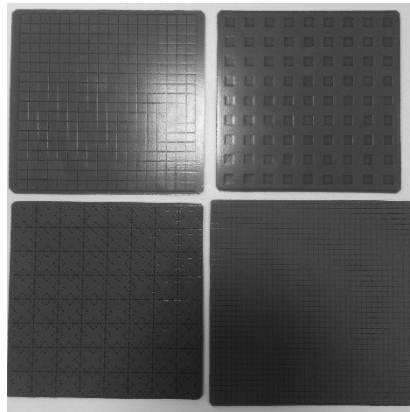


**Figure 4.5:** Designed AMC structures.

At VHF-UHF frequencies, the thickness and/or permeability necessary for reasonable AMC bandwidth is excessively large for antenna ground-plane applications (Gregoire, White, & Colburn, 2011). Artificial magnetic conductors (AMCs) having canonical frequency selective surface (FSS)-type two-dimensional periodic structures to be used as back reflectors for an aperture antenna (Agarwal, Nasimuddin, & Alphones, 2013). We present in the simulation result that PRFE antenna with loaded AMC substrate's can produce higher E-field and H-field (Figure 4.6). It is expected that antenna with AMC has higher H-field, as shown in Table 4.1.

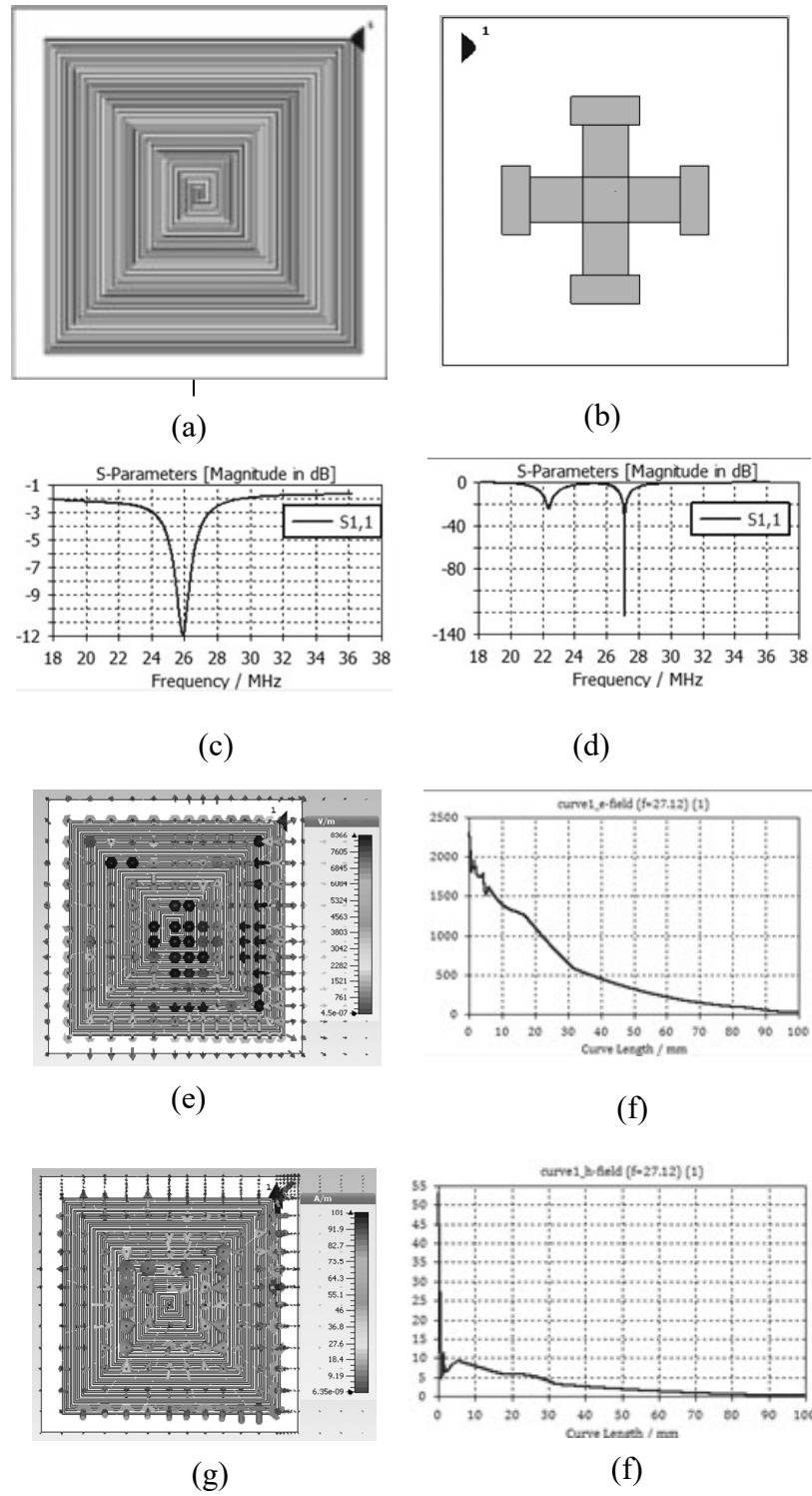


**Figure 4.6:** Simulation results of the proposed antenna with AMC (a) Front view (b) Back view (c) Simulation result of S11 (d) Simulation result of S11 with matching (e) E-field simulation result (f) E-field result through 10 cm line from the antenna (g) H-field simulation result (h) H-field result through 10 cm line from the antenna.

**Table 4.1:** Performance Parameter results of Flat Spiral Antenna.

	Reference Antenna (Without AMC)		Antenna with AMC	
	Simulation	Measurement	Simulation	Measurement
<b>Material</b>	FR4 & Copper	FR4 & Copper	FR4 & Copper	FR4 & Copper
<b>Size</b>	120 x 120 x 1.6 mm <sup>3</sup>	120 x 120 x 1.6 mm <sup>3</sup>	120 x 120 x 1.6 mm <sup>3</sup>	120 x 120 x 1.6 mm <sup>3</sup>
<b>Connector</b>	Discrete Port	Copper Female	Discrete Port	Copper Female
<b>Resonant Frequency (@ fr)</b>	27 MHz	27 MHz	27 MHz	27 MHz
<b>Input Impedance @ fr</b>	50 Ω	50 Ω	50 Ω	50 Ω
<b>Return Loss @ fr</b>	~-2 dB wo matching & ~-120 dB with matching	~-2.5 dB wo matching & ~-13 dB with matching	~-7 dB wo matching & ~-100 dB with matching	-
<b>Mean E-Field (V/m) @ fr</b>	5000	-	4000	-
<b>Mean H-Field (A/m) @ fr</b>	100	-	150	-

#### 4.6.3 A Multi layers Flexible Flat Spiral Antenna on PDMS/Kapton Substrate

Polymers are rapidly becoming important among materials for microwave and biomedical applications. Flexible electronics have drawn significant attention in the past decades. More and more flexible electronics have been developed, such as flexible displays, smart tags, and wearable products. Polymers such as polydimethylsiloxane (PDMS) widely adopted for microwave microsystem fabrication in recent years (Chih-Peng, Chieh-Hsiang, Cheng, & Jou, 2011).

Kapton is used as a substrate in the flexible circuit industry. Its long flex life and ability to withstand copper etching makes it excellent choice for these applications. It issued heavily in the electronics market as the industry moves to smaller, lighter and faster components (Rufus, 2014). Previous sections discussed various antenna designs with FR4 substrate. Subsequently a flexible flat spiral antenna using Artificial Magnetic Conductor (AMC) as a reflector is explained. Prior to implementing the multi-layer antenna design the fabrication process for the embedded Kapton in PDMS material can be seen in Figure 4.7.

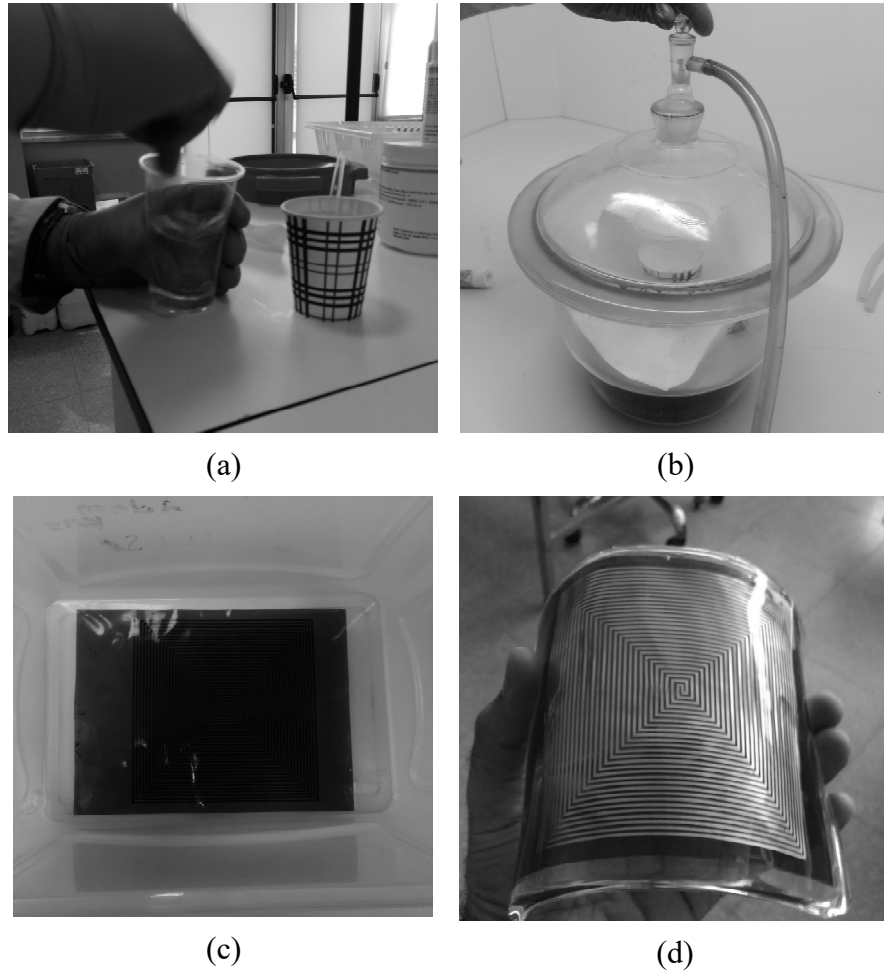


**Figure 4.7:** Fabrication process for PDMS-Kapton substrate based antenna, (a) Mixing PDMS silicone gel and cure agent (10:1 v/v) (b) Degas for 30 minutes, (c) Pour the mixture into a container attached antenna with Kapton substrate at the bottom and degas for 1 hour (d) Fabricated Antenna Prototype.

The antenna was optimized and electrical properties of 27 MHz frequency were determined by simulations (Figure 4.8). This section presents the design, fabrication and analysis of the flexible antenna. The development of a flexible thick polydimethylsiloxane (PDMS)/Kapton microstrip antenna at 27 MHz is presented.

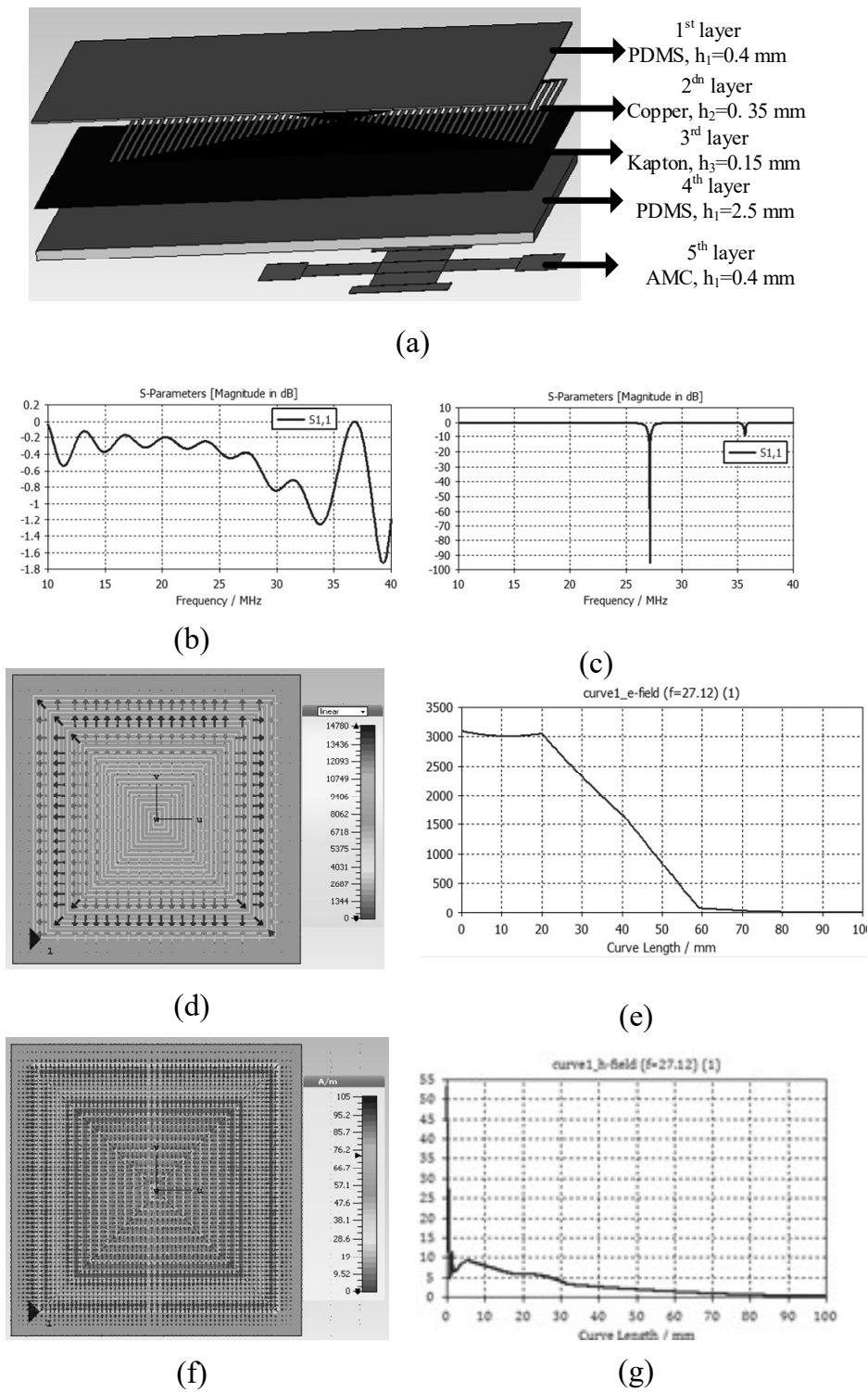


**Figure 4.8:** (a) Schematic diagram of the multilayer microstrip patch antenna identifying each layer and its thickness, (b) Simulation result of S11 (c) Simulation result of S11 with matching (d) E-field simulation result (e) E-field result through 10 cm line from the antenna (f) H-field simulation result (g) H-field result through 10 cm line from the antenna.

#### **4.6.4 Antimicrobial Effects of Non-Thermal Plasma on PDMS Layer of the Antenna**

Recently, there has been growing interest on applications of cold plasma biomedicine with potential applications in dentistry, blood coagulation, wound healing, infection prevention and control, and fighting some types of cancers (Machala, Hensel, & Akishev, 2012). These studies have revealed that cold plasma applications can take place into the medical and therapeutic fields. Plasma may accelerate wound healing when it is generated directly on the skin (Isbary et al., 2013). Furthermore, the antimicrobial effects of plasma have been demonstrated on broad range of microorganisms such as bacteria, virus, fungal pathogens, and even prions (Montie, Kelly-Wintenberg, & Roth, 2000). Researches indicated that potent antimicrobial effect of non-thermal plasma is through generation of free radicals, reactive oxygen (ROS), and nitrogen species (RNS), such as hydrogen peroxide, superoxide, singlet oxygen, nitric oxide, peroxy nitrite, etc. (Ahn et al., 2014). In addition to antimicrobial activity of direct plasma treatment, there are reports demonstrating that also, plasma treated materials such as various liquids and gels can gain antimicrobial activity. Poor et al., 2014 have shown that non-thermal DBD air plasma treated calcium alginate gels can gain antimicrobial activity, which is capable of inactivating broad range of bacteria and fungus. Thus, in the present study, PDMS layer of PRFE applicator was treated using non-thermal dielectric barrier discharge (DBD) air plasma to evaluate possible antimicrobial activity, which could be considered as an auxiliary feature for enhancing wound healing on infected wounds. In the present study, 10x10 mm pieces of PDMS gels were prepared as previously described and treated using non-thermal DBD air plasma at 15 kHz, 31.6 kV which yields 14 W power, by fixing discharge gap to 2 mm. Shortly after plasma treatment,  $10^4$  CFU/ml *E. coli* was placed on the treated surface of PDMS and held for 30 minutes. Following 30 minutes of holding time bacteria was homogenized, diluted and plated for colony counting assay. Our results revealed that, 3-minute plasma treated PDMS gel is capable of inactivating up to 1.5 log bacteria, and when PDMS treated for 5 minutes, a total inactivation (>4 log) was achieved (Figure 4.9).

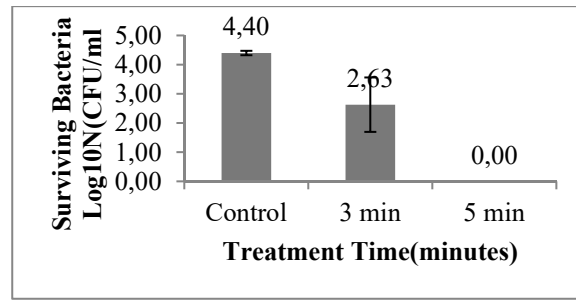


**Figure 4.9:** PDMS exposed for 5 mins to non-thermal plasma completely inhibited  $10^4$  CFU/mL of E. Coli.

#### 4.6.5 Comparison of the PRFE Applicator with Simulation Results

Three selected antennas were compared as shown in Figure 4.10. Through the CST simulations, performance characteristics of the antennas were determined in terms of S11, E-field and H-field. Although the performances are similar to each other, the multilayer antenna has advantages over other antennas, specifically, flexible and more biocompatible.

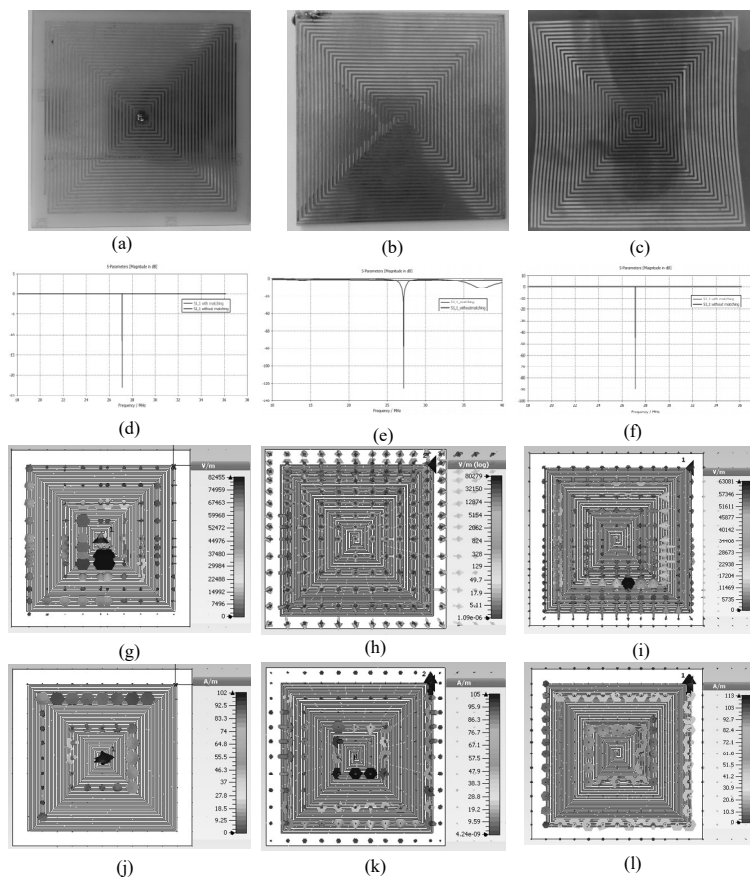


**Figure 4.10:** Flat spiral antennas simulation results (a) 1.6 mm FR4  $\epsilon_r = 4.3$ , middle feeding (b) 1.6 mm FR4  $\epsilon_r = 4.3$ , side feeding (c) 1.6 mm PDMS  $\epsilon_r = 2.4$ , side feeding (d), (e), (f) S11 results with and without matching circuit (g), (h), (i) E-field results (j), (k), (l) H-field results.

Figure 4.11 shows spectrum analyzer based measurement of S11 and S21 performed on some PRFE antennas. From these results it can be seen with  $S_{11} < -10\text{dB}$  as a requirement, our designed antennas can operate at resonant frequency of 27 MHz. We can also obtain transmission performance that signal coming out from antenna 2 entering to antenna 1 with S21 result. The measurement results have a good agreement with the simulation results.

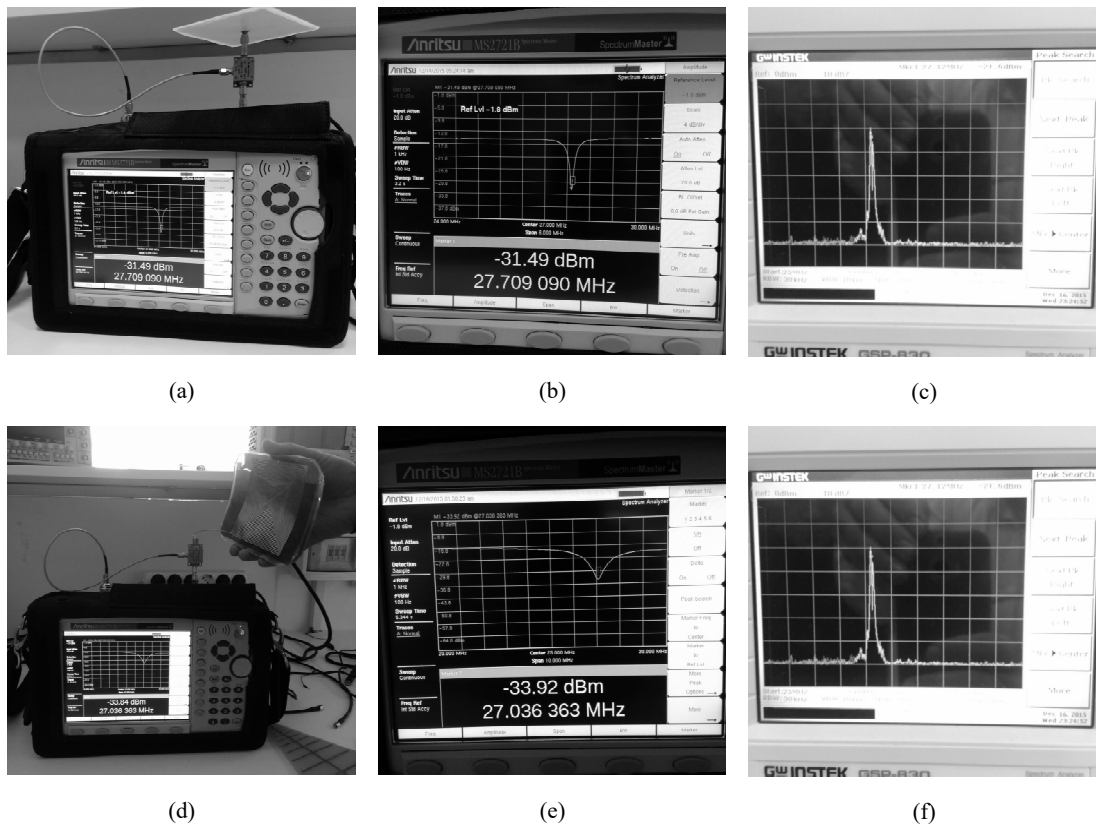


**Figure 4.11:** (a) Measurement setup of S11 for middle feeding flat spiral antenna (b) S11 result of the antenna, (c) S21 result of the antenna (d) Measurement setup of S11 for side feeding flat spiral antenna flexible flat spiral antenna (e) S11 result of the antenna, (f) S21 result of the antenna



## **5. PEMF PRFE EXPOSURE SYSTEMS, MEASUREMENTS and BIOLOGICAL RESULTS**

### **5.1 Overview**

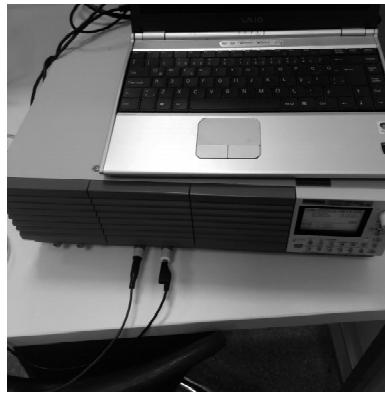
The design and development of the PEMF coil and PRFE antenna were detailed in Chapter 4. The introduction of the therapy had a significant and positive effect on all the chronic wounds under study. This chapter presents and discusses the application of the developed exposure system to study the effects of varying parametric changes of PEMF exposures on breast cancer cells (MDA-MB-231), adipose tissue-derived stem cells (ASCs), bone marrow derived mesenchymal stem cells (BMSC), mouse neuroblastoma cells (Nb2a), and 3T3 fibroblast cells. Cells were grown in culture flasks in a humidified incubator at 37° C with 5% CO<sub>2</sub> and were used at the proliferation and confluent stages.

### **5.2 Experimental Equipment**

General types of equipment used for investigating the effect PEMF/PRFE on wound healing are; Signal Generators (Kikusui bipolar power supply for PEMF, Suin signal Generator for PRFE), Coils or applicators (Pasco Helmholtz Coil (PEMF), The proposed 27 MHz antennas for PRFE), Pasco Magnetic Field Sensor to measure PEMF magnetic field intensity, GW Instek and Anritsu Spectrum analyzers to measure S11, S21, Anritsu Network Analyser to measure S11.

The systems used for investigating the efficacy of PEMF and PRFE exposures in affecting the wound healing of selected cell cultures are given below:

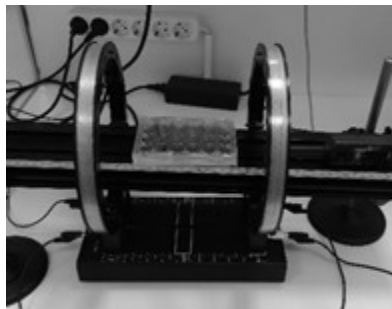
- i. PEMF exposure system is used to generate uniform time varying magnetic fields in the low frequency range, with magnetic induction (magnetic flux density) up to 5 mT (Figure 5.1).



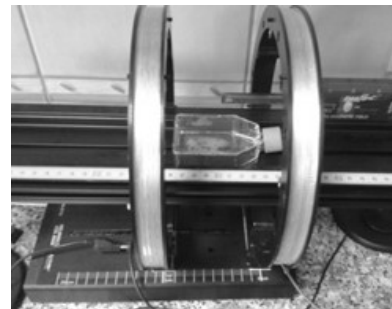
(a)



(b)



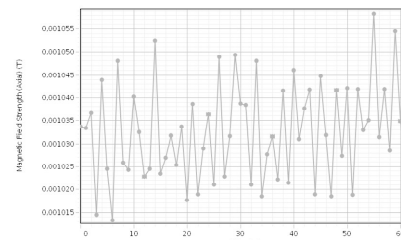
(c)



(d)



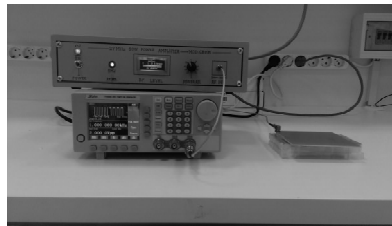
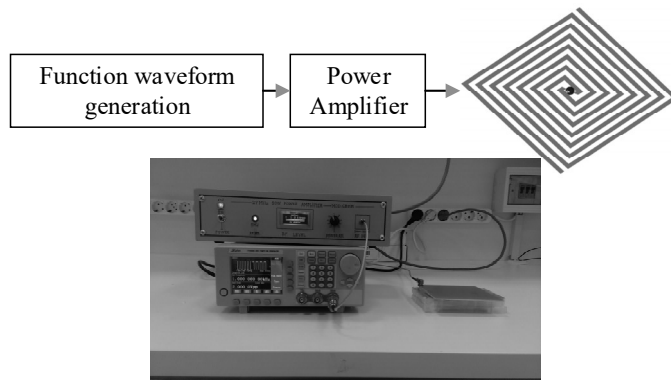
(e)



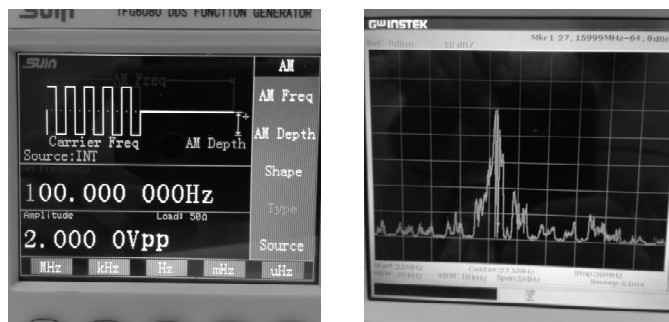
(f)

**Figure 5.1:** PEMF exposure System (a) Kikusui power generator (b) Pasco function generator and Pasco universal interface (c), (d) Pasco Helmholtz coils with cell cultures, (e) 75 Hz PEMF signal (f) B-Field (Tesla) measurement result with a hall effect sensor.

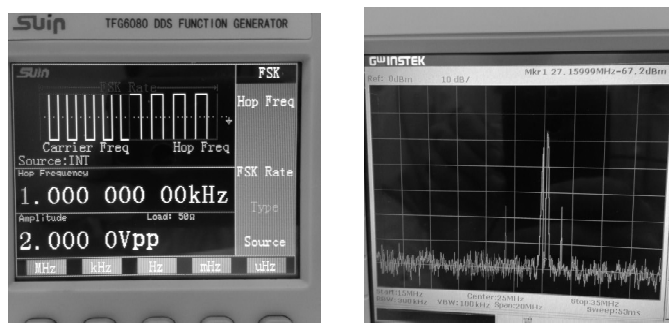
- ii. PRFE exposure system with different signal modulations (PFS, FSK, AM...) is used to generate uniform time varying magnetic fields at 27.12 MHz (Figure 5.2).



(a)



(b)



(c)

**Figure 5.2:** (a) PRFE system (b) AM signal of PRFE application (c) FSK application of PRFE.

### 5.3 The PEMF/PRFE exposure systems

Cells were exposed for PEMF and PRFE 5 hours to. The PEMF exposure system consisted of one Helmholtz coil system in 20 cm diameter and the PFRE exposure system consisted of a square patch applicator antenna, 12 cm edge length. A current flow of 0.4 Ampere passed through two 500-turn Helmholtz Coils setup consists of two field coils mounted on a base to provide a uniform magnetic field between the coils. The copper wire diameter is 0.645 mm. The system allows exposure with low frequencies and magnetic field strength up to 5 mT. The coils were connected in series and each coil was powered by 75 Hz frequency with a pulse duration of 1.3 ms, square

waveform, 1 mT magnetic field intensity. The magnetic field was measured using a magnetic field sensor. Cells were placed in the central part of the system which presented the highest field homogeneity as shown in Figure 5.3.

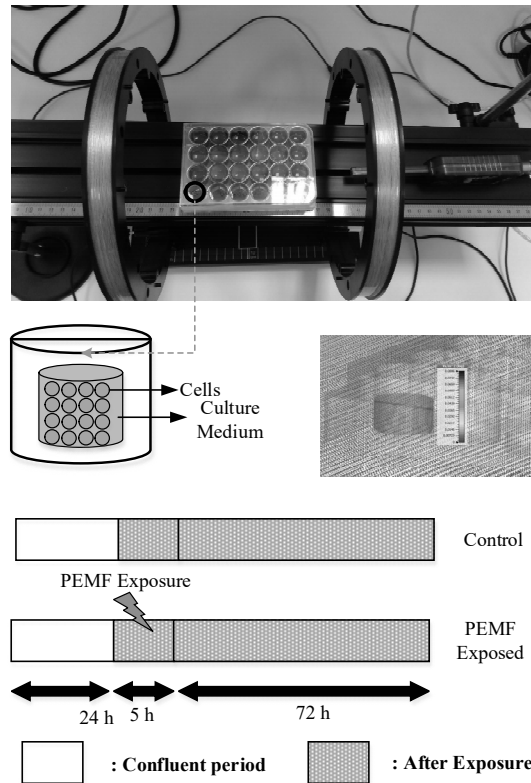


**Figure 5.3:** PEMF exposure setup and experimental timeline.

The wound model was examined for the closure of the wound area by the acquired pictures. After the scratch was initiated, cells exposed with a PEMF signal to 5 hours. A separate flask was kept as control at the same condition without exposure. All photographs were acquired with 10 x magnification at different time points which is summarized in Figure 5.4.

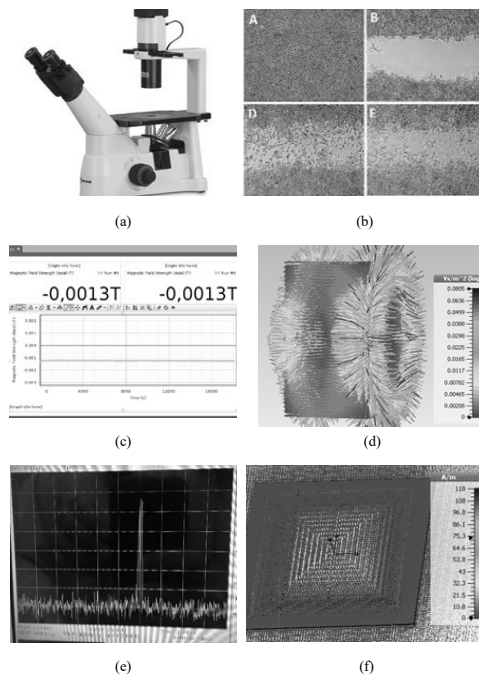


**Figure 5.4:** Summary of steps for methodology of the study. (a) Inverted microscope, (b) Cell culture images, (c) Measured B-field in the Helmholtz coil, (d) Simulated B-field in the Helmholtz coil, (e) Measured power in dB, (f) Simulated H-field.

The PRFE exposure system consists of a field generator, an amplifier and a wideband antenna. Signal Generator fed the antenna with 27.12 MHz frequency, PSK modulation, and 13 dBm amplitude signal for PRFE system. Same processes have been followed to investigate PEMF and PRFE systems. The stimulated samples were maintained outside the incubator, at room temperature (Figure 5.5).

Cell behavior and morphological changes were examined by phase contrast microscopy. Same cell lines were kept in the same condition without exposure used as control groups. The statistical analysis of wound healing images were performed by graphed software and evaluated by blind scoring the results with a scale starting from weak (+1) to strong (+5).

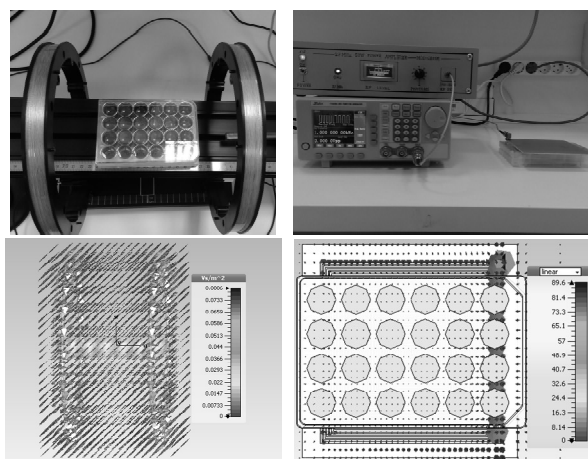


**Figure 5.5:** *In Vitro* exposure systems and conditions. Cells: MDA-MB-231, (ASCs), (BMSC), (Nb2a), and 3T3; Exposure: PEMF (75 Hz, 1.3 ms pulse width, 1 mT, 5h) PRFE (27.12 MHz frequency, PSK or AM, 20 mW, 5h).

Results from comparative analysis of changes in the cell metabolism activity of the exposed vs. non-exposed samples are presented for the selected frequencies of 75 Hz and 27.12 MHz. The simulation results of the experiment system are given with biological results

#### 5.4 *In Vitro* Wound Healing Assays

*In Vitro* wound healing assays have been used for decades to study the major signalling transduction pathways in wound healing (Sammak, Hinman, Tran, Sjaastad, & Machen, 1997; van Horssen, Galjart, Rens, Eggermont, & ten Hagen, 2006). These assays have also been used to examine various mechanisms responsible for cell sheet movement (Bindschadler & McGrath, 2007; Trepot et al., 2009). The most commonly used setup is the “scratch” wound assay, which is performed by denuding an area of a confluent cell sheet using a small tool (e.g., pipette tip). Three different methods have been used to determine the effect of PEMF/PRFE application:

***In Vitro* Scratch Assay:** The *In Vitro* scratch assay is an easy, low-cost and well-developed method to measure cell migration *in vitro*. The basic steps involve creating a “scratch” in a cell monolayer, capturing the images at the beginning and at regular intervals during cell migration to close the scratch, and comparing the images to quantify the migration rate of the cells. Compared to other methods, the *in vitro* scratch assay is particularly suitable for studies on the effects of cell–matrix and cell–cell interactions on cell migration, mimic cell migration during wound healing *in vitro* and

are compatible with imaging of live cells during migration to monitor intracellular events if desired. Besides monitoring migration of homogenous cell populations, this method has also been adopted to measure migration of individual cells in the leading edge of the scratch. Not taking into account the time for transfection of cells, *in vitro* scratch assay per se usually takes from several hours to overnight (Liang, Park, & Guan, 2007).

**Measurement of Cell Viability by MTT Assay:** MTT is a colorimetric assay for measuring the mitochondrial reductase activity in living cells that reduce MTT to formazan dyes giving a blue/purple color. It is based on the cleavage of membrane-permeable yellow tetrazolium salt MTT to formazan crystals by metabolically active cells (figure 5.6).

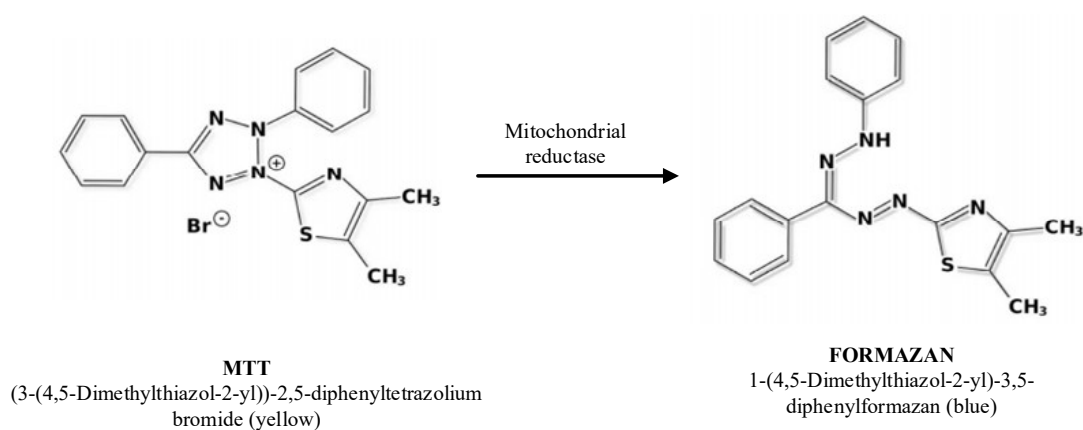


**Figure 5.6:** MTT metabolization to formazan salt in metabolically active cells.

A solubilization solution is then added to dissolve formazan into a colored solution. Spectrophotometric measurement of MTT-formazan at 540 nm allows quantitation of cell viability. Reagents used yield low background absorbance; a strong correlation between cell number and signal produced exists, allowing an accurate measurement of cell viability.

**MTT Assay Protocols:**

- Plate 1.0 ml of cells (50,000-100,000 cells/ml) into each well of 24-well culture plate.
- Incubate cells for 24 h in CO<sub>2</sub> incubator.
- After treatment of cells for 24-72 h, experimental media are removed, and cells are washed with PBS.

- The cells are incubated with basal medium containing 0.5 mg/ml MTT in CO<sub>2</sub> incubator at 37 °C for 4 h.
- The medium is aspirated, and the formazan product is solubilized with dimethyl sulfoxide (DMSO).
- Absorbance at 540 nm is measured for each well using a microplate reader.

**Immunohistochemistry Analysis:** The morphology of the human breast cancer cell line(MDA-MB-231), bone marrow derived mesenchymal stem cells (BMSC) and mouse neuroblastoma cell line was immunohistochemically.

**Immunohistochemistry Protocols:**

- Seed and culture cells in a 24-well plate until they become confluent.
- Wash each well 3 times with 0.5 ml of room temperature PBS.
- Fix each well by adding 0.5 ml of 4% paraformaldehyde in PBS and incubating for 20 minutes at room temperature.
- Aspirate 4% paraformaldehyde and wash each well 3 times with 0.5 ml of PBS for 5 minutes with gentle agitation.
- Add 0.5 ml per well of Blocking Buffer to block non-specific antibody binding.
- Incubate at room temperature for 1 hour.
- Dilute the primary antibody in Blocking Buffer according to the manufacturer's instructions.
- Aspirate the Blocking Buffer and add 200 µl of the diluted antibody to each well.
- Incubate at 4°C overnight.
- After overnight incubation, wash each well 3 times with 0.5 ml of PBS for 10 minutes with gentle agitation.
- Dilute an appropriate secondary antibody (fluorophore-conjugated) in Blocking Buffer according to the manufacturer's instructions.
- Add 200 µl of diluted secondary antibody to each well.
- Incubate at room temperature for one hour, protecting the plate from light.



- Wash each well 3 times with 0.5 ml of PBS for 10 minutes with gentle agitation, protecting the plate from light.
- For nuclear visualization during fluorescent imaging, prepare a 2 µg/ml working solution of DAPI by diluting the stock solution in PBS. Add to each well and incubate for 10 minutes at room temperature, protecting the plate from light.
- Wash each well once with 0.5 ml of PBS for 5 minutes with gentle agitation, protecting the plate from light.
- Aspirate any PBS remaining in wells and, if desired, add 1 to 2 drops of mounting medium to each well to preserve the samples for fluorescence microscopy imaging.

### **5.5 Simulation and Biological Results of PEMF/PRFE Exposure to MDA-MB-231, BMSC, and NA2B**

MDA-MB-231 breast cancer cell line is used to determine cell proliferation and differentiation, mouse neuroblastoma cell line is used to detect neurites extending and no extending cells further mesenchymal stem cells (bone marrow derived mesenchymal stem cells, BMSC) are used to investigate the effects of PEMF and PRFE applications on wound healing. Breast cancer is one of the most common cancers in women worldwide and a cause of cancer-related death. It is reported that some of hormones including estrogen (E2) play a role in the development of breast cancers and the breast cancers could not occur without the hormones (KOYUNOĞLU, KONAR, & SANDAL, 2013). Breast cancer cell lines are used as an *in vitro* cancer models for experimental research. MDA-MB-231 breast cancer cell line is useful for in vitro research area (Zhu et al., 2006). Another cell line used in our study Nb2a cells are the mouse neuroblastoma cell line derived from brain. In the presence of dibutyryl cyclic adenosine monophosphate (cAMP) or fibroblast growth factor (FGF)/epidermal growth factor (EGF) in serum-free media, Nb2a cells were induced extent of neurite elongation and cells become neuronal cells (Vural & Tuğlu, 2011). Stem cells are cells that can self-renew and differentiate into diverse specialized cell types and are classified according to differentiation potentials and sources from which they obtained. Recently, stem cells can be obtained from many sources to use for

therapeutic purposes and hematopoietic and mesenchymal stem cells derived from bone marrow are the most studied. Although surgery, chemotherapy and radiotherapy are used to treat cancer but they are still not effective. Hence the alternative treatments are being researched. In our study, we aimed that effect of PEMF and PRFE exposures on the wound healing in the cells of MDA-MB-231 ( $ER\alpha$ ), Nb2a cell line and BMSCs with wound model. A part of Na2b cells were suspended in serum-free medium and cause neurite extension in the presence of fibroblast growth factor and epidermal growth factor. Hence they transformed into induced typical neuronal cells.

Electric and magnetic fields generated by the antenna on the cell culture was simulated with CST Microwave Studio program. According to results about 40 V / m electric field and 0.2 A/m magnetic field occurred on the cell cultures (Figure 5.7).

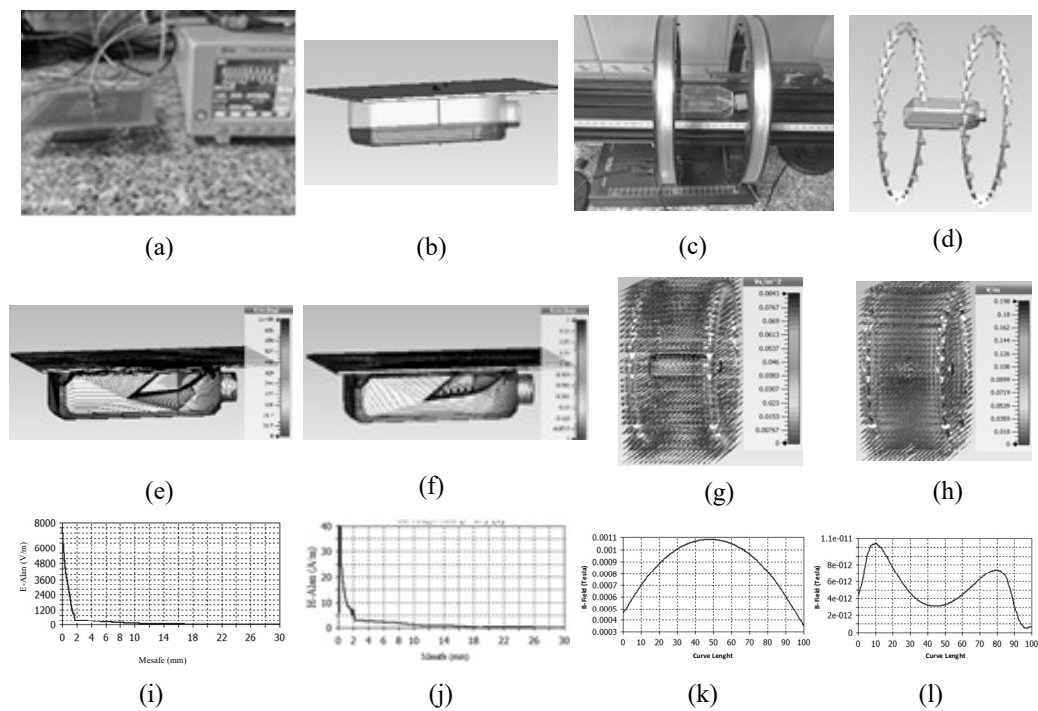


**Figure 5.7:** PEMF and PRFE system simulations with petri dish, (a) PRFE application with petri dish, (b) PRFE simulation with petri dish, (c) PEMF application petri dish, (d) PEMF simulation with petri dish, (e) E-field simulation result of PRFE application, (f) H-field simulation result of PRFE application, (g) E-field simulation result of PEMF application, (h) H-field simulation result of PEMF application, (i) E-Field result of PRFE application through 10 cm line from center of the applicator, (j) H-Field result of PRFE application through 10 cm line from center of the applicator, (k) E-Field result of PEMF application through 20 cm diameter of the applicator, (l) H-Field result of PEMF application through 20 cm diameter of the applicator.

## 5.6 The effect of PEMF and PRFE on mouse neuroblastoma (Na2b) and adipose tissue

End of the experiment exposed groups compared to the control group, wounds in neuroblastoma cell lines hadn't closed yet and cell proliferation decreased while in the neurites extended neuron cells inhibition dependent effects were observed at lower rate Adipose-derived stem cell lines (ASCs) (See in Figure 5.8).

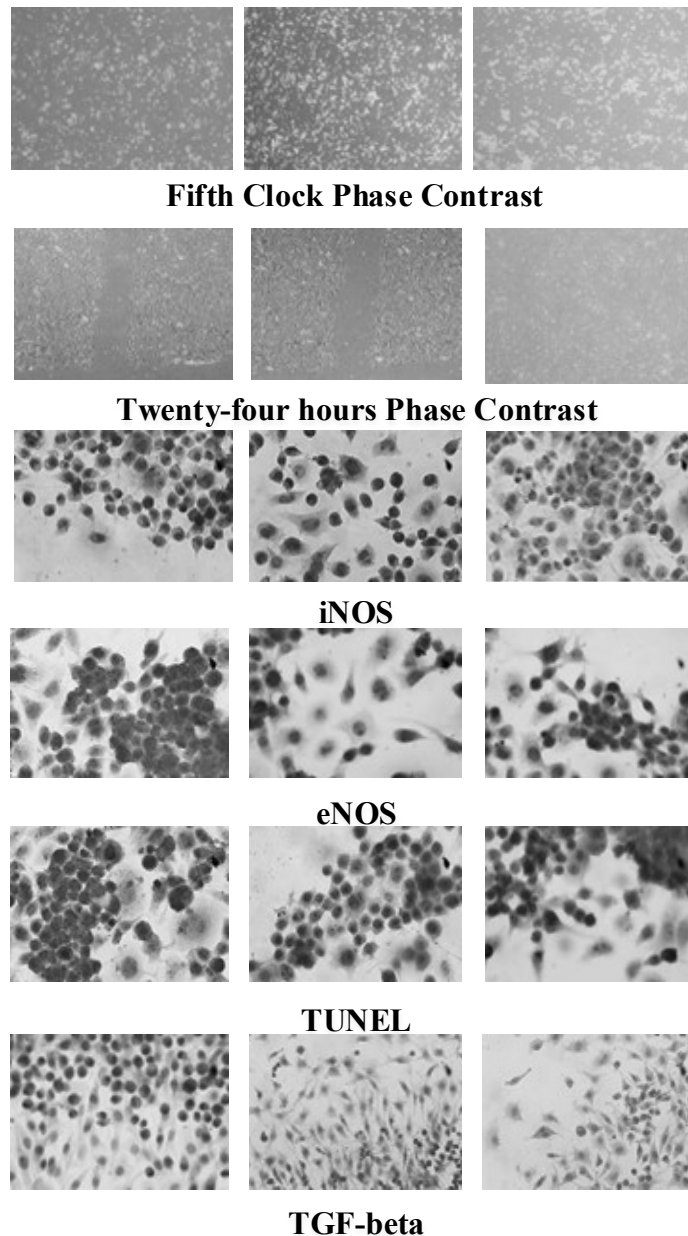


**Figure 5.8:** The death of cells were observed during the stage of proliferation and that is because oxidative stress (NOS), apoptosis (TUNEL), and inflammation (TGF-beta) increased.

The PEMF effects were found to be significantly better than PRFE with morphometric analysis done with scoring (Figure 5.9).

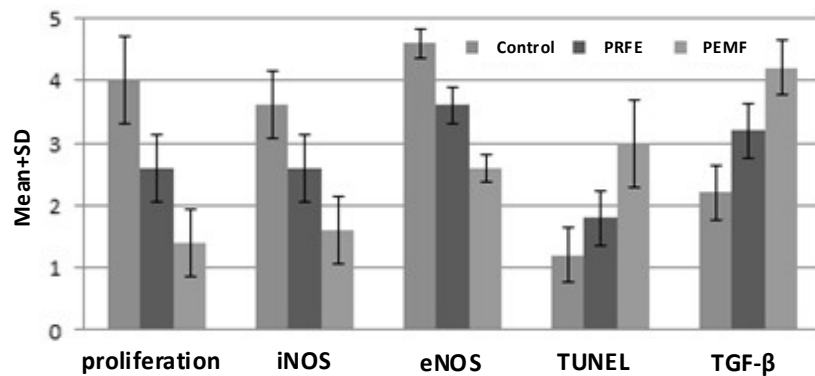


**Figure 5.9:** The effects of PEMF and PRFE Na2b in mouse neuron-like cell culture.

Electromagnetic fields affect the behavior of cancer cell lines at the stage of proliferation was examined by the differentiation stage of extending neurites (Figure 5.10).

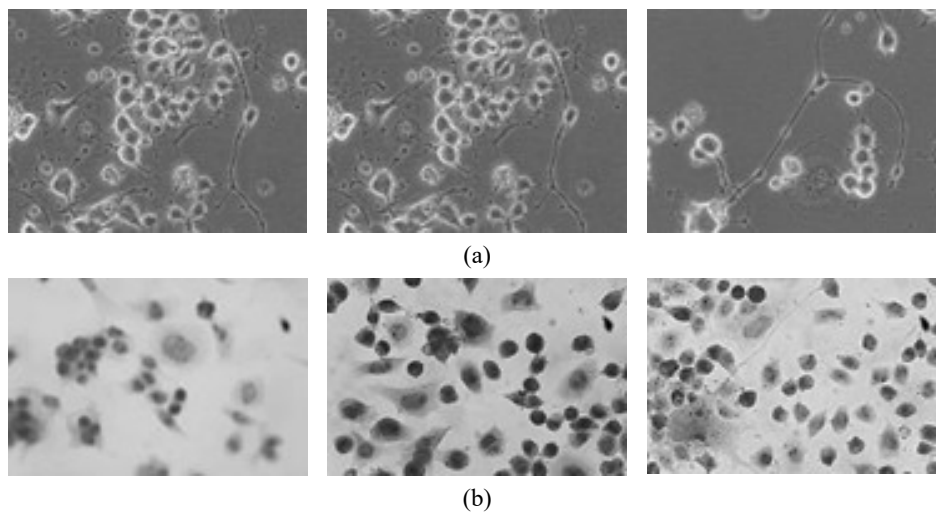


**Figure 5.10:** Oxidative stress (NOS), apoptosis (TUNEL) and increase of inflammation (TGF-beta) (a) Proliferation Stage (b) Differentiation Stage.

Consequences of the application of electromagnetic field therapy was observed while proliferation of non-cancerous cells were increased, the proliferation of cancer cells were stopped. To show the efficacy of treatment, inhibition of neurite was found to be significant. This finding shows us that PEMF and PRFE exposure to the cancer cells may be effective to stop proliferation which is the main problem in cancer.

This observation is important since these treatments don't have any harmful side effect. Effect of EMF on somatic cells was more interesting, which they cause proliferation of the cells even in wound closure. This effect could be useful for accelerated wound healing. As a result, proliferation of proliferative cells which indicating the cancer progression was stopped and were found to lead them to death. To achieve this result, reduction of oxidative stress was shown by NOS, decreased of cell death was shown by apoptosis, and reduction of inflammation, was demonstrated by TGF. The efficacy of this application without any observed side effect showed by MTT. Moderate formation of neurite inhibition suggests the development and involvement of this application in medicine. More importantly, curative effect may be possible on the cancer caused by nerve cells were shown in the culture medium. It was suggested to study and show these results *in vitro* could be more significant.

### **5.7 The Effect of PEMF on 3T3 cells during *In Vitro* Wound Healing**

We investigated the effects of 75 Hz square waveform PEMF with intensity of 1 mT and 27.12 MHz carrier frequency PRFE for up to 5 h on the cell growth rate of 3T3 cells as described previously in this section. Electric and magnetic fields generated by the antenna on the cell culture were simulated with CST Microwave Studio program. According to results of 50 V / m electric field and 0.8 A/m magnetic field occurred on the cell cultures showed on Figure 5.11.

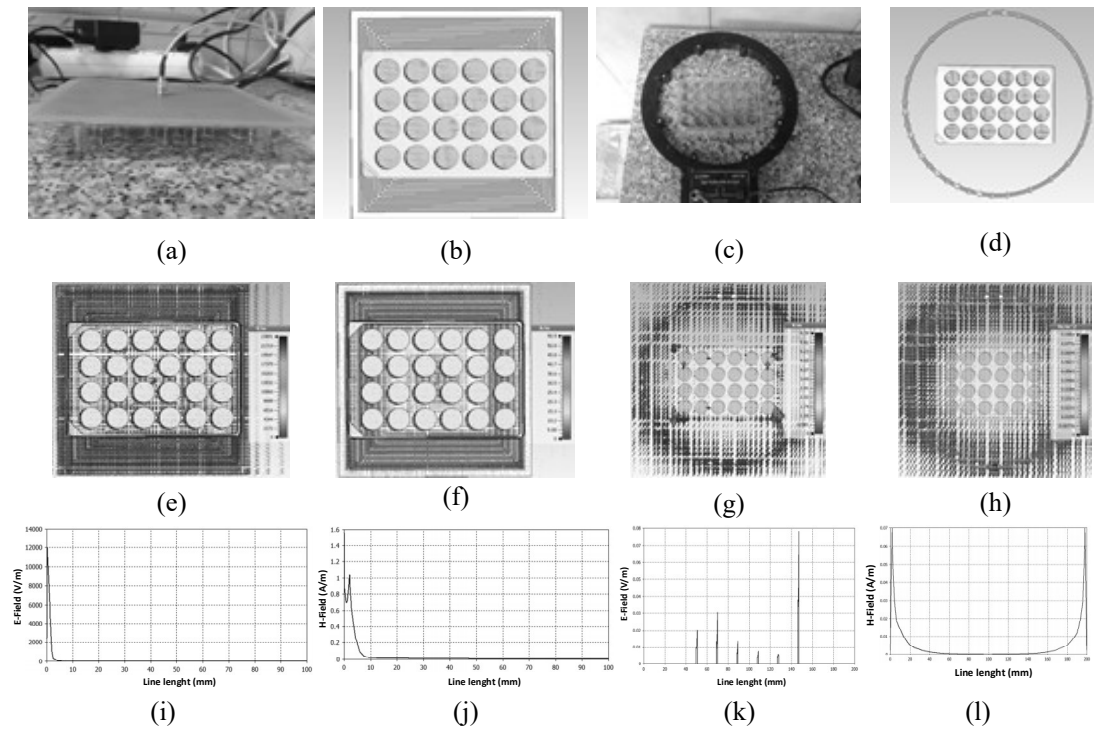


**Figure 5.11:** PEMF and PRFE system simulations with 24 well plate cell culture (a) PRFE application with 24 well plate (b) PRFE simulation with 24 well plate (c) PEMF application 24 well plate, (d) PEMF simulation with 24 well plate, (e) E-field simulation result of PRFE application, (f) H-field simulation result of PRFE application (g) E-field simulation result of PEMF application, (h) H-field simulation result of PEMF application (i) E-Field result of PRFE application trough 10 cm line from center of the applicator, (j) H-Field result of PRFE application through 10 cm line from center of the applicator, (k) E-Field result of PEMF application through 20 cm diameter of the applicator, (l) H-Field result of PEMF application through 20 cm diameter of the applicator.

3T3 fibroblast cell line (the 3T3 abbreviation comes from three-day transfer inoculum  $3 \times 10^5$  cells) were obtained from Ege Research Group of Animal Cell Culture and Tissue Engineering. Cells were routinely grown in Dulbecco's Modified Eagle's Medium (DMEM) (Sigma-Aldrich, STEINHEIM) containing 10% FBS (Sigma-Aldrich), 1% L-glutamine (Gibco, Grand Island, US) (required in cell metabolism reactions), 10% fetal bovine serum (contains growth factors), and 0.1% penicillin/streptomycin (for preventing infections)]. Cells were cultured in 75 cm<sup>2</sup> culture flasks at 37 °C, in a 5 % CO<sub>2</sub> atmosphere. All cultures were passaged two or three times per week at 80% confluence by trypsin/EDTA detachment. In this study passage P19 was used.

Figure 5.12 shows by representative images that PEMF and PRFE substantially increased the wound healing process compared to control cells. Images were acquired

at 0, 12, 24, 48 and 72 hours after the applications using an inverted phase contrast microscopy with a 10x phase objective. As shown in the Figure 5.12 the ability of wound repair was significantly higher in 3T3 cells treated with PEMF and PRFE at each time point investigated and compared to control cells.

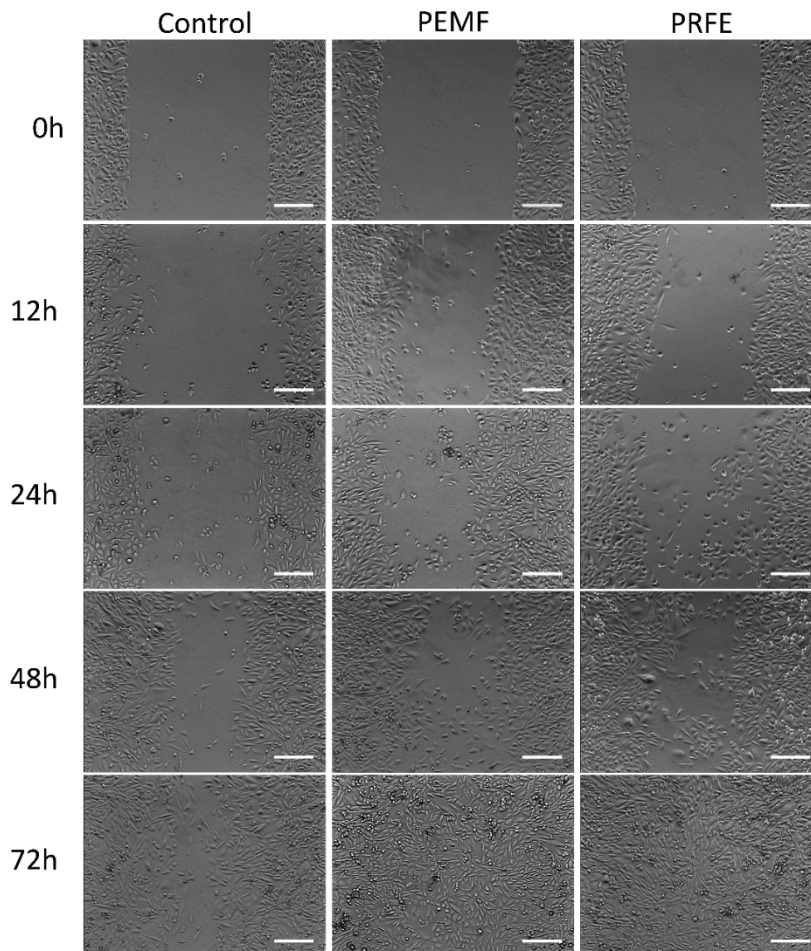


**Figure 5.12:** Acquired microscope images of the Control and PEMF/PRFE exposure 3T3 fibroblast cell groups.

The primary finding of the present study was that PEMF and PRFE enhanced the proliferation of 3T3 cells in culture. The results of experiments on cell cycle using MTT assay provided support to this conclusion (Figure 5.13). Furthermore, 27.15 MHz carrier frequency PRFE had a superior effect on 3T3 cell proliferation compared to PEMF at 75 Hz.

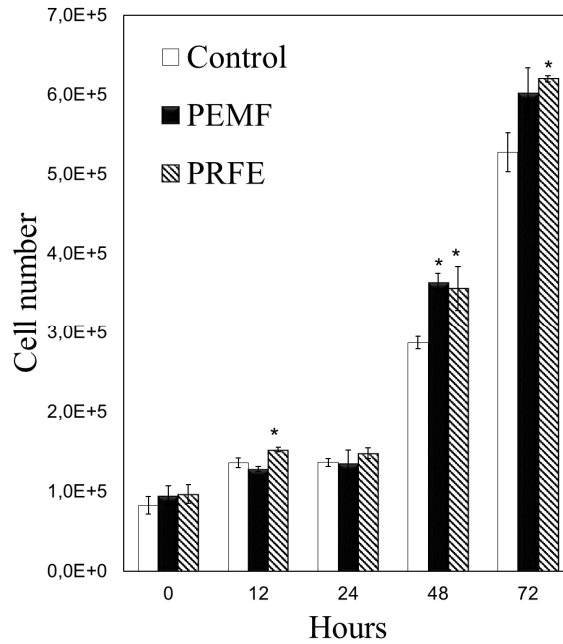


**Figure 5.13:** MTT result of Acquired microscope images of the Control and PEMF/PRFE exposure 3T3 fibroblast cell groups.

The migration of fibroblast cells to cover the scratch created to mimic wound was captured using light microscope attached to a camera, at time interval of 0, 12, 24, 48, and 72 hours (Figure 5.13). On the consecutive days, the wound area was occupied by fibroblasts. The percentage of healed wound area was measured and analysed quantitatively at 0 and 72 hours. The ability of wound closure of PEMF and PRFE treated groups was seen to be more significant ( $P < 0.05$ ) compared to control group. (Figure 5.14).

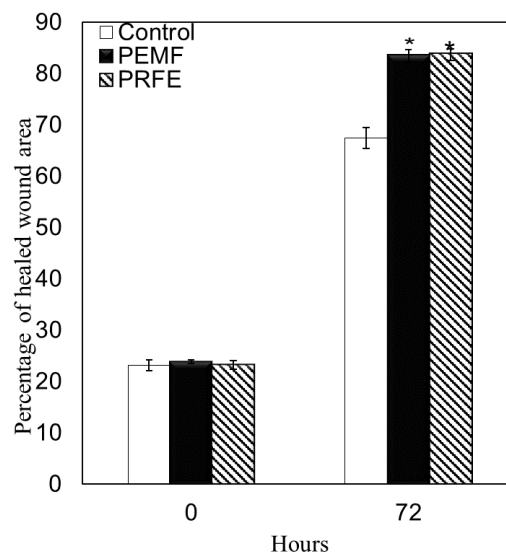


**Figure 5.14:** Percentage of wound closure of PEMF and PRFE treated groups



## 5.8 Thermal Effect of Pulsed Electromagnetic Fields

Diathermy is the application of electromagnetic waves in the radio frequency range of the electromagnetic spectrum to the tissues of the body. The most common form of diathermy in use today utilizes 27.12 MHz frequency waves from the short wavelength range of radio frequency waves and is commonly referred to as shortwave diathermy (SWD). The radio frequency waves produced by diathermy devices will pass through the tissues of the body and initially are not detected. Gradually, absorption of energy by the tissues may cause an increase in tissue temperature, depending on the intensity of the waves and whether the waves are continuous or pulsed. Patients may perceive a feeling of warmth as the tissue temperature rises. Generally, the closer the diathermy applicator is to the patient's skin, the greater the effect on the tissues (Michlovitz et al., 2011).

Pulsed shortwave diathermy can be adjusted to provide a thermal response or to produce no tissue heating. When shortwave diathermy is adjusted to a low frequency (less than 500 pulse per second) with a short pulse duration (65  $\mu$ s into the non-thermal range), it is often classified as pulsed electromagnetic field (PEMF) or pulsed radio frequency energy (PRFE). This reclassification is important because diathermy implies heating, whereas the labels PEMF and PRFE imply a non-thermal therapy (Denegar, Saliba, & Saliba, 2015). Figure 5.14 shows typical thermal images acquired that showing the temperature differences of petri dish surface which applied PEMF. There are no differences with the applications.

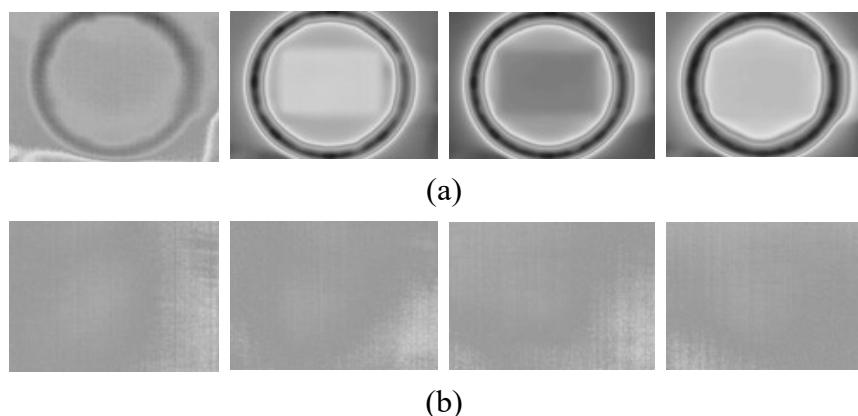


**Figure 5.15:** Thermal image of PEMF applied cultures. (a) Culture with PEMF coil, (b) Closer thermal images of culture dish.

## 6. CONCLUSIONS

New methods of rapid tissue regeneration are being investigated to shorten the wound healing process. In recent years' effects of physical forces such as electric currents, laser beams and ultrasound on repair of the tissue injury are shown in experimental studies. Novel knowledge is needed to determine the appropriate type of energy to provide significant contribution to wound healing. In this study, we intended to design an applicator by examining the effects of pulsed radiofrequency energy (PRFE) carried with 27.12 MHz on the experimental wound healing in cell culture media containing mouse neuroblastoma cells and differentiating neural stem cells. Pulsed electromagnetic field (PEMF) was applied on the same cell lines as well and its effects on wound healing were investigated.

While the exact mechanism by which PEMF interacts with cells to initiate the therapeutic effect is not fully understood, cell studies have given a valuable insight into the downstream biological effects of PEMF therapy. Pulsed electromagnetic fields (PEMF) provide a non-invasive, no-touch means to apply an electric field which can target intra and extracellular biochemical pathways. PEMF signals have recently been configured to modulate  $\text{Ca}^{2+}$  binding to calmodulin (CaM), followed by Ca/CaM binding to an enzyme such as constitutive nitric oxide synthase (cNOS) which leads to transient nitric oxide (NO) release. Manipulation of this pathway is known to be anti-inflammatory. Direct evidence on modulation this pathway by PEMF signal has been reported for chondrocytes, as well as neuronal cells in culture, and in a rat thermal injury model of cardiac ischemia. Strong indirect clinical evidence has also been reported for post-surgical pain relief, chronic wound repair, and for cardiac myopathy patients with chronic angina.

Dielectric properties of biological tissues have been extensively studied theoretically and experimentally (Peratta & Peratta, 2010). A basic understanding has been achieved of the mechanisms and structures that determine the electromagnetic properties of tissue materials. It has been demonstrated that tissue materials are nearly nonmagnetic, and thus have permeabilities close to that of free space and are independent of

frequency. On the other hand, electrical properties of tissue materials have been shown to display a characteristic dependence on frequency. They possess very high dielectric constants compared to many other types of homogeneous liquids and solids. Due to nature of nonhomogeneous tissues are, in which tissues are composed of cells, macromolecules, and other membrane-bound substances.

The concept and prospects of PEMF effects on wound healing are introduced. In the following, I present the main conclusion of this study:

- It was shown that well-designed loop antennas operating around 27 MHz can be used as applicators for the PRFE application. Given the loops operate in very close proximity to each other and that their resonant frequencies are susceptible to slight changes in the distance and the environment, proper matching of their impedance under a deterministic scenario will ensure higher efficiency.
- Non-Thermal Plasma treated PDMS layer of the antenna can gain antimicrobial activity.
- PEMF and PRFE applications inhibited neurite extension in Neuroblastoma cells. The proliferation in these cells has not been occurred yet comparing with control cells.
- At the end of the 24 hours the wounds in culture were not closed by the cells of MDA-MB-231 and Na2b which were under the effect of PEMF and PRFE exposures compared to those of control cultures. Neurite inhibition of Na2b was also observed after EMF exposure. Interestingly, BMSCs were showed more proliferation instead of inhibition and this behavior more obvious with wound healing. BMSCs had more proliferative activity with PEMF and PRFE exposure compared to control cultures.

The effect of low-frequency PEMF and 27.12 MHz PRFE on different cells in wound healing remains to be investigated. Therefore, this study focuses on the effects of pulsed electromagnetic fields on the healing process in an *in vitro* wound healing model. Our findings contributes to a better understanding wound healing and could support the development of new strategies for tissue regeneration.

## REFERENCES

- Agarwal, K., Nasimuddin, & Alphones, A.** (2013). Unidirectional wideband circularly polarised aperture antennas backed with artificial magnetic conductor reflectors. *IET Microwaves, Antennas & Propagation*, 7(5), 338-346. <http://digital-library.theiet.org/content/journals/10.1049/iet-map.2012.0580>
- Ahn, H. J., Kim, K. I., Hoan, N. N., Kim, C. H., Moon, E., Choi, K. S., . . . Lee, J.-S.** (2014). Targeting Cancer Cells with Reactive Oxygen and Nitrogen Species Generated by Atmospheric-Pressure Air Plasma. *PLoS ONE*, 9(1), e86173. doi: 10.1371/journal.pone.0086173
- Andreuccetti, D., Fossi, R., & Petrucci, C.** (1997). An Internet resource for the calculation of the dielectric properties of body tissues in the frequency range 10 Hz–100 GHz. *Internet document*.
- Balanis, C. A.** (2012). *Advanced Engineering Electromagnetics*: Wiley.
- Behari, J.** (2009). *Biophysical Bone Behaviour: Principles and Applications*: Wiley.
- Behm, B., Babilas, P., Landthaler, M., & Schreml, S.** (2012). Cytokines, chemokines and growth factors in wound healing. *Journal of the European Academy of Dermatology and Venereology*, 26(7), 812-820.
- Bindschadler, M., & McGrath, J. L.** (2007). Sheet migration by wounded monolayers as an emergent property of single-cell dynamics. *J Cell Sci*, 120(Pt 5), 876-884. doi: 10.1242/jcs.03395
- Blank, M., & Findl, E.** (2013). *Mechanistic approaches to interactions of electric and electromagnetic fields with living systems*: Springer Science & Business Media.
- Cheng, D. K.** (1993). *Fundamentals of Engineering Electromagnetics*: Addison-Wesley Publishing Company.
- Chih-Peng, L., Chieh-Hsiang, C., Cheng, Y. T., & Jou, C. F.** (2011). Development of a Flexible SU-8/PDMS-Based Antenna. *Antennas and Wireless Propagation Letters, IEEE*, 10, 1108-1111. doi: 10.1109/LAWP.2011.2170398
- Cooke, S. J., Shtokhamer, R., Mondelli, A. A., & Levush, B.** (2006). A finite integration method for conformal, structured-grid, electromagnetic simulation. *Journal of Computational Physics*, 215(1), 321-347. doi: <http://dx.doi.org/10.1016/j.jcp.2005.10.032>
- Dargaville, T. R., Farrugia, B. L., Broadbent, J. A., Pace, S., Upton, Z., & Voelcker, N. H.** (2013). Sensors and imaging for wound healing: a review. *Biosensors and Bioelectronics*, 41, 30-42.
- Didouh, S., Abri, M., & Bendimerad, F. T.** (2012). Multilayered BOW-TIE Antennas Design for RFID and Radar Applications Using a Simple Equivalent Transmission Line Model. *International Journal of Computer Networks & Communications*.
- Duck, F. A.** (2013). *Physical Properties of Tissues: A Comprehensive Reference Book*: Elsevier Science.
- El Hatmi, F., Grzeskowiak, M., Alves, T., Protat, S., & Picon, O.** (2011, 8-10 Sept. 2011). *Magnetic loop antenna for wireless capsule endoscopy inside the*

- human body operating at 315 MHz: Near field behavior*. Paper presented at the Mediterranean Microwave Symposium (MMS), 2011 11th.
- Faktorová, D., & Isteniková, K.** (2011). Modelling of scattering parameters in biological tissues. *Skin*, 1(41), 0.7.
- Fleming, T., & Bauer, E.** (2014). *Inside the Photon: A Journey to Health*: Pan Stanford.
- Gabriel, C.** (1996). Compilation of the Dielectric Properties of Body Tissues at RF and Microwave Frequencies: DTIC Document.
- Garg, R.** (2008). *Analytical and Computational Methods in Electromagnetics*: Artech House, Incorporated.
- Gordon, G. A.** (2007). Designed electromagnetic pulsed therapy: Clinical applications. *Journal of Cellular Physiology*, 212(3), 579-582. doi: 10.1002/jcp.21025
- Goswami, D. Y.** (2004). *The CRC Handbook of Mechanical Engineering, Second Edition*: CRC Press.
- Gregoire, D. J., White, C. R., & Colburn, J. S.** (2011). Wideband artificial magnetic conductors loaded with non-Foster negative inductors. *Antennas and Wireless Propagation Letters, IEEE*, 10, 1586-1589.
- Habash, R.** (2007). *Bioeffects and therapeutic applications of electromagnetic energy*: CRC press.
- Habash, R. W. Y.** (2001). *Electromagnetic Fields and Radiation: Human Bioeffects and Safety*: Taylor & Francis.
- Harden, R., Remble, T., Houle, T., Long, J., Markov, M., & Gallizzi, M.** (2007). Prospective, Randomized, Single-Blind, Sham Treatment-Controlled Study of the Safety and Efficacy of an Electromagnetic Field Device for the Treatment of Chronic Low Back Pain: A Pilot Study. *Pain Practice*, 7(3), 248-255.
- Hilger, I., Dahlke, K., Rimkus, G., Geyer, C., Seifert, F., Kosch, O., . . . Sachs, J.** (2013). *ultraMEDIS – Ultra-Wideband Sensing in Medicine*.
- Hubing, T. H.** (1991). Survey of numerical electromagnetic modeling techniques. *Department of Electrical Engineering, University of Missouri-Rolla, USA*.
- Hug, K., & Rööslı, M.** (2012a). Therapeutic effects of whole-body devices applying pulsed electromagnetic fields (PEMF): A systematic literature review. *Bioelectromagnetics*, 33(2), 95-105. doi: 10.1002/bem.20703
- Hug, K., & Rööslı, M.** (2012b). Therapeutic effects of whole-body devices applying pulsed electromagnetic fields (PEMF): A systematic literature review. *Bioelectromagnetics*, 33(2), 95-105.
- Isbary, G., Stolz, W., Shimizu, T., Monetti, R., Bunk, W., Schmidt, H. U., . . . Zimmermann, J. L.** (2013). Cold atmospheric argon plasma treatment may accelerate wound healing in chronic wounds: Results of an open retrospective randomized controlled study in vivo. *Clinical Plasma Medicine*, 1(2), 25-30. doi: <http://dx.doi.org/10.1016/j.cpme.2013.06.001>
- Karacolak, T., Cooper, R., & Topsakal, E.** (2009). Electrical properties of rat skin and design of implantable antennas for medical wireless telemetry. *Antennas and Propagation, IEEE Transactions on*, 57(9), 2806-2812.
- KOYUNOĞLU, F., KONAR, V., & SANDAL, S.** (2013). İnsan meme kanseri hücre serileri (MCF-7) üzerine apelin-13'ün etkilerinin araştırılması: In vitro bir çalışma. *İnönü Üniversitesi Sağlık Bilimleri Dergisi*, 1(1), 23-28.
- Liang, C. C., Park, A. Y., & Guan, J. L.** (2007). In vitro scratch assay: a convenient and inexpensive method for analysis of cell migration in vitro. *Nat Protoc*, 2(2), 329-333. doi: 10.1038/nprot.2007.30

- Lin, J. C., Guy, A. W., & Johnson, C. C.** (1973). Power deposition in a spherical model of man exposed to i-20-mhz electromagnetic fields. *Microwave Theory and Techniques, IEEE Transactions on*, 21(12), 791-797.
- Lin, J. C., & Michaelson, S. M.** (2013). *Biological effects and health implications of radiofrequency radiation*: Springer Science & Business Media.
- Lin, J. C., & Michaelson, S. M.** (2014). *Biological Effects and Health Implications of Radiofrequency Radiation*: Springer.
- Machala, Z., Hensel, K., & Akishev, Y.** (2012). *Plasma for Bio-Decontamination, Medicine and Food Security*: Springer Netherlands.
- Markov, M. S.** (2007). Expanding use of pulsed electromagnetic field therapies. *Electromagnetic Biology and Medicine*, 26(3), 257-274.
- Markova, A., & Mostow, E. N.** (2012). US skin disease assessment: ulcer and wound care. *Dermatologic clinics*, 30(1), 107-111.
- Michaelson, S., & Lin, J.** (1987). Radio and Microwave Dielectric Properties of Biological Materials *Biological Effects and Health Implications of Radiofrequency Radiation* (pp. 93-136): Springer US.
- Michlovitz, S. L., Bellew, J. W., & Nolan, T. P.** (2011). *Modalities for Therapeutic Intervention*: F.A. Davis Company.
- Montie, T. C., Kelly-Wintenberg, K., & Roth, J. R.** (2000). An overview of research using the one atmosphere uniform glow discharge plasma (OAUGDP) for sterilization of surfaces and materials. *Plasma Science, IEEE Transactions on*, 28(1), 41-50.
- Peratta, C., & Peratta, A.** (2010). *Modelling the Human Body Exposure to ELF Electric Fields*: WIT.
- Pesce, M., Patrino, A., Speranza, L., & Reale, M.** (2013). Extremely low frequency electromagnetic field and wound healing: implication of cytokines as biological mediators. *European cytokine network*, 24(1), 1-10.
- Pirmohamed, M., James, S., Meakin, S., Green, C., Scott, A. K., Walley, T. J., . . . Breckenridge, A. M.** (2004). Adverse drug reactions as cause of admission to hospital: prospective analysis of 18 820 patients. *Bmj*, 329(7456), 15-19.
- Poor, A. E., Ercan, U. K., Yost, A., Brooks, A. D., & Joshi, S. G.** (2014). Control of Multi-Drug-Resistant Pathogens with Non-Thermal-Plasma-Treated Alginate Wound Dressing. *Surgical infections*, 15(3), 233-243.
- Rufus, E.** (2014). *Microstrip antenna on kapton substrate for strain sensing applications*. Paper presented at the Advanced Communication Technology (ICACT), 2014 16th International Conference on.
- Sammak, P. J., Hinman, L. E., Tran, P. O., Sjaastad, M. D., & Machen, T. E.** (1997). How do injured cells communicate with the surviving cell monolayer? *J Cell Sci*, 110 ( Pt 4), 465-475.
- Silver, H. W., & Wilson, M.** (2008). *The ARRL Extra Class License Manual for Ham Radio*: ARRL.
- Singh, S., & Kapoor, N.** (2015). Occupational EMF exposure from radar at X and Ku frequency band and plasma catecholamine levels. *Bioelectromagnetics*, 36(6), 444-450.
- Trepat, X., Wasserman, M. R., Angelini, T. E., Millet, E., Weitz, D. A., Butler, J. P., & Fredberg, J. J.** (2009). Physical forces during collective cell migration. *Nat Phys*, 5(6), 426-430. doi: [http://www.nature.com/nphys/journal/v5/n6/supinfo/nphys1269\\_S1.html](http://www.nature.com/nphys/journal/v5/n6/supinfo/nphys1269_S1.html)

- Trock, D. H.** (2000). Electromagnetic fields and magnets: investigational treatment for musculoskeletal disorders. *Rheumatic Disease Clinics of North America*, 26(1), 51-62.
- Ueno, S.** (1996). *Biological effects of magnetic and electromagnetic fields*: Springer.
- van Horssen, R., Galjart, N., Rens, J. A. P., Eggermont, A. M. M., & ten Hagen, T. L. M.** (2006). Differential effects of matrix and growth factors on endothelial and fibroblast motility: Application of a modified cell migration assay. *Journal of Cellular Biochemistry*, 99(6), 1536-1552. doi: 10.1002/jcb.20994
- Vural, K., & Tuğlu, M.** (2011). Neurotoxic effect of statins on mouse neuroblastoma NB2a cell line. *European review for medical and pharmacological sciences*, 15(9), 985-991.
- Wade, B.** (2013). A review of pulsed electromagnetic field (PEMF) mechanisms at a cellular level: A rationale for clinical use. *Am J Health Res*, 1, 51-55.
- Zhang, K., & Li, D.** (2013). *Electromagnetic Theory for Microwaves and Optoelectronics*: Springer Berlin Heidelberg.
- Zhu, Y., Wang, A., Liu, M. C., Zwart, A., Lee, R. Y., Gallagher, A., . . . Clarke, R.** (2006). Estrogen receptor alpha positive breast tumors and breast cancer cell lines share similarities in their transcriptome data structures. *International journal of oncology*, 29(6), 1581-1589.

## APPENDICES

### APPENDIX A: ELECTROMAGNETIC MODELLING of HUMAN LEG and ITS APPLICATION ON THE INTERACTION BETWEEN HELMHOLTZ COILS, ELECTROMAGNETIC MODELLING of HUMAN TISSUE and ITS APPLICATION ON THE INTERACTION WITH A LOOP ANTENNA

Mathematical formulation of magnetic field of circular ring is given by;

$$\vec{B} = \frac{\mu_0 I}{4\pi} \int \frac{d\vec{l}'}{|\vec{R} - \vec{R}'|^3} \times (\vec{R} - \vec{R}') \quad (\text{A1.1})$$

$$\vec{R} - \vec{R}' = (x - x')\vec{a}_x + (y - y')\vec{a}_y + (z - z')\vec{a}_z \quad (\text{A1.2})$$

$$\vec{B} = \frac{\mu_0 I}{4\pi} \int \frac{R d\phi' \vec{a}_{\phi'}}{\left((x - x')^2 + (y - y')^2 + (z - z')^2\right)^{3/2}} \times \left((x - x')\vec{a}_x + (y - y')\vec{a}_y + (z - z')\vec{a}_z\right) \quad (\text{A1.2})$$

$$\vec{a}_{\phi'} = -\sin(\phi')\vec{a}_x + \cos(\phi')\vec{a}_y \quad (\text{A1.3})$$

$$\vec{B} = \frac{\mu_0 I}{4\pi} R \int_0^{2\pi} \frac{\left(-\sin(\phi')(y - y') + \cos(\phi')(x - x')\right)\vec{e}_z + \sin(\phi')(z - z')\vec{e}_y + \cos(\phi')(z - z')\vec{e}_x}{\left((x - x')^2 + (y - y')^2 + (z - z')^2\right)^{3/2}} d\phi' \quad (\text{A1.4})$$

where R is the radius of circular ring;

$$x' = R \cos(\phi') \quad (\text{A1.5})$$

$$y' = R \sin(\phi') \quad (\text{A1.6})$$

$$z' = 0 \quad (\text{A1.7})$$

By the numerical integration of mathematical formulation of B for magnetic field computation of one ring and the superposition of magnetic field components in the vectorial form for magnetic field computation of more than one circular rings, the



magnetic field components of different arrangements of multiple circular rings with different radii can be computed.

The electric and magnetic fields are formulated for y-polarized z direction propagating plane wave in all three different media as;

$$\vec{E}_1 = (E_0 e^{-jk_1 z} + \Gamma E_0 e^{jk_1 z}) \vec{e}_y \quad (\text{A1.8})$$

$$\vec{H}_1 = \frac{(-jk_1 E_0 e^{-jk_1 z} + jk_1 \Gamma E_0 e^{jk_1 z})}{j\omega\mu_1} \vec{e}_x \quad (\text{A1.9})$$

$$\vec{E}_2 = (A e^{-jk_2 z} + B e^{jk_2 z}) \vec{e}_y \quad (\text{A1.10})$$

$$\vec{H}_2 = \frac{k_2 (-A e^{-jk_2 z} + B e^{jk_2 z})}{\omega\mu_2} \vec{e}_x \quad (\text{A1.11})$$

$$\vec{E}_3 = E_3 e^{-jk_3 z} \vec{e}_y \quad (\text{A1.12})$$

$$\vec{H}_2 = \frac{-k_3 E_3 e^{-jk_3 z}}{\omega\mu_2} \vec{e}_x \quad (\text{A1.13})$$

The field continuity conditions of tangential electric and magnetic fields at two different boundaries,  $z=0$  and  $z=L_1$  have to be satisfied as boundary conditions.

$$E_1 \Big|_{z=0} = E_2 \Big|_{z=0} \Rightarrow E_0(1+\Gamma) = A+B \quad (\text{A1.14})$$

$$H_1 \Big|_{z=0} = H_2 \Big|_{z=0} \Rightarrow -\frac{E_0 k_1 (1-\Gamma)}{\mu_1} = \frac{k_2 (-A+B)}{\mu_2} \quad (\text{A1.15})$$

$$E_2 \Big|_{z=L_1} = E_3 \Big|_{z=L_1} \Rightarrow A e^{-jk_2 L_1} + B e^{jk_2 L_1} = E_3 e^{-jk_3 L_1} \quad (\text{A1.16})$$

$$H_2 \Big|_{z=L_1} = H_3 \Big|_{z=L_1} \Rightarrow \frac{k_2}{\omega\mu_2} (-A e^{-jk_2 L_1} + B e^{jk_2 L_1}) = -\frac{E_3 k_3}{\omega\mu_3} e^{-jk_3 L_1} \quad (\text{A1.17})$$

All four unknown field parameters, A, B, E3 and  $\Gamma$  can be calculated from four linear equations in terms of E0 by presetting the power density of incoming wave. The reflection coefficient,  $\Gamma$  can be formulated as

$$\Gamma = \frac{\frac{\mu_1 k_2}{\mu_2 k_1} \left( \cos(k_2 L_1) + j \frac{\mu_3 k_2}{\mu_2 k_3} \sin(k_2 L_1) \right) - j \sin(k_2 L_1) - \frac{\mu_3 k_2}{\mu_2 k_3} \cos(k_2 L_1)}{-\frac{\mu_1 k_2}{\mu_2 k_1} \left( \cos(k_2 L_1) + j \frac{\mu_3 k_2}{\mu_2 k_3} \sin(k_2 L_1) \right) - j \sin(k_2 L_1) - \frac{\mu_3 k_2}{\mu_2 k_3} \cos(k_2 L_1)} \quad (\text{A1.18})$$

The mathematical model has been applied to the evaluation of the currents induced in human leg and tissue models exposed to 75 Hz and 27 MHz electric and magnetic fields. The human leg has been modelled considering actual shapes and dimensions, as shown in Figure A.1. In this study, a 27 MHz carrier frequency electromagnetic radiation as generated by a loop antenna at a distance of 10 cm to a multilayer model of human tissue, as in Figure A.2, was assumed. Each internal region has been characterized by proper dielectric properties following the indications available in literature (Table A.1). The human leg is exposed to an electric field whose intensity ranges from 0.0027 to 0.0297 V/m, and a magnetic flux density from 152 to 1.6 mT. The human tissue is exposed to an electric field whose intensity ranges from 47.8 to 525 V/m, and a magnetic flux density from 0.0472 to 0.519 A/m.

**Table A.1** : Dielectric properties of fat and muscle layers at different frequencies.

Frequency	Wave length [m]	Type of EM Radiation*	Fat Dielectric Properties		Muscle Dielectric Properties		Ref
			Relative Permittivity	Conductivity [S/m]	Relative Permittivity	Conductivity [S/m]	
75 Hz	4x10 <sup>6</sup>	PEMF	746910	0.020	12777000	0.253	(Andreuccetti, Fossi, & Petrucci, 1997)
13.56 MHz	22	PRFE	177.132	0.055	125.715	0.683	
27.12 MHz	11	PRFE	17.926	0.061	91.605	0.707	
40.68 MHz	7.5	PRFE	15.354	0.064	80.120	0.721	(Gabriel, 1996)
915 MHz	0.33	MWD	11.328	0.110	56.845	1.001	
2450 MHz	0.12	MWD	10.820	0.268	54.418	1.882	

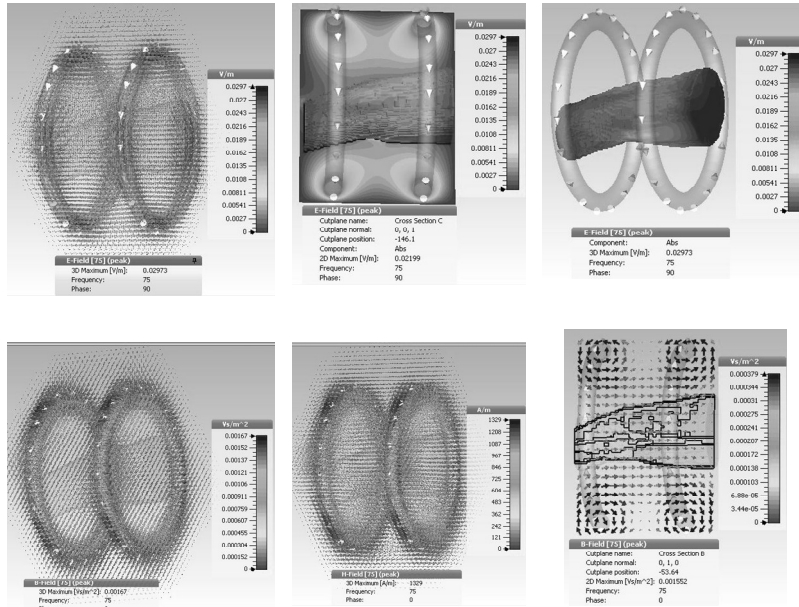


**Figure A.1 :** Induced electric and magnetic field by low frequency electromagnetic fields to human leg model

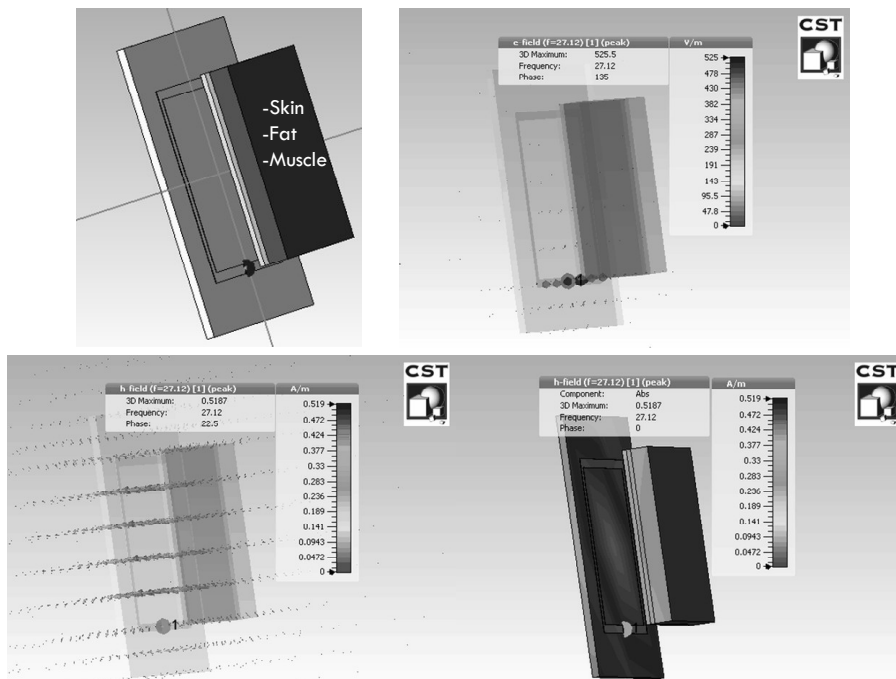


**Figure A.2 :** Simulation result of 27 Mhz electromagnetic field exposed of human tissue model by a loop antenna

The human body is a multilayer medium constituted of different organs such as muscles, bones, blood, cells, skin, stomach, etc. Every layer contains its own electric properties, which also depends on the frequency (El Hatmi, Grzeskowiak, Alves, Protat, & Picon, 2011). To simplify the 27 MHz antenna study, the different layers of the human tissue can be considered in only three homogeneous layers (1.3 mm skin, 6

mm fat, 50 mm muscle). The antenna is placed 10 cm from the homogeneous human tissue surrounded by an air box. Figure A.3 shows that the absolute component of the electric and magnetic field distribution on 57.3 mm thickness of skin, fat, muscle layers. The total E field decreases in the tissue with the distance, whereas, the magnetic field is also decreasing.

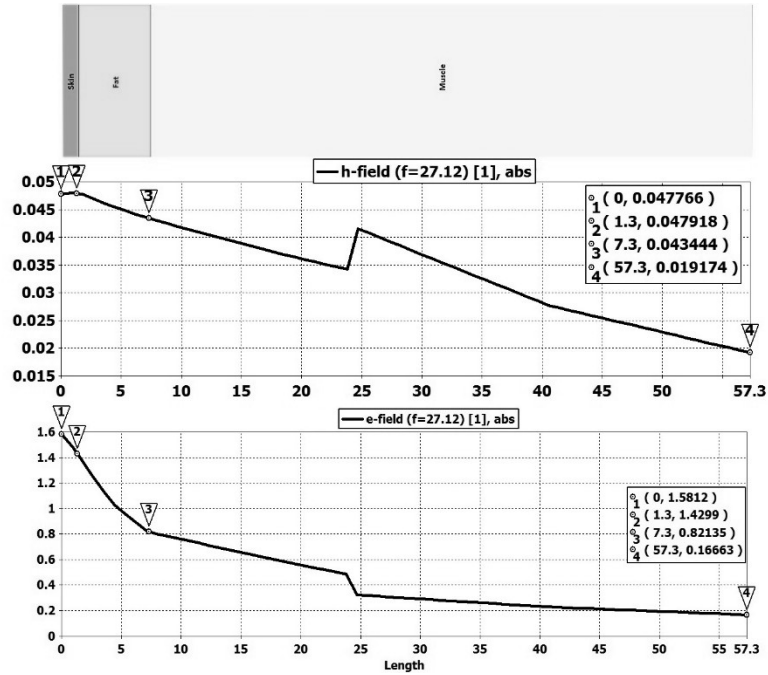
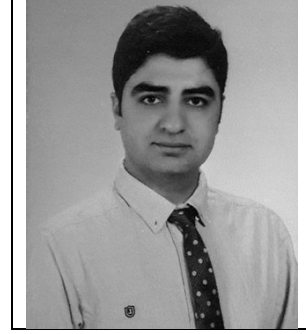


**Figure A.3 :** E-field and H-field distributions generated by 27 MHz antenna in human tissue layers

## CURRICULUM VITAE



**Name Surname:** Mehmet GÜMÜŞAY

**Place and Date of Birth:** MARDIN-01/07/1989

**Address:** Izmir Katip Celebi University Graduate School of Science and Engineering Department of Biomedical Technologies Balatcik Mh. No: 33/2 Postcode: 35620 Cigli/IZMIR/ TURKEY

**E-Mail:** mehmet.gumusay@ikc.edu.tr

**M.Sc.:** Izmir Katip Celebi University, Department of Biomedical Technologies, 2013-

**B.Sc.:** Ege University-Engineering Faculty Department of Bioengineering, 2013

### PROFESSIONAL EXPERIENCE AND REWARDS:

- Researcher, Izmir Katip Celebi University Scientific Research Projects, Design of Chronic Wound Healing Device by Pulsed Electromagnetic Fields, 2015-
- Tubitak Research Project Graduate Student Scholarship, 2014-2016
- Certificate On Laboratory Animal Usage and Care, Ankara University, 2014
- Research Assistant, Izmir Katip Celebi University, Department of Biomedical Technologies, 2013-

### COMPUTER SKILLS AND COMPETENCES

- Operating System: Windows
- Softwares: Microsoft Office, CST Studio Suite (Computer Simulation Technology), Antenna Magus, Proteus, Multisim, Matlab

### PUBLICATIONS, PRESENTATIONS AND PATENTS ON THE THESIS:

- **M. Gümüőay**, S. Saygılı, I. Aydemir, İ. Tuđlu, A. KAYA, “Yara İyileőme Tedavisinde 27.12 MHz Darbeli Elektromanyetik Alan Iőıması Etkilerinin İncelenmesi ve Aplikatör Tasarımı”, *Elektromanyetik Alanlar ve Etkileri Sempozyumu*, Mersin, 13-14-15 Kasım 2015
- S. Saygılı, **M. Gümüőay**, I. Aydemir, İ. Tuđlu, A. KAYA, “Yara İyileőme Tedavisinde Darbeli Elektromanyetik Alan Tedavisi (PEMF) Etkilerinin

İmmünohistokimyasal Analizi” *Elektromanyetik Alanlar ve Etkileri Sempozyumu, Mersin*, 13-14-15 Kasım 2015

- S. Saygılı, **M. Gümüřay**, I. Aydemir, A. KAYA, “Elektromanyetik alanın nöroblastom dizin hücrelerinde yara iyileřmesine etkisi” *13. Ulusal Sinirbilim Kongresi, Selçuk Üniversitesi*, 30 Nisan-3 Mayıs 2015
- **M. Gümüřay**, Kaya, A, “Düşük Enerjili Darbeli Elektromagnetik Alanların Yara İyileřtirmesine Etkileri” *Tıp Teknolojileri Kongresi (Tiptekno 2014)*, Kapadokya, 25-27 Eylül 2014
- **M. Gümüřay**, Kaya, A, “Pulsed Electromagnetic Field (PEMF) Effect on Biochemical Pathways” III. Uluslararası Moleküler Biyoloji Kongresi, İzmir Yüksek Teknoloji Enstitüsü, 10-12 Eylül 2014.
- **M. Gümüřay**, Kaya, A, “Düşük Enerjili Darbe Elektromagnetik Dalga Teknięi İle Kronik Yara İyileřtirme Analizi” *URSI-TÜRKİYE’2014 VII. Bilimsel Kongresi*, Fırat Üniversitesi, 28-30 Ağustos 2014.